Technische Universität München

Wissenschaftszentrum Weihenstephan für Ernährung, Landnutzung und Umwelt

Lehrstuhl für Waldwachstumskunde

Allometric Estimation of Aboveground Forest Biomass using Forest Structure Parameters estimated by means of Multi-Baseline SAR Measurements

Astor Toraño Caicoya

Vollständiger Abdruck der von der Fakultät Wissenschaftszentrum Weihenstephan für Ernährung, Landnutzung und Umwelt der Technischen Universität München zur Erlangung des akademischen Grades eines

Doktors der Forstwissenschaft (Dr. rer. silv.)

genehmigten Dissertation.

Vorsitzender: Priv.-Doz. Dr. Thomas Rötzer

Prüfer der Dissertation:

1. Prof. Dr. Dr. h.c. Hans Pretzsch
2. Prof. Dr. Michael Weber
3. Prof. Dr. Irena Hajnsek

Die Dissertation wurde am 30.11.2015 bei der Technischen Universität München eingereicht und durch die Fakultät Wissenschaftszentrum Weihenstephan für Ernährung, Landnutzung und Umwelt am 16.03.2016 angenommen.

Doctoral Thesis

Allometric Estimation of Aboveground Forest Biomass using Forest Structure Parameters estimated by means of Multi-Baseline SAR Measurements

presented by

Astor Toraño Caicoya

For the degree:

Dr. rer. silv.

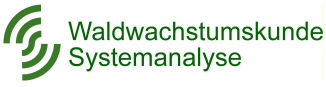

Submitted to: **Technische Universität München (TUM)**

Lebenslauf

1.1 PERSONALDATEN

Name: **Toraño Caicoya, Astor**

Geburtsort: Oviedo, Asturias, Spanien

Geburtsdatum: 27. Oktober 1983

Nationalität: Spanisch

Adresse: Lindwurmstrasse 8 München, Deutschland, D-80337

Tel. +49 172 8277363

1.2 BILDUNG

2010 – 2016: **Doktorarbeit** in der Technische Universität München (TUM), Lehrstuhl für Waldwachstumskunde, Freising in zusammen Arbeit mit dem Deutschen Zentrum für Luft- und Raumfahrt (DLR), Oberpfaffenhofen, Deutschland

2007 – 2010: **MSc** Sustainable Resource Management (Note: 1.3/sehr gut),
Technische Universität München (TUM), Studienfakultät Forstwissenschaft und Ressourcemangement, Freising, Deutschland
Spezialisierung in Landschaftsmanagement und nachhaltige Forstwissenschaft

2004 – 2007: **MSc** Waldingenieur (Ingeniero de Montes) (Note: 7.48/10),
Polytechnic University of Valencia (UPV), School of Agricultural Engineering and Environment, Valencia, Spain

2001 – 2004: **Bhc** Waldingenieur (Ingeniero Técnico Forestal) (Note: 7.21/10),
University of Oviedo, Polytechnic School of Mieres, Mieres, Asturias, Spanien
Spezialisierung in Waldbewirtschaftung

1999 – 2001: **Gymnasium** (Bachillerato): IES Escultor Juan de Villanueva, Pola de Siero, Asturias, Spanien

1.3 BERUFSERFAHRUNG

Seit 02/2010: **Deutsches Zentrum für Luft- und Raumfahrt (DLR), Oberpfaffenhofen, Deutschland, Hochfrequenz und Radarsysteme Institut (HR)**

- Entwicklung von Algorithmen zur Bestimmung der Waldbiomasse mittels vertikaler/horizontaler Vermessung der Waldinventur bzw. muli-baseline interferometrischer und tomographischer SAR Daten. Waldbiomasseklassifikation in der borealen Region mit TanDEM-X Aufnahmen.

2009/2010: **Deutsches Zentrum für Luft- und Raumfahrt (DLR), Oberpfaffenhofen, Deutschland, Hochfrequenz und Radarsysteme Institut (HR)**

- Masterarbeit und Prakikum: Modellierung von Waldbiomasse 3D-Strukturen mittels Waldinventur-Datenbanken und vertikalen LiDAR-Struktur Profilen

2008: **Technische Universität München (TUM), Freising, Deutschland**
Lehrstuhl für Waldwachstumskunde, Studienfakultät Forstwissenschaft und Ressourcemangement

- Terrestrische LiDAR Erfassung von Wäldern zur Unterstützung von „Leaf Area Index" Bestimmungen

2007: **Polytechnic University of Valencia, Spanien,**
Department of Agroforestry Ecosystems

- Forschungsarbeit zur Simulation der Schwierigkeiten bei der Löschung von Waldbränden

1.4 WISSENSCHAFTLICHE AUSZEICHNUNGEN UND PREISE

- **Franz-Xavier-Erlacher Förderpreis (2010)** für Doktoranden im Bereich der Fernerkundung von Atmosphäre, Klima und Umwelt
- **Preis der Audi Stiftung für Umwelt (2010)** für die beste Masterarbeit im „Sustainable Resource Management" Programm: "Forest Biomass Estimation Derived from 3D Forest Structure in Remote Sensing (LiDAR, Radar)"
- **Sonderauszeichnung der School of Agriculture and Forest Sciences (Polytechnic University of Valencia) (2007)** für die Masterarbeit: "Index of Difficulty of Wildfire Extinction (IDEIF) for Chiva, Valencia"

1.5 SOFTWARE

- Sehr gute Kenntnisse der Programmiersprache IDL, MS Office (Word, Excel, Access, Powerpoint, MSProject), von GIS/CAD/RS (ArcGIS 9.x, ArcVIew, ENVI) und Statistikprogramme (Statgraphics, SPSS, Statbox). Kenntnisse von Python, ERDAS, Matlab und eCognition

1.6 SPRACHEN

- Spanisch (Muttersprache)
- English (berufliche Kompetenz)
- Deutsch (berufliche Kompetenz)

Abstract

Forest biomass is an essential part of the terrestrial carbon pool; therefore, it is one of the most important contributions to the global carbon cycle. Moreover, forest biomass is a main variable for mapping the amount and geographic distribution of forests and its change in time is required to understand the development of carbon fluxes. Even more, the changes in forest biomass are the most uncertainly measured variable in the carbon cycle.

A common method for estimating forest biomass is based on allometric equations which connect biomass to other accessible forest variables. However, in order to measure these variables for global estimations, with sufficient spatial and temporal resolution, Remote Sensing (RS) systems need to be used. Therefore, in this dissertation, the potential of allometric relationships that can be applied to RS variables, especially focusing on Synthetic Aperture Radar (SAR) data, is investigated. Height-to-biomass allometries are known to estimate biomass actually from RS data. Here, a large-scale biomass classification methodology for the boreal region, based on forest height and proposed for the satellite mission with global coverage, TanDEM-X, is performed. High accuracy and a measurable error for 4- and 5- class biomass maps are produced. However, these allometric relationships can only be applied in forest ecosystems which, like the boreal forests, are characterized by homogenous structures. Changes in structure diversity increase the variance of the relationship and make the biomass estimation inaccurate. For this reason, new allometric relationships are investigated.

SAR systems are capable of estimating vertical distribution of forest volumes providing with stand vertical structure variables. In this dissertation, the allometric relationships existing between the vertical distribution of biomass and the aboveground biomass content are studied. Using inventory data to model vertical biomass profiles it is demonstrated that the novel structure-to-biomass relationship can improve the biomass estimation accuracy by an average of a 20% respect to only height relationships. Moreover, useful management parameters, like the allometric level, are also estimated using vertical structures. Finally, the expression derived for inventory data is adapted and applied to SAR reflectivity profiles, estimated using tomographic techniques from L-band airborne data. Similar performances are observed for all the tested scenarios and biomass maps with accuracies closed to r^2 =0.8 are produced.

Kurzfassung

Waldbiomasse ist Hauptbestandteil des terrestrischen Kohlenstoffpools und damit ein zentraler Parameter im globalen Kohlenstoffkreislauf. Waldbiomasse ist somit eine der Hauptvariablen für die Erfassung von Waldmengen. Aus ihrer geographischen Verteilung sowie ihrer zeitlichen Veränderung kann die Entwicklung des Kohlenstoffkreislaufs abgeleitet werden. Änderungen in der Waldbiomasse gehören noch immer zu den am ungenauesten gemessenen Variablen des Kohlenstoffkreislaufs.

Eine verbreite Methode zur Bestimmung von Waldbiomasse beruht auf allometrischen Gleichungen, die den Zusammenhang von Waldbiomasse mit anderen gemessenen Waldkenngrößen beschreiben. Um diese weiteren Kenngrößen mit der notwendigen räumlichen und zeitlichen Auflösung weltweit erfassen zu können, müssen Fernerkundungssysteme eingesetzt werden. Diese Dissertationsarbeit untersucht daher das Potenzial der Anwendung allometrischer Gleichungen im Bereich der Fernerkundung, im speziellen mit Synthetic Aperture Radar (SAR). Es ist bekannt, dass allometrische Beziehungen zwischen Wuchshöhe und Waldbiomasse mit einer hohen Genauigkeit aus Fernerkundungsdaten abgeleitet werden können. In dieser Arbeit wird eine Methode für großflächige Waldbiomasseklassifikation borealer Regionen entwickelt, die auf der Erfassung der Baumwuchshöhe unter Verwendung der Satellitenmission TanDEM-X beruht. Die gewonnenen 4- und 5- Klassen Kartierungsdaten besitzen eine hohe Genauigkeit inkl. Angabe des auftretenden Messfehlers, wobei die dabei angewandten allometrischen Berechnungen nur in borealen Ökosystemen gültig sind, die sich durch eine homogene Struktur auszeichnen. Veränderungen in der Strukturvielfalt erhöhen die Varianz der Berechnungen und führen zu Ungenauigkeiten bei der Bestimmung von Biomasse. Aus diesem Grund ist es notwendig, neue allometrische Zusammenhänge zu untersuchen.

SAR-Systeme sind in der Lage die Vertikalverteilung des Waldvolumens zu bestimmen und liefern damit die Berechnungsgrundlage der Vertikalstruktur des Waldes. Die bestehenden allometrischen Beziehungen zwischen der Vertikalverteilung der Waldbiomasse und dem messbaren oberirdischen Biomasseanteil werden in dieser Dissertation untersucht. Unter Zuhilfenahme von Datenbanken (Vorratsdaten) werden Vertikalverteilungsprofile der Waldbiomasse erstellt, deren Berechnungsgrundlage auf den Beziehungen zwischen Struktur und

Biomasse basiert. Dabei kann gezeigt werden, dass die hierbei erreichte Genauigkeit der Biomassebestimmung um mindestens 20% im Vergleich zur konventionellen Methode bei der nur die Wuchshöhe berücksichtigt wird, verbessert werden kann. Zusätzlich können durch die Bestimmung der Vertikalstruktur nützliche Management-Parameter wie z.B. das allometrische Niveau gewonnen werden. Abschließend werden Beziehungen, die aus Vorratsdaten abgeleitet wurden, angepasst und auf SAR-Rückstreuungsprofilen angewendet, welche aus luftgestützten tomographischen L-Band Techniken gewonnen wurden. In allen getesteten Szenarien wurde eine vergleichbare Leistung beobachtet und die kartographierte Biomasse konnte mit einer Genauigkeit von r^2=0.8 ermittelt werden.

Acknowledgements

With this dissertation I close one of the most important periods of not only my career but also my life. The challenges that I have gone through these years have helped to grow and have definitely prepared me to face whatever it is to come. Frustrations and satisfactions together with disappointments and achievements were part of this trip, and brought me where I am, personally and professionally. Therefore, I would like to kindly thank my supervisors Irena Hajnsek and Kostas Papathanassiou, for giving this outstanding opportunity, together with Florian Kugler who gave me my first chance in DLR and guided my thesis since the very beginning. Moreover, I would like to acknowledge Peter Biber who, through my master thesis started all of this, and Prof. Hans Pretzsch for allowing me to present my thesis at his Chair and for his valuable support both theoretically and towards the conclusion of this work.

The life in DLR not only gave me the chance to meet great scientists and professionals, but also to make a bunch of real good friends who I am sure I will keep forever. And for this I have to especially thank Matteo for the daily coffees and chats, getting everyday his bright view and knowledge, and Hannah for all the talks and support not only in the German writing but also in everything else. Maria and Giuseppe, always there ready to share a frustration or a chat and all together for making every day, conference, trip and meeting a great experience. I could not have made it without you guys. I also want to thank all my PolInSAR colleagues, from master to postdocs who passed through DLR during this quite some years and enriched the experience.

Finally, I am particular grateful to my family to which I dedicate my last words, the Spanish and the German one: my parents who have never doubted or stopped encouraging me, and my real good friends, who are my family in Munich and stood me without hesitation though all this process. Kleo, Gemma, Saša, Pablo, Roger, thanks for being there, thanks for all.

Contents

List of symbols and acronyms

Acronyms:

3-D	Three dimensional
AGB	Aboveground Biomass
ALOS/ALOS-2	Advanced Land Observing Satellite; are Japanese earth observation satellite with an L-band SAR antenna
ALOS PALSAR	L-band SAR of ALOS
ASAR	Advanced Synthetic Aperture Radar operated at C-band on ESAs' earth observation satellite Envisat
AVHRR	Advanced Very High Resolution Radiometer multispectral remote sensing sensor operated by the National Oceanic and Atmospheric Administration of the US government
BIOMASS	future radar earth observation satellite operating at P-band (from ESA)
CORINE	Coordination of Information on the Environment; European land cover classification
dbh	Diameter at Breast Height
DEM	Digital Elevation Model
DSM	Digital Surface Model
DTM	Digital Terrain Model
ENVISAT	Environmental Satellite, an inoperative Earth-observing satellite
ERS	European Remote Sensing Satellites was operated by ESA and carries beside other sensors also a C-band SAR
ESA	European Space Agency
FSC	Forest Stewardship Council (Forest Certification System)
GLAS	Geoscience Laser Altimeter System on board of ICESat; large footprint LiDAR sensor
GtC	Giga-tone of Carbon
InSAR	Interferometric SAR

JERS	Japanese Earth Resources Satellite carried L-band SAR (operated until 1998)
LAI	Leaf Area Index
LiDAR	Light Detection And Ranging
LOS	Line of Sight
MB	Multi-baseline
MODIS	Moderate-resolution Imaging Spectroradiometer is a sensor on board of the NASA earth observation satellites Terra and Aqua
NOAA	National Oceanic and Atmospheric Administration
PCT	Polarimetric Coherence Tomography
Pol-InSAR	Polarimetric-Interferometric SAR
PRF	Pulse Repetition Frequency
Radar	Radio Detection and Ranging; microwave region of the electromagnetic spectrum
REDD	Reducing Emissions from Deforestation and Forest Degradation
RMSE	Root Mean Square Error
RS	Remote Sensing
RVoG	Random Volume over Ground Model
SAR	Synthetic Aperture Radar
ScanSAR	SAR acquisition mode offering the opportunity cover broad stripes
SLC	Single Look Complex image
SNR	Signal to Noise Ratio
TanDEM-X	TerraSAR-X add-on for Digital Elevation Measurement; Radar earth observation satellite operating at X-band
Tandem-L	future radar earth observation satellite operating at L-band (from Germany)
TerraSAR-X	radar earth observation satellite operating at X-band (from Germany)
TomoSAR	SAR Tomography
UNFCC	United Nations Framework Convention on Climate Change

Roman symbols:

A	amplitude of a complex number or received power
A_{ML}	A radar amplitude multilooked
a	allometric factor
AGB	Aboveground forest biomass
B	biomass
B_{az}	azimuth bandwith
B_{forest}	forest stand biomass
B_{rg}	bandwith of the transmitted signal
$B_{\perp}$	perpendicular baseline
b_{stem}	tress stem biomass
c	allometric exponent or speed of light constant
dbh	diameter at breast height of a single tree
$\bar{d}$	mean dimeter
f_z	species specific shape factor
f_{ref}	allometric reference function
$f(z)$	function of the vertical distribution of scatterer
g	basal area of a tree
G	total basal area of a forest stand
H	forest dominant height
h	scatering profile height, tree height or altitude
h_{mid}	mean height
i	imaginary unit
k	Reneinke's allometric factor
l_a	allometric level
L_{ant}	length of the antenna
L_{SA}	length of the syntetic aperture

m	ground to volume ratio or plant biomass
N	tree number
S_m	complex backscattered signal of the master aquistion
SNR	SNR decorrelation
S_{rat}	Forest vertical structure ratio
S_s	complex backscattered signal of the slave aquistion
v	forward speed of the platform

Greek symbols:

$\tilde{\gamma}$	interferometric complex coherence
$\tilde{\gamma}_v$	volume decorrelation
$\tilde{\gamma}_{temp}$	temporal decorrelation of the volume
γ_{SNR}	noise decorrelation
γ_{VoG}	Volume-over-Ground coherence
δ_{rg}	range resolution
δ_{az}	azimuth resolution
τ_p	pulse duration
θ	local incidence angle
κ_z	vertical wavenumber
λ	wavelength
ϕ	interferometric phase
π	3.14159265359 – mathematical constant (circles)
ρ	wood density
ρ_{mid}	mean wood density of the forest stand
σ	backcattering extinction coefficient

1 Introduction

The most important environmental challenge in the early 21st century is the improvement of our understanding of global change and how this will affect the Earth system and the feedbacks within the system. The carbon cycle is fundamental for the functioning of Earth, involving many layered and interconnected processes through which carbon is exchanged between the atmosphere, land and ocean. Quantifying this global cycle is essential for the understanding of many changes taking place in the Earth system.

Terrestrial processes play a crucial role in the carbon cycle through carbon uptake and respiration associated with vegetation growth and emissions from disturbance caused by both natural processes, such as wildfires and land-use changes and through human activity. However, the status, dynamics and evolution of the terrestrial biosphere are the least understood and most uncertain elements in the carbon cycle.

1.1 Carbon cycle

Atmospheric CO^2 represents the main atmospheric phase of the global carbon cycle, which can be viewed as a series of reservoirs of carbon in the Earth System, which are connected by exchange fluxes of carbon (Figure 1) (Intergovernmental Panel on Climate Change and Stocker, 2014, chap. 1). It is therefore fundamental to understand accurately how much carbon is stored in the atmosphere.

There are very large uncertainties in our knowledge of the carbon fluxes between land and atmosphere. This is in sharp contrast with the other components of the carbon cycle. The terrestrial terms in the global carbon balance are less certain that the oceanic, atmosphere, and fossil fuel terms. The land flux has two components, a source term mainly due to deforestation and forest degradation and a poorly understood sink (Solomon et al., 2007).

The source term can only be estimated from current observations, and reported estimations have an average value of 1.1 GtC/year. Moreover, the net emissions of carbon from land use

change are uncertain because neither current rates of deforestation nor the biomass density are well known, especially in the tropical region (Houghton et al., 2009). From this, the land use change contributed from a 4 to 26% of the total anthropogenic flux to the atmosphere. To balance the carbon budget the land must be absorbed around 2.6 GtC/year if the mean value for the land emission is taken (Figure 2).

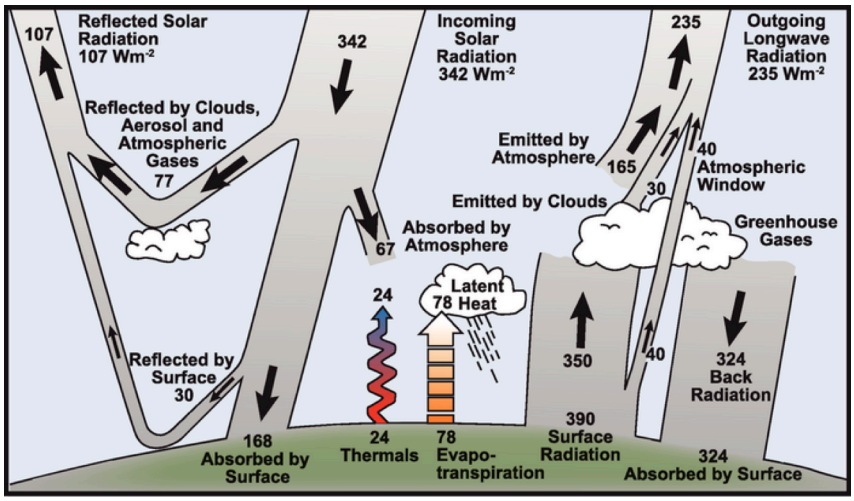

Figure 1: The global carbon cycle showing estimated sizes in GtC/year of the atmospheric, ocean and terrestrial carbon pools, and the net annual fluxes between them (Solomon et al., 2007).

The land sink is calculated as the difference between the net land sink and the estimated emissions from land-use change, and is known as the residual land sink. There is an uncertainty of roughly 70% (low) to 150% (high) of the mean value, and the location and the processes underlying it are still highly discussed (Fletcher and European Space Agency, 2012, bk. Biomass). The residual carbon sink is even more poorly constrained in part because of uncertainty surrounding the emissions from land use change. If a biomass observing system enabled determination of the global distribution of aboveground biomass density once, the uncertainties of land use could be reduced to 20% or less (Houghton et al., 2009). Nonetheless, the residual carbon sink is clearly important in controlling climate warming.

The terrestrial carbon sink, as of yet unidentified, represents 15–30% of annual global emissions of carbon from fossil fuels and industrial activities. Some of the missing carbon is sequestered in vegetation biomass and, under the Kyoto Protocol of the United Nations Framework Convention on Climate Change, industrialized nations can use certain forest biomass

sinks to meet their greenhouse gas emissions reduction commitments (Myneni et al., 2001). Therefore, accurate estimates of terrestrial carbon storage are required to determine its role in the global carbon cycle, to estimate the degree that anthropogenic disturbance (i.e. land use/land cover change) is hanging that cycle, and for monitoring mitigation efforts that rely on carbon sequestration through reforestation.

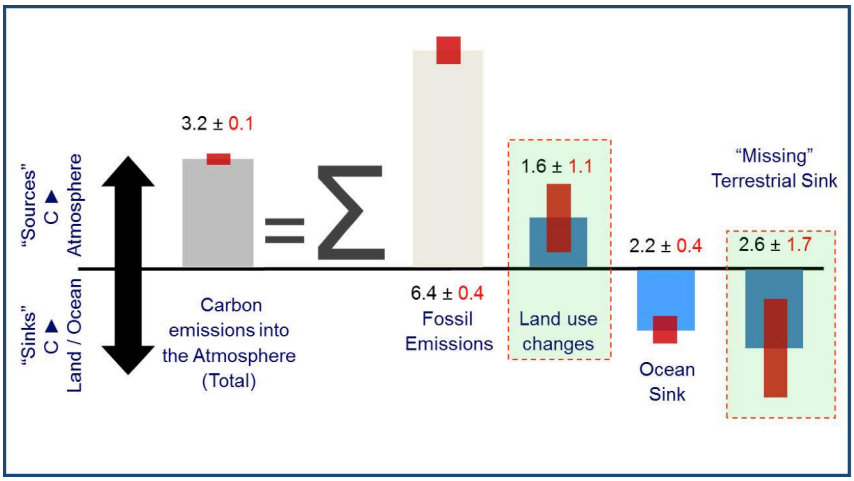

Figure 2: Global carbon budget for the 2000s, portioned into emissions to the atmosphere from the burning of fossil fuels and land-use change and uptake from the land and ocean.

1.2 Forest aboveground biomass (AGB)

The role of vegetation in reducing atmospheric levels of CO_2 has been recognized in a number of international agreements (e.g., United Nations Framework Convention on Climate Change (UNFCCC), Kyoto Protocol), which specifically require countries to quantify their carbon stocks and changes. Plants store carbon in above- and belowground biomass, 90% of the aboveground carbon is stored in tree stems, which are being reduced through natural (diseases, wildfires, drought/flooding) and anthropogenic impacts (logging, pollution, human-induced fires), or vice versa, increased through regeneration or promoted growth associated with elevated CO_2 levels in the atmosphere (Wardle et al., 2003).

From the whole biomass stored in vegetation, forest biomass is the most important part of the terrestrial carbon pool and therefore, a main participant in the global carbon cycle (Drake, 2002). It is a main variable in mapping the amount and geographic distribution of forest and its change in time is needed for understanding the development of the carbon fluxes (Brown, 2001;

Treuhaft, 2009). According to Brown (Estimationg biomass and biomass change of tropical forests, 1997) forest biomass is defined as the total amount of aboveground living organic matter in trees expressed as oven-dry tons per unit area. This biomass accounts for the greatest fraction of the total living biomass in forests and does not pose too many logistical problems in its estimation. Biomass is of interest for another number of reasons. It is the raw material of food, fiber and fuelwood. It is also important for soil, fire, water management. It is related to vegetation structure, which in turn influences biodiversity and it determines the magnitude and rate of autotrophic respiration.

Biomass density (the quantity of biomass per unit area, or Mg dry weight ha) determines the amount of carbon emitted to the atmosphere (as CO_2, CO, and CH_4 through burning and decay) when ecosystems are disturbed (Houghton et al., 2009). Maps of biomass stocks are the basis for calculating emissions based on land use change, and serve to determine the amount of carbon emitted to the atmosphere when ecosystems are disturbed (Houghton, Hall, & Goetz, 2009). In addition, biomass maps are of enormous value in themselves as they tell us about the world's forest resources. For the development of such maps and information systems, first, knowledge of biomass is required for the calculation of the sources and sinks of carbon that result from converting a forest to clear land, and vice versa. While average biomass values have been used in most calculations of carbon flux to date, the possibility that deforestation occurs in forest with biomass that is significantly different from the average suggests that linking specific locations of disturbance with geographically specific estimates of biomass would improve estimates of flux (Houghton, 2005). Second, knowledge of the spatial distribution of biomass enables the measurement of change through time

The estimates of AGB are the largest proportion of carbon uncertainty (Saatchi et al., 2007), accountings for 70–90%, as well as spatial variability (Cairns et al., 1997). Reducing the uncertainty in emissions estimates requires estimates of forest carbon content at a spatial scale that is fine enough to capture the variability over the landscape and at the scale of forest disturbances. Such information would improve carbon stock estimates in large scales as well as assist in the development of baseline projects required for reducing emissions from deforestation and degradation (REDD) (Saatchi et al., 2011).

Finally, AGB stocks are also a key parameter in assessing the economic, conservation, and biofuel potential of land surfaces. The provision of a sensor that measures these stocks and their change in space and time is therefore paramount. Global data sets like Global Tree Cover (Figure 3) exhibit high uncertainties for forest cover estimates and amount of carbon stored in different types of forest (Defries et al., 2000; Hese et al., 2005). However, even if steadily increasing, our knowledge of the amount of carbon stored in forests is incomplete.

The knowledge of the distribution and amount of terrestrial biomass is based almost entirely on ground measurements over an extremely small, and possibly biased sample with many regions still unmeasured. In conclusion, biomass is not consistently defined (Houghton et al., 2009):

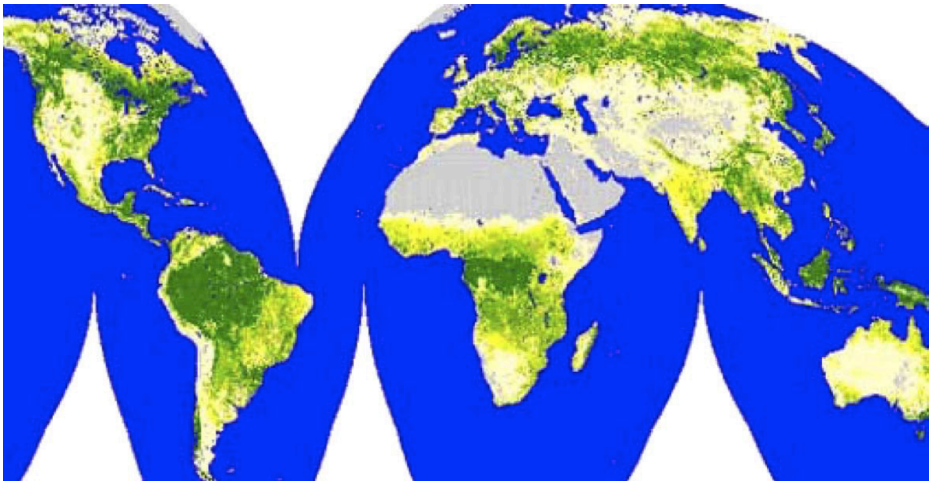

Figure 3: Global Tree Cover in percent (white: 0%; dark green: 100%) retrieved from NOAA AVHHR (Defries et al., 2000). Uncertainties exist for global forest cover estimates (between 30 and 60 Mio km²) and carbon stored in different types of forests (stock ranges from 100 to 400 Mg/ha with biomass). (For interpretation of the references to color in this figure legend, the reader is referred to the web version of this article (Hese et al., 2005).

1.3 Global missions for forest biomass monitoring and requirements

Forest biomass cannot be measured directly on any but the smallest scales (< 1ha). This is because it involves the complete harvest of the trees and very laborious measurements to determine the mass of wood in stems, roots and branches. Terrestrial biomass measurements are time consuming, expensive (destructive methods are based on highly precise measurements), and

rare (Houghton, 2005). Forestry science aimed to reduce the effort of measuring biomass with the help of allometric functions which can estimate biomass from easier measurable tree variables, like diameter at breast height (dbh), basal area, tree height and form factor (first order parameters). However, single tree measurements remain ineffective for large area and global applications. Thus, the limited utility of field inventories owing to the natural spatial variability of forest biomass, together with the wide extent of world's forest and the difficult of the accessibility to a high proportion of them, the efforts in the estimation biomass distribution rely on space observation based on remote sensing (RS) techniques (Gibbs et al., 2007; Houghton, 2005). Although various studies used RS for forest characterization (Koetz et al., 2006; Mette et al., 2003), a region-wide coverage is still missing.

Houghton (2009) laid out the required specifications for a future satellite RS mission to significantly reduce the currently existing uncertainties. Therefore, in order to reduce the large uncertainty in the global net flux, carbon from land use change requires biomass to be measure with accuracy better than 10 Mg/ha for biomass less than 50 Mg/ha and better than 20% (95 % confidence interval) for biomass values above this, at a scale of maximum 4 ha (Fletcher and European Space Agency, 2012, bk. Biomass). While these precisions can be achieved on managed areas, focused on timber productions, on most other areas a regular forest inventory system is missing or the sampling density is insufficient, then the combination of uncertainty sources and errors affect the estimation precision (Santoro et al., 2011).

RS has been a key technology in existing efforts to monitor carbon storage and fluxes (Cohen et al., 1996; Running et al., 1999), and has been identified as a probable tool for monitoring compliance with treaties such as the Kyoto protocol (Ahern et al., 1998). However, direct estimation of carbon storage in moderate to high biomass forests remains a major challenge for RS. For example, RS has had considerable success in measuring the biophysical characteristics of vegetation in areas where plant canopy cover is relatively sparse, but the quantification of vegetation structure where leaf area index (LAI) exceeds three has been less successful (Lefsky et al., 2002).

Other approaches have been based on relating RS measured variables to estimate biomass, as they are capable to measure some forest stand parameters, like forest height and vertical structure, in short time periods and over large regions of the Earth (Saatchi et al., 2011). New

approaches using Light imaging and ranging (LiDAR) and (radar) from airborne sensors have been used in oder to provide high-resolution estimates of forest carbon density, but only for small areas (Asner et al., 2010; Drake et al., 2002; Saatchi et al., 2011). For this reason, the spaceborne sensors needed to use the approaches developed on an airborne basis to extrapolate them for large-scale mapping and monitoring.

Studies based on conventional forest stand parameters from yield-related averages have tended to neglect three-dimensional stand structures, probably the most important of all stand characteristics (Onaindia et al., 2004). The study of the Stand Density Index (SDI) in Pretzsch and Biber (2005), e.g. shows a strong relationship between AGB and horizontal forest structures. Several methods have tried to quantify and measure forest vertical structure (Drake et al., 2002; Hall et al., 2005; Parker and Russ, 2004; Treuhaft et al., 2010) where AGB is estimated assuming that it is correlated with the vertical organization of the canopy of a forest stand. New RS devices and techniques like, polarimetric synthetic aperture radar (SAR) interferometry (Pol-InSAR) and LiDAR, allow getting, besides forest height, vertical backscattering profiles which are connected to forest vertical structure (Cloude, 2006; Lefsky et al., 1999). Some methods like Fourier series (Treuhaft et al., 2010) or height metrics (Harding et al., 2001) have shown the potential of using these RS-derived structural parameters for the estimation of AGB. LiDAR or SAR interferometry nowadays accurately estimate forest parameters like forest height as well as other parameters (tree density, Leaf Area Index) that can improve second order forest parameter estimates like AGB (Lefsky et al., 1999; Mette et al., 2003)

RS methods, primarily multi- and hyper-spectral have been explored as cost effective means of measuring structural characteristics in a spatially continuous manner. However, these systems have shown poor potential to access vertical structures (Hyde et al., 2005). Active RS systems have also the potential to penetrate through the forest volume begin sensitive to forest structures. LiDAR has been extensively studied in the last decade and multiple studies, with small and large footprints, show the potential of these techniques to evaluate forest structures and to use these to improve biomass estimations (Harding et al., 2001; Lefsky et al., 2005). For example, a systematic approach, the Global Land Cover 2000 Maps project provides a global harmonized land cover map with an overall classification accuracy of 68.6% (Mayaux et al., 2006).

1.4 Objectives

The main objective of this thesis was to investigate and describe the relevance of stand structural variables, especially vertical structure and forest height to estimate AGB on a global scale. Initially an allometric model is studied to derive a forest vertical biomass function from field-inventory data in order to establish a new methodology that is able to characterize forest vertical structure and to investigate the allometric relationships of these variables with AGB.

The second main objective was to investigate the applicability of allometric relationships to RS global applications. A first approach could be tested in forest scenarios of a comparatively low structure complexity, as the boreal forest ecosystems. The potential of the TanDEM-X mission for biomass classification was investigated and the performance of single height-to-biomass allometric equations derived from these data was evaluated.

The last objective and therefore step of the thesis was the implementation of the structure theories in highly structured forest ecosystems. Airborne multi-baseline SAR data sets in L-band were used over a temperate forest in order to retrieve vertical structure profiles. The adaptation of the field-derived biomass allometric theories into a remotely sensed variable was investigated and a new inversion approach was tested.

2 Methodology

2.1 Synthetic Aperture Radar

The main application of the studies developed in this thesis is focused on radar (SAR) data. Synthetic Aperture Radar (SAR) has entered into a golden age. More than 16 spaceborne SAR sensors are being operated today and 9 new SAR systems will be launched within the next 5 years. SAR is unique in its imaging capability: It provides high-resolution two dimensional images independent from daylight, cloud coverage and weather conditions (Moreira et al., 2013).

The basic principles and radar techniques that have been used and/or are needed for a better understanding and interpretation of the results presented in this thesis, are summarized in the following sections. The section begins with SAR principles, interferometry and the Random Volume over Ground (RVoG), necessary for the estimation of forest height; and ending with Tomography, which is the methodology used to estimate vertical reflectivity profiles and is, therefore, needed for the retrieval of structure.

2.1.1 SAR principles

The radar system transmits electromagnetic pulses with high power and receives the echoes of the backscattered signal in a sequential way. The values for the pulse repetition frequency typically vary from a few hundred to thousand Hertz for airborne and spaceborne systems, respectively. The swath width can vary from a few kilometers to 20 km in the airborne case or from 30 to 500 km in the spaceborne case. The transmitted pulse interacts with the Earth surface and only a portion of it is backscattered to the receiving antenna. The amplitude and phase of the backscattered signal depends on the physical (i.e., geometry, roughness) and electrical properties (i.e., permittivity) of the imaged object. However, depending on the frequency band, considerable penetration can occur so that the imaged media can be behaved and be modeled as a volume (e.g., vegetation, ice and snow, dry soil). More penetration of the

electromagnetic pulses in media will occur for radar systems using longer wavelengths (Moreira et al., 2013). The most frequently used bands in SAR systems are shown in Table 1.

In general, the SAR system is mounted on a flying platform, such as an aircraft or a spaceborne platform/satellite to image terrain. While in flight, the radar transmits pulses with a certain Pulse Repetition Frequency (PRF) and receives the backscattered signals, which are sampled and stored in a matrix. This matrix is commonly known as raw data because these data still have to be compressed in order to obtain information. After SAR processing (Hein 2004, Cumming and Wong 2005), a focused 2D radar image, generally called single look complex (SLC) SAR image, is obtained.

Table 1: Commonly used frequency bands for SAR system s and the corresponding frequency and wavelength ranges (Moreira et al., 2013).

Frequency Band	Ka	Ku	X	C	S	L	P
Frequency [GHz]	40-25	17.6-12	12-7.5	7.5-3.75	3.75-2	2-1	0.-0.25
Wavelength [cm]	0.75-1.2	1.7-2.5	2.5-4	4-8	8-15	15-30	60-120

A SAR system scans the Earth's surface in a specific geometry. Figure 4 shows the geometry of a conventional monostatic side-looking SAR. The platform moves at a uniform speed *v* on an altitude *H*. The antenna looks slant-wise towards the ground and perpendicularly to the flight direction. The two coordinates of the SAR image are the azimuth dimension along the flight direction and the slant range dimension along the line-of-sight. The antenna is normally directed to one side of the platform to avoid left-right ambiguities. The illustrated beam is wide in the vertical direction and intersects a certain surface in across track (range) direction. The radar footprint is the area of illumination for each pulse, generally defined as the half power (3db) antenna beamwidth at the surface. The entire image strip illuminated by many pulses is referred to as the image swath. While the beamwidth along range determines the swath size, the beamwidth along azimuth results in the length of the synthetic aperture (L_{SA}).

$$L_{SA}(r) = 2r\tan\left(\frac{\theta_{az}}{2}\right), \tag{1}$$

where θ_{az} is the azimuth antenna beam at -3dB and r the range distance between the antenna and the target (Figure 4). Despite of a physically small antenna, a synthesized much longer antenna can be attained.

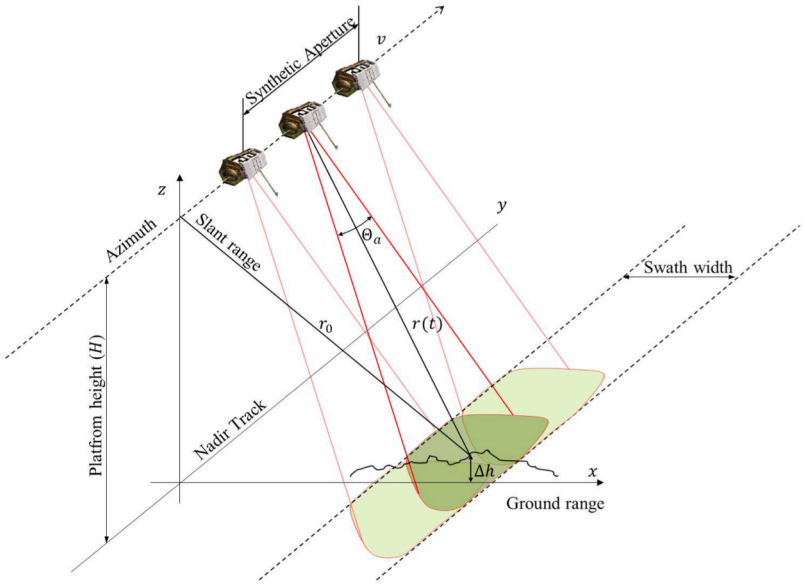

Figure 4: SAR imaging geometry. r_0 stands for the shortest approach distance, Θ_0 for the azimuth beamwidth and v for the sensor velocity.

One of the most important advantages of SAR images is its spatial resolution. It is a measure of how two close point-like objects can be located to each other in order to still be separated in the image. For SAR imaging sensors, the spatial resolutions in range and azimuth are differently defined due to the two different scanning mechanisms (Bamler and Hartl, 1998). In range, the improvement of the resolution is performed by compressing the chirped signal whose frequency varies linearly in time. After filtering (Cumming and Wong 2005), the energy of a single target is focused at its range position. The achievable resolution δ_{rg} is determined by the system bandwidth of the transmitted signal B_{rg} yielding (Bamler and Hartl, 1998):

$$\delta_{rg} = \frac{c}{2\,B_{rg}} = \frac{c\,\tau_p}{2}, \tag{2}$$

where c is the speed of light, τ_p the pulse duration which is inversely proportional to B_{rg} and the factor ½ comes from the two-way path between the antenna and target. For example, the L- and P- band E-SAR system with 100 MHz system bandwidth provides a high slant-range resolution

of approximately 1.49 m. Note that the resolution in range direction is independent of the distance of the SAR sensor to the target and the movements in azimuth direction.

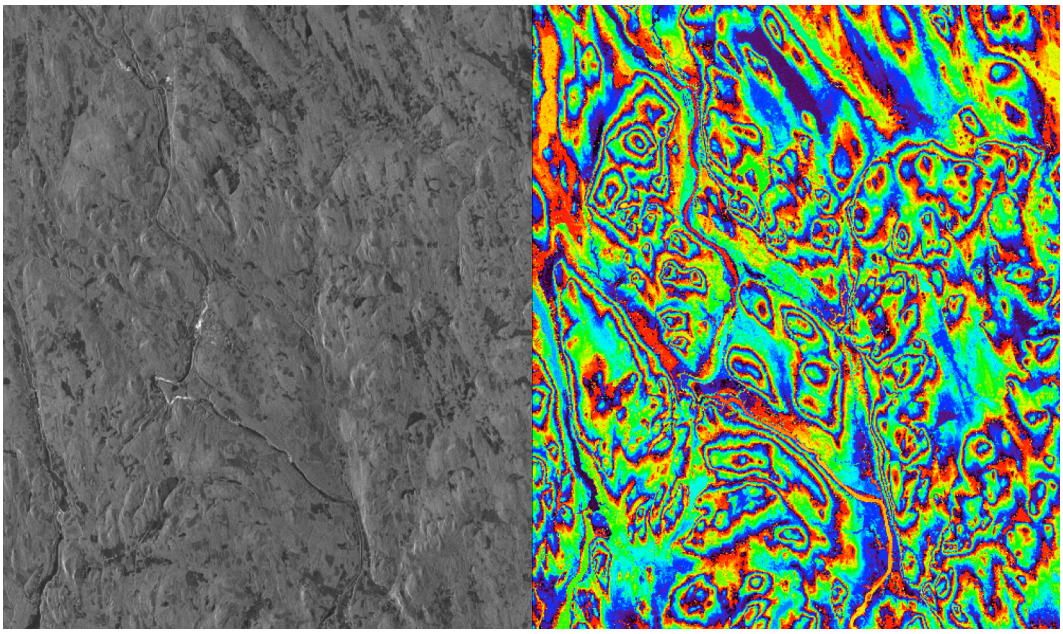

Figure 5: SAR data example from Krycklan site (Northern Sweden) acquired with TanDEM-X in bistatic mode. On the left side: the amplitude image. On the right side: interferometric phase (ϕ) scaled from $-\pi$ to π rad.

On the other hand, the azimuth resolution is improved by synthesizing a long antenna in time with the movement of the platform. A single target is illuminated by the radar at multiple locations along the flight direction (Figure 4). Thus, a small antenna with a broad beamwidth contains frequency information of a point scatter's response, resulting in a broad azimuth bandwidth (Bamler and Hartl, 1998). All echoes from many pulses need to be coherently combined to achieve the maximum resolution. The azimuth resolution δ_{az} is given by:

$$\delta_{az} = \frac{v}{B_{az}} \approx \frac{L_{ant}}{2}, \tag{3}$$

where L_{ant} is the physical azimuth length of the antenna, v the forward speed of the platform and B_{az} the azimuth bandwidth. It is interesting to note that the theoretical azimuth resolution (assuming perfect signal processing) depends only on the physical antenna size L_{ant}. It is independent of range and sensor velocity. Thus, this break-through enabled to operate high azimuth resolution SAR systems not only on air- but also spaceborne platforms. An image example acquired in X-band with the TanDEM-X constellation is shown in Figure 5-left.

2.1.2 SAR interferometry (InSAR)

SAR interferometry (InSAR) measures the range difference by measuring the phases of a given scatterer in two independent SAR images that are separated in time, space, or frequency, known as baselines. The interpretation of the interferometric phase varies depending on the types and combinations of these baselines (Bamler and Hartl, 1998). With zero spatial baselines but non-zero temporal baselines, the interferometric phase is solely due to the deformation or the movement of the scatterer in the line-of-sight (LOS) direction between two acquisition times. Detectable motion velocities depend on the temporal baseline. Fast movements are detected in short temporal baselines, whereas the long temporal baselines are fit for detecting slow deformations. In the case of zero temporal baselines but non-zero spatial baselines, the interferometric phase is due to the alteration of the LOS direction, and (geometrically) reveals information about the terrain's topography. Most spaceborne SAR system configurations acquire interferograms in repeat-pass mode, with non-zero temporal and spatial baseline components at the same time.

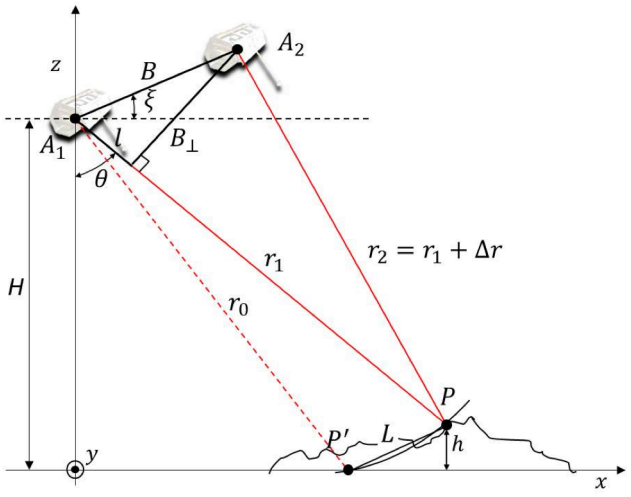

Figure 6: Geometry of Interferometric SAR (InSAR).

In InSAR applications, the images must be co-registered to remove the image distortion due to the parallax between two acquisitions. The acquisition used for the reference of the co-registration is conventionally called the master acquisition, while the other one is called slave.

The geometry of InSAR for a non-zero spatial baseline is shown in Figure 6. The spatial separation between the position of the antennas is assigned by $B_\perp$, which is for the normal baseline measured perpendicularly, in the elevation direction, to the LOS direction from the master antenna. The horizontal line indicates the reference plane for the estimated terrain topography (solid curve). The intersection points of an equirange (r_0) arc with the reference plane and the terrain topography are P'' and P, respectively. In the imaging geometry of the master, points P' and P cannot be distinguished, as they have the same range distance to the master. However, the distance of P' and P are different from the slave antenna. This distance difference is estimated by means of the interferometric phase that also allows the estimation of the terrain topography.

When the master antenna images P', a right-angles triangle A_1A_2P' is drawn. It can be assumed that $A_1P' = A_2P' = r_0$ because $r_0 \gg B_\perp$:

$$\frac{r_0}{L} = \frac{B_\perp}{l}, \tag{4}$$

and using $L = h \,/\, \sin\,\theta$ for a given look angle θ, and $l = \lambda\phi \,/\, 4\pi$, the relation between the interferometric phase ϕ, and the normal baseline $B_\perp$ and the topographic altitude h becomes:

$$\phi = 4\pi \frac{\lambda B_\perp}{r_0 \sin\theta} h. \tag{5}$$

The vertical wave number κ_z is defined as the change rate of the interferometric phase with respect to the altitude and is given by:

$$\kappa_z = \frac{d\phi}{dh} = \frac{4\pi B_\perp}{r_0 \sin\theta}. \tag{6}$$

An image of the interferometric phase ϕ, scaled from $-180°$ to $180°$, for the test site of Krycklan located in Northern Sweden and acquired with the TanDEM-X constellation, is shown in Figure 5-right.

2.1.3 Decorrelation

The similarity of two independent InSAR observations is expressed by means of coherence $\tilde{\gamma}$, which is defined in the time domain as:

$$\tilde{\gamma} = \frac{\langle S_M S_s^* \rangle}{\sqrt{\langle S_M S_m^* \rangle \langle S_s S_s^* \rangle}}. \tag{7}$$

S_M and S_s stand for the complex backscatter in the master and the slave acquisitions, respectively. The absolute value of the coherence $|\tilde{\gamma}|$ can reach one if and only if $S_M = S_s$, so otherwise it is always lower than 1. An interferogram of high coherence is characterized by a small deviation of its interferometric phase ϕ, and increases when decreasing $|\tilde{\gamma}|$. The decrease or loss of coherence $|\tilde{\gamma}|$ is called decorrelation, and it is a fundamental factor that limits the application of InSAR. In Figure 7-left an example of a coherence image is shown. Coherence images are typically displayed in a linear gray scale where black corresponds to 0 and white to 1.

After spectral filtering, there are some physical reasons that still prevent the two independent acquisitions of an InSAR pair from being identical. The dominant decorrelation factors are: temporal, Signal-to-Noise ratio (SNR) and volume decorrelations. The coherence can be modeled as the multiplication of the three components:

$$\tilde{\gamma} = \tilde{\gamma}_{temp} \cdot \gamma_{SNR} \cdot \tilde{\gamma}_v \,. \tag{8}$$

1) The temporal decorrelation ($\tilde{\gamma}_{temp}$): The evolution of the scatterers with time is a critical factor of decorrelation. The Earth's surface itself is a complex and dynamic system and its scattering behavior is never stationary in terms of shape and dielectric constants. Any InSAR acquisition pair with a non-zero temporal baseline suffer from temporal decorrelation, which is difficult if not impossible to predict and address

2) SNR decorrelation (γ_{SNR}): The white noise on the received signal also contributes to the decorrelation of the InSAR application. If SNR is the same at both acquisitions, as in typical monostatic SAR observations, the coherence γ_{SNR} is:

$$\gamma_{SNR} = \frac{SNR}{1 + SNR}\,. \tag{9}$$

SNR is not only dependent on the output power of the antenna, but is also related to the radar backscatter from the surface.

3) Volume decorrelation ($\tilde{\gamma}_v$): in foliage or in dray sand and snow, $\mathcal{F}(\sum \vec{x})$ along the f_z-axis is no longer constant, which adds to decorrelation. This type of decorrelation is called volume decorrelation and cannot be corrected by spectral filtering. Due to its importance in the estimation of forest variables, it will be addressed in more detail in the following chapters.

2.1.4 The Random Volume over Ground (RVoG) model

Volume decorrelation is a function of the scatterer distribution in height. This makes it principally possible to invert forest heights from coherence, as long as the other decorrelation processes can be neglected or compensated.

For a simple scatterer distribution, that is, a uniform scattering profile in height, volume decorrelation is described to resolve to a since-function. The Random Volume over Ground (RVoG) model alters the uniform scattering profile by introducing the parameters extinction (σ) and ground-to-volume ratio (m). In this sense, the RVoG models the forest as a decorrelation volume of randomly distributed scatterers with a certain height h and extinction σ, above a non-decorrelating ground with a certain backscatter contribution m. These parameters: height, extinction and ground contribution cannot be inverted from a single coherence, and an extension of the observation space is required. The options are more baselines, frequencies and polarizations.

The volume decorrelation γ_v in (10) describes the relation between the interferometric coherence and the scatterer height distribution $\sigma(z)$ inside a resolution cell. In order to develop the RVoG, three simple scattering profiles can be modelled: 1) a uniform scattering profile, 2) an extinct scattering profile and 3) a uniform scattering profile with ground.

$$\gamma_v = \frac{\int \sigma \cdot \exp(-i \cdot \Delta\kappa_z \cdot z) dz}{\sigma \int \sigma dz'} = \exp(i \cdot {}^1/_2 \cdot \Delta\kappa_z \cdot h) \tag{10}$$

1) Uniform scattering profile, the sinc-solution: For a uniform backscatter height profile, the solution of the volume decorrelation in (10) is a sinc function. The relation between height and coherence is called by the vertical wave number $\Delta\kappa_z$

$$\sigma(z) = const \cdot \int_0^h exp(2\sigma/cos\theta) dz \tag{11}$$

2) Extinct scattering profile: if the radar wave is extinct along its path through the volume, the backscattered from the deeper parts of the volume is damped. For a constant extinction along the volume depth, the backscattering coefficient $\sigma(z)$ becomes an exponential function of the extinction σ and the 2-way penetration through the height z of the volume.

In comparison to the volume without extinction, the absolute of the coherence for a given height is always higher. The interferometric phase, i.e. the scattering center is dragged towards the volume top. For no extinction, $\sigma = 0$, the canopy becomes a surface with volume a coherence of 1 and a phase center at the volume top. For the lowest extinctions, the coherence of the extinct volume does not deviate strongly from the sinc-function. The effect of extinction increases for high look angles, because the effective path through the volume is longer than for steep look angles.

$$\gamma_v = \exp(i\phi_0) \cdot \frac{\int \exp(2\sigma z/cos\theta) \cdot \exp(-i \cdot \Delta\kappa_z \cdot z) dz}{\int \exp(2\sigma z/cos\theta) dz} = \frac{\frac{\exp\left(-\frac{2\sigma z}{cos\theta} \cdot i\Delta\kappa_z \cdot h\right) - 1}{-(2\sigma/cos\theta \cdot i\Delta\kappa_z)}}{\frac{\exp(2\sigma z/cos\theta \cdot h) - 1}{-(2\sigma/cos\theta)}} \quad (12)$$

3) Volume over ground: when the ground contributes to the backscattering, the total backscatter $\sigma(z)$ is the coherent sum of the effective ground σ_G and the volume backscattering $\sigma_V(z)$ after extinction. A ground-to-volume ratio m can be defined, and the Volume-over-Ground coherence γ_{VoG} can be resolved (Papathanassiou and Cloude, 2001):

$$\sigma(z) = \sigma_G + \sigma_V(z) = \sigma_G \cdot \exp(-2\sigma h) + \int_0^h \sigma_V \cdot \exp(2\sigma z)\, dz, \quad (13)$$

$$m = {}^{\sigma_G}/_{\sigma_V(z)}, \quad (14)$$

$$\gamma_V = \frac{m + \gamma_{vol}}{m + 1}, \quad (15)$$

$$\gamma_{VoG} = \gamma_{vol} + (1 - \gamma_v) \cdot \frac{m}{m + 1}. \quad (16)$$

The Volume-over-Ground coherence γ_{VoG} describes a linear function in the unite circle. An increasing in the ground contribution drags the scattering center to the ground. The coherence-height relation is ambiguous. Compared to the since ($m = 0$), the coherence decreases for a low ground contribution, and increases for a high ground contribution.

Ground an extinction act as antagonists: extinction drags the location of the scattering center towards the canopy top which leads to an increase in the coherence; however, ground contribution drags the scattering center towards the ground leading to a decrease in the coherence (except if the ground contribution is very high). The ground can become, especially important when double bounces occur between the tree trunks and the ground surface, or when extinction is

very small in open forests. Extinction becomes critical if the response from lower volume parts and the ground is effectively shielded.

Both extinction and ground contributions are function of the wavelength (Papathanassiou and Cloude, 2001), what means and increase of the ground contribution when decreasing frequency and the opposite effect for the extinction. The polarization and the look angle also affect both parameters: ground contribution is in general stronger in co-polarized channels (HV-VH), and high look angles increase the effective way of the radar wave through the volume.

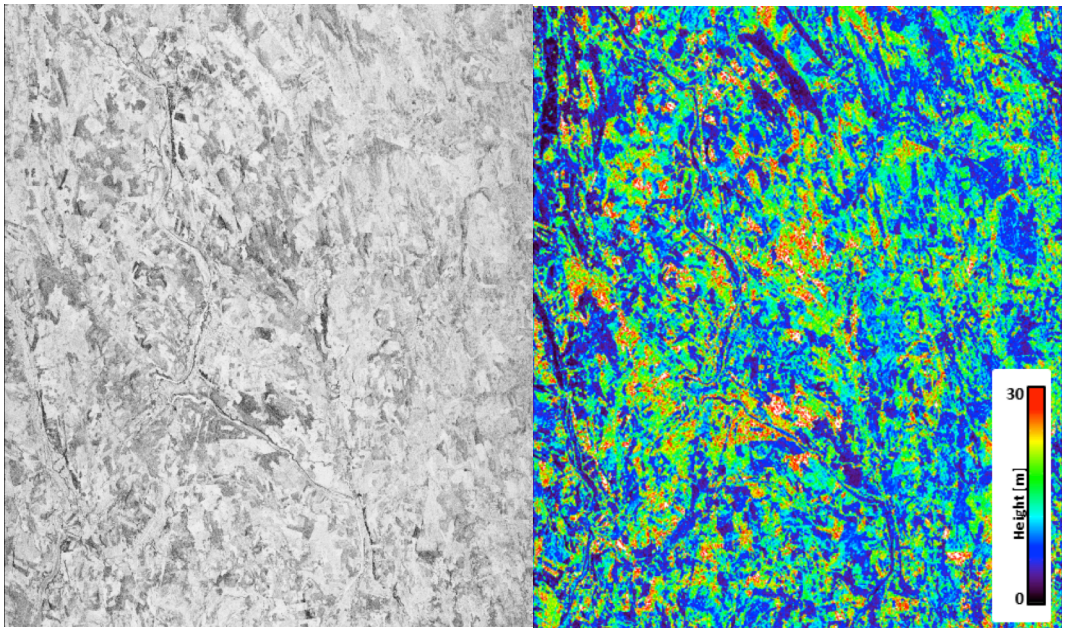

Figure 7: SAR data example from the Krycklan site (Northern Sweden) acquired with TanDEM-X in bistatic mode. On the left: amplitude of the complex interferometric coherence ($|\tilde{\gamma}|$), scale from 0 (black) to 1 (white). On the right side: forest height inversion example using the RVoG model.

In Figure 7-right a height inversion example, scaled from 0 to 30 m, using the RVoG model is shown. The interferometric coherence (Figure 7-left) in the case of a bistatic acquisition is not affected by temporal decorrelation. Therefore, after estimating the SNR decorrelation from the system parameters (provided in the TanDEM-X data) the volume decorrelation can be estimated from the interferometric coherence as:

$$\tilde{\gamma}_v = \frac{\tilde{\gamma}}{\gamma_{SNR}}. \tag{17}$$

Introducing $\tilde{\gamma}_v$ in (16) and assuming reasonable values for σ and m, forest (volume) height h can be estimated (see (12)).

2.1.5 SAR Tomography

The transmitted electromagnetic wave signal can penetrate through semi-transparent media; hence, it is sensitive to 3-D distribution of the scatterers in the volume of the observed objects. For instance, forest even being such a prominent volume scatterer, at lower frequencies the transmitted signal penetrates (depending on the structure and dielectric properties of the forest) down to the ground even in very dense vegetation (Moreira et al., 2013; Pardini et al., 2014).

In order to retrieve the whole vertical distribution of the scatterers through the forest volume, and therefore to separate their responses, it is necessary to exploit the synthetic aperture concept, which requires the use of multiple passes of the SAR sensor over the same area but at different positions, i.e. realizing a multibaseline (MB) acquisition. In this way the SAR resolution cell becomes fully 3-D (Moreira et al., 2013). Such an acquisition concept is known as SAR Tomography, abbreviated TomoSAR. TomoSAR exploits both the amplitude and the phase information of the MB signals in any pixel in order to fully reconstruct the 3-D reflectivity profile. Intuitively, it is apparent that, differently from InSAR, an accurate and detailed TomoSAR inversion in principle needs many short (high coherence) and long (low coherence) baselines in order to follow the complete spatial decorrelation behavior of the scatterers in each cell (Pardini et al., 2014).

A common method used in TomoSAR is the Capon method, which is a non-model based method, originally derived for time-series analysis of seismic signals (Capon, 1969). Using a back of bandpass filters, this estimator allows to adaptively reject interference coming from noise and scattering from other directions than the selected one, varying the shape of its frequency response during the spectral scan depending on the input data (Pardini et al., 2014).

Figure 8 shows a tomogram obtained using Capon, over a forested area in the test site of Traunstein obtained with data acquired in 2008 by DLR's E-SAR airborne system. The campaign was performed at L-band and a total of 5 tracks with an equidistant separation of 5 m. The forest slice taken from west (near range) to east (far range) is color coded according to the

maximum power of each pixel. The tomogram is sensitive to the forest structures. In the mature spruce stand the maximum appears close to the top of the canopy while in the mixed stand this tends to appear closer.

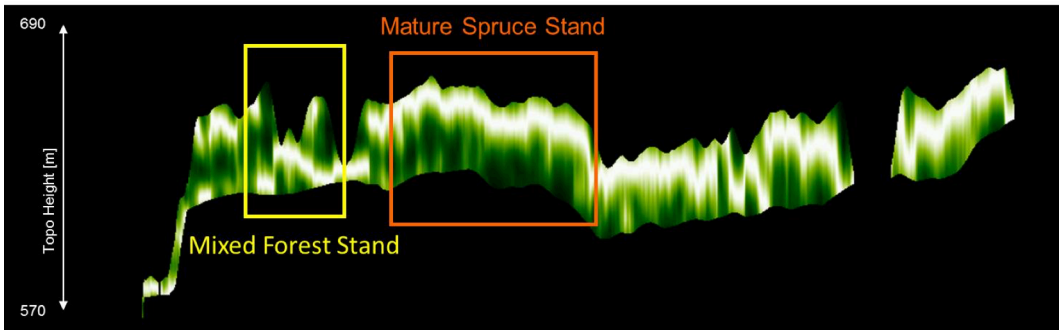

Figure 8: Capon tomographic slice calculated in test site of Traunstein (South-east Germany)

2.2 Theory of allometry

Allometry, the science concerning the relations between size dimensions of living systems, is the key to the understanding of the forces that shape the structure, function, and dynamics of ecosystems, which is a fundamental goal of ecology (Enquist et al., 2009). Originally, allometry concerns itself to the relationships of parameters of organs during growth (Burschel, 1997). The connection between allometry and growth is lined out in the theory of 'dynamic morphology' (Bertanlanfly 1942), which states that any organic system is essentially a hierarchy of processes in a dynamic balance between anabolism and catabolism. Forest allometry refers to the size dimensions of forests. Nowadays, size relations are understood as the result of phylo- and ontogenetic evolution that have optimized and still optimize functional advantages and obligations: "Organic proportionalities often reflect consequences of natural selection operating on the relation between form and function" (Niklas, 1994). In this sense, the study of allometry is motivated by the attempt to understand the adaptations of the living organisms to their environment.

According to (Enquist and Niklas, 2001), extensions of a general allometric framework obtained from a simulation model reveal how several main organismal, community and ecosystem level properties can be explained from relatively few allometric and biomechanical relationships, which dictate how metabolic production and biomass are partitioned among

different body parts at the level of the individual plant. Furthermore, they provide a quantitative basis for the development and study of connections between numerous features of organismal biology, ecology and ecosystem.

If allometric scaling laws holds for entire communities, organismal relationships can be used to link to larger scale properties of communities across different ecosystems. Thus allometric scaling laws generalize the size-dependent structural relationships, partitioning and trade-offs between different organs' or ecosystem elements' growth (Pretzsch, 2006). It is then, from the interpretation that any organism receives part of the total growth energy that is proportional to its relative size, where the physiological relevance of allometric functions lies. Similarly, the relationship between the community size and some of its parameters can also be studied using allometric relationships. For example, extensions of allometric and biomechanical theory predict that total standing community biomass will be invariant with respect to species composition (or latitude). Furthermore, the intrinsic capacity to produce biomass on an annual basis will vary little across communities (Enquist and Niklas, 2001).

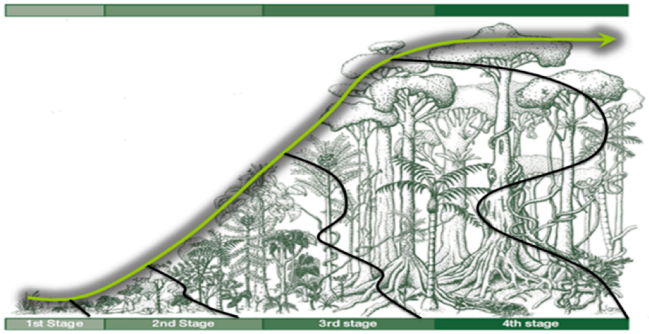

Figure 9: Diagram of forest evolution. The forest development over time results in an evolution of the structural arrangements. The black lines represent the possible evolution of the vertical biomass profiles and the green arrow the change of the dominant height.

Besides the physiological and evolutionary implications, allometric relationships are quite practical when estimating a size dimension from another that is much easier to measure (Mette, 2007). Theory of allometry is applicable when estimations of forest biomass can be used from measurable parameters like forest height or forest vertical structure. Figure 9 shows a scheme which illustrates these principles, relating the possible vertical structure (as a biomass distribution) to the forest dominant height during its growth until the climax state.

2.2.1 The allometric equation

The allometric reference equation and the allometric level that are the basis for the concept of the height-biomass allometry, as explained in Mette (2007).

The allometric relations are based on the development of specific equations that involve first order parameters and empirically calculated coefficients. The allometric equation is defined as the power function of the mathematical solution of a relative growth equation (Mette, 2007):

$$y = a \cdot x^c \,. \tag{18}$$

This equation can also be formulated logarithmically:

$$lny = lna + c \cdot lnx \,, \tag{19}$$

where x represents a measured parameter (first order) and a and c are the coefficients. The allometric factor is denoted by a, the allometric exponent c.

The logarithmic expression is more frequently applied due to its linearity it is an easily visible indicator of allometric and study objects that may vary over several orders of magnitude. However, for limited size ranges with linear intervals the logarithmic representation emphasizes low values.

For a set of allometric relations with a similar allometric exponent c, the ratio of the allometric factors a is a directly scale of the functions to each other. Often, it makes sense to choose one equation as the "allometric reference function" f_{ref} with a certain c_{ref} and a_{ref}. If for an allometric function f_1 the exponent c_{ref} is enforced, then the ratio of the allometric factors a_1 / a_{ref} shall be defined as the "allometric level l_a".

$$f_{ref} = a_{ref} \cdot x^{c(ref)} \tag{20}$$

$$f_1 = a_1 \cdot x^{c(ref)} \tag{21}$$

$$l_a = {a_1}/{a_{ref}} \tag{22}$$

2.2.2 Self-thinning rule

One of the most prevalent allometric patterns observed for both plant and animal communities is the inverse relationship between body mass (biomass) and abundance (density).

Biomechanical and allometric theory predicts that the total body mass of an individual tree is proportional to the stem diameter of any size class (Enquist and Niklas, 2001).

First studies done to develop allometric relationships, associating forest structural parameters in forest stands, are lined out in Pretzsch (2009). Based on Galilei's principle of the similarity of forms, the biologists, Spencer (1864) and Thompson (1917) introduced the allometric relationships between parameters like demand on area, basal area dependent energy consumption, stand density and biomass of organisms. The stand density rule postulated by Reineke (1933) for woody plants is an early empirically based species invariant scaling law with considerable importance in forest practice and forest science. For the relationship between tree number N and mean diameter $\overline{d}$ in fully stocked, even-aged forest stands the stand density rule was defined as:

$$N = k\overline{d}^{-1.605}. \tag{23}$$

In Figure 10 Reinieke's rule is illustrated for two test sites, Traunstein and Ebersberg test sites, both located in SE Germany (site characteristics are summarized in Torano (2015b), publication I).

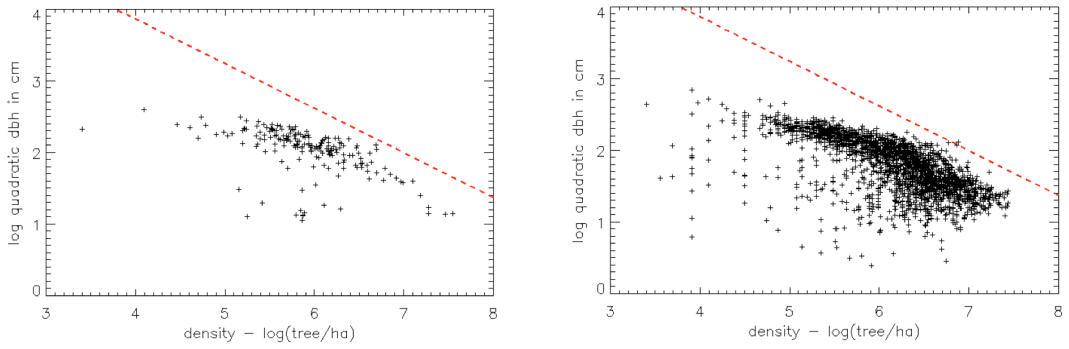

Figure 10: Stand density rule of Reineke for the test sites Traunstein (left) and Eberbserg (right), both located on SE Germany. The red line corresponds to the Reineke's rule for a $k = 10.2$.

Later, Yoda et.al (1963) connected a decreasing biomass, in terms of plant weight, with increasing density (numbers of plants per unit area) for herbaceous plants from which they derived the -3/2 self-thinning rule. By establishing an allometric relationship, using this coefficient, between the biomass (m) per plant and the number of plants per unit area (N) in even-aged stands at maximum density, this rule combines production and population ecological

aspects ($m \propto N^{-3/2}$). Numerous authors consider this the most important rule or even the law with the greatest significance in population biology. This rule is illustrated for the Traunstein and Ebersberg test sites in Figure 11.

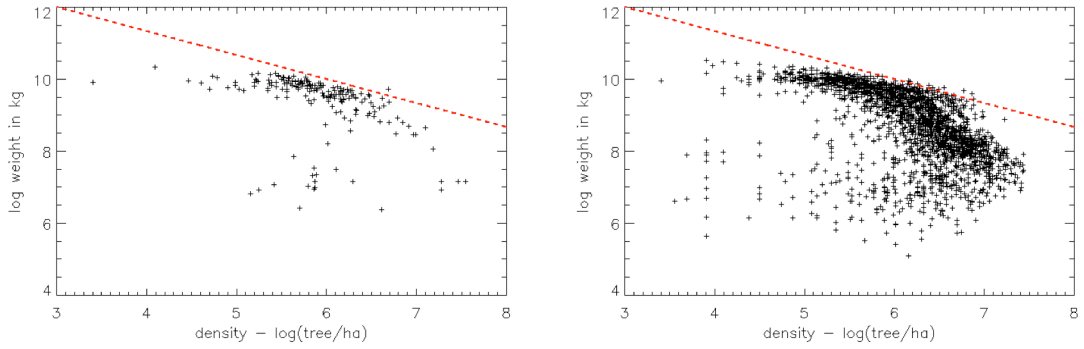

Figure 11: Rule of Yoda for the test sites Traunstein (left) and Eberbserg (right), both located on SE Germany. The red line corresponds to the line $m = kN^{-3/2}$ for $k = 21$.

2.2.3 Height-to-biomass allometric relationships

The work developed in this thesis is greatly motivated by the studies done by Mette about the allometric relationships between forest height and biomass (Mette 2007). This allometric relationship based on an allometric power law serves as basis for the structure-to-biomass relationships, as forest height is the main contributor to the forest structure.

The beginning of the study of the statistical relationships existing between the total forest volume productions and the stand mean height resulted in the Eichorn's rule. According to Pretzsch (2009), the first version of the Eichhorn's rule, was valid for more or less untreated stands. Gehrhardt (1930) refined Eichhorn's rule based on the extended database from experimental plots. First, he found that total volume production was also closely related to mean height. Then Gerhard refined this relationship by specifying mean height - total volume relationships for each site index. In the first variation of the rule, Gehrhardt describes a site-independent height-volume relationship, later referred to as the common yield level by Assmann (1961, pp. 161–168). The second variation is a site-dependent height-volume relationship termed the "special" yield level by (Assmann, 1961). The interpretation of Eichhorn's rule according to Assmann lies on the estimation of total production in relationship with age, height, and yield

classes and reveals the increasing precision of the intermediate relationship which allows a more realistic estimation of stock volume production (Pretzsch, 2006).

Forest aboveground biomass estimation

In the most general formulation, forests are defined as plant formations that are constituted mainly from trees and cover with sufficient extent for the development of a characteristic forest climate (Burschel and Huss, 1997). The first criterion "tree" refers to woody upright, perennial plants with branching at the tip, reaching at maturity at least 5-7 m. The second criterion "characteristic forest climate" depends on height, density and extension of the forest. The main parameters that characterize a tree in a dendrometric scene sense are:

- Tree species: relates to wood density and tree shape.
- Tree dbh (m): diameter at breast height (1.3m) aboveground.
- Tree height (m): vertical distance between ground and tree tip.
- Tree volume (m3) or biomass (Mg): most integrative structural parameter.

While volume is more of a forestry standard, biomass is the ecological standard. Biomass can be calculated from volume through multiplication with species-specific wood density weight ρ (g cm^{-3}):

$$Biomass = Volume \cdot \rho \tag{24}$$

Volume and biomass are typically defined as stem volume or biomass, usable wood volume or biomass, or total wood volume or biomass, although biomass can also include non-woody parts of the tree.

The stem volume can be calculated from tree height h, diameter dbh and the shape factor f_z; tree biomass b_{stem} is obtained after the multiplication with the woody density ρ (25). In this way, biomass is considered as a first order parameter as it has been obtained by the multiplication of directly measured parameters (Chave et al., 2005).

$$b_{stem} = h \cdot \pi\left({}^{1}/_{2}\, dbh\right)^{2} \cdot f_z \cdot \rho \tag{25}$$

The shape factor accounts for the stem shape, for the height of the reference diameter and for the definition of volume. It typically assumes values around 0.5.

Finally, forest biomass density is calculated as the sum of the individual stem biomasses related to an area unit (typically ha). If tree dimensions are more or less similar, i.e. in an even aged forest, then biomass can be calculated using mean height h_{mid} and mean dbh dbh_{mid}, denoted by *mid*, and multiplied by the tree number per hectare *N*:

$$B_{forest} = \sum_{i=0}^{n} b_{stem} \tag{26}$$

$$B_{forest} = h_{mid} \cdot N \cdot \pi(\frac{1}{2} \quad dbh_{mid})2 \cdot f_z \cdot \rho_{mid} \tag{27}$$

Height-to-biomass allometric considerations

The study of Mette (2007) is based on German standard forestry tables from Spruce single even aged forest stands. Thus, the parameters used for the height-to-biomass allometry are derived for these specific conditions. These are stand conditions and age, forest management and forest species. Since the allometry is based on yield tables these relations are forest type-specific and therefore it is needed to discuss how strong the height-biomass allometry depends on the forest type.

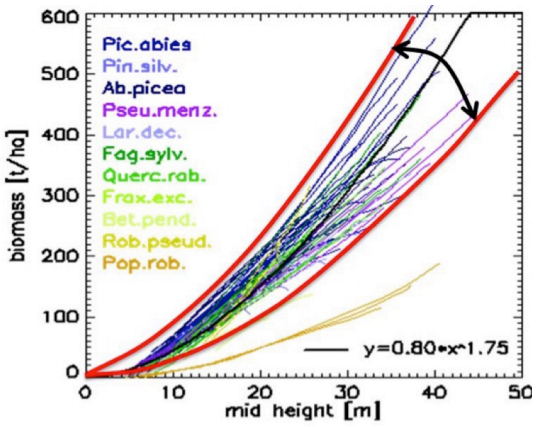

Figure 12: Regression curves for the collection of yield tables used by Mette (2007). In black it is represented the curved used for the allometric equation. The red curves indicate the ~15% biomass estimation error.

The consideration of these three parameters is fundamental to understand the strength and limitations of the height-biomass allometry under such particular stand conditions. The main considerations can be summarized as follows:

1) For one even-aged species the height-to-biomass relationship can be considered stand condition independent: When estimating stem biomass from tree height, the influences of stand conditions is almost negligible: a specific height corresponds to a specific biomass, no matter whether it is at a young age by fast growing forest (under favorable conditions) or at an old age by a slow growing forest (under adverse stand conditions).
2) The variability of the height-to-biomass relationship for single-species stands: The forest yield tables, used in the allometric relation (Mette, 2007), were only registered for managed forest systems, where the growth rate is maximized through a moderate to strong thinning of weaker trees. Therefore, allometric relations will always possess certain variability due to the missing information about the forest management and structure.
3) The effect of species: Depending on the species the allometric exponent varies so the height-to-biomass relationship between different species can vary within a limited range of +/- 15% (tested with central European species in the test site of Traunstein), which can be wider depending on the conditions and variety (mixture) of species within the site (see also Figure 12).

2.2.4 Structure interactions and dynamics

The dynamics of single-layered mono-specific stands can be modeled from stand level data, without taking into account the spatial stand structure. However, if 3D structure is not modeled in multilayered pure or mixed stands the characteristic of theses stands that affects their dynamics will be neglected. Therefore, due to the importance of forest structure for the understanding of forest dynamics, new research approaches need to be based on the spatial structure of the tree, stand or forest (Pretzsch, 2009).

As explained in the previous section, the applications of height-to-biomass allometric relationships are, for this reason, optimal just for homogeneous forest conditions: even aged, single species stands; but forests on a global scale present, on the other hand, a much higher diversity. Thus, natural forests in the tropical region and in the temperate zones tend to form mixed stands with complex structures that make the height-to-biomass allometric relations inaccurate. Even in managed forests, especially in central Europe, forest management increasingly tends to create complex structures to make stands more resistant against the

changing climatic conditions. In fact, the study of forest structures offers the possibility to access to new allometric relationships, which are of value not only to improve biomass estimations with new parameters, but also to provide with a better understanding of the forest dynamics (improve forest management) in the frame of climate change (Rötzer et al., 2005).

Forest structure is described, in the most general terms, as the distribution of biomass in space, that is a vertical and horizontal spatial arrangement of plant species, plant sizes, or age distributions (Zenner and Hibbs, 2000), characterized by variation in species and age classes, arrangement of species into different canopy layers and distribution of individuals among diameter classes. However, while these definitions recognize the 3-dimensionality of forest structure, quantitative and ecologically relevant measures of the structural complexity that allow comparisons among forest stands are yet missing.

The stand structure determines the integrity and stability of a forest to a large extent. Since trees are rooted to the ground, and develop and acquire their structure over long periods of time, their existing structures enable them to influence those factors, which in term influence growth, such as light, temperature and precipitation. Consequently, the tree and stand structures, which have developed in a forest ecosystem, have a major influence on the life cycle of all organisms within the stand, so that, stand structure determines the competition among tress in a stand for resources and the biomass production within the stand (Pretzsch, 2014).

The interaction between structures and process in dynamic systems can be illustrated by a river system. The structure of the riverbed influences the water flow and this modifies the riverbed changing the water flow and shaping it. The feedback mechanism, characteristic of many dynamic systems, it is really apparent here. The structure determines the processes directly and immediately, whereas, in turn, the processes modify structures over a longer period of time in a slower feedback system. The existence of this feedback system means an understanding of the processes is only possible if the one recognizes the structural patterns that these processes actually follow (Pretzsch, 2009). The recognition of structures is essential to understand the developments that can be influenced effectively through changes in the structure.

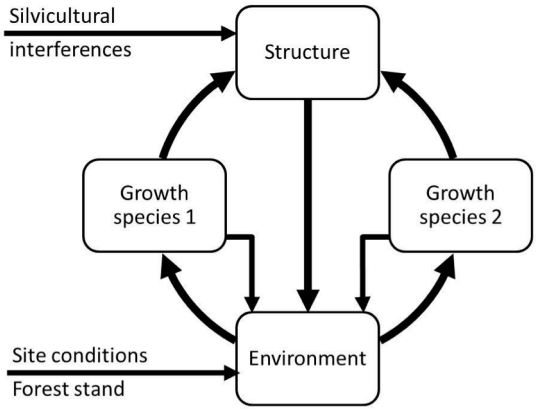

Figure 13: Feedback loop between stand structure, environmental conditions, and tree growth in a two-species stand. The outer feedback loops structure environment→ growth→ structure (bold arrows) are slow, the inner loops environment→ growth→ environment work faster (Pretzsch, 2014).

Two feedback loops proceeding at different time scales can be recognized. First, by forming the local environmental conditions within the stand (e.g. interception of light and precipitation) the structure of the canopy is crucial for the feedback between structure-environment-growth, which drives population dynamics (Figure 13). While this applies to all forest types, it is particularly relevant in shaping the forests of the future, and the transition from homogenous even-aged stands to structurally-rich, mixed stands with complex intraspecific and interspecific interactions. In the second loop, the structure determines the processes directly and immediately whereas in turn, the processes modify structures over a longer period of time in a slower feedback system. The existence of this feedback system means that an understanding of the processes is only possible if one recognizes the structural patterns these processes follow. As processes modify structures, the resulting measured structures can assist the interpretation of those processes which are often more difficult to measure or observe (Pretzsch, 2014). These structural relationships of processes of individual trees, also, "scale up" to generate emergent properties of forests, such as size, structure and spacing relationships (Enquist et al., 2009). Moreover, the structural patterns of the trees in the overstory affect the canopy gap structure due to the participation of light and precipitation received by the understory layers, and the limited availability of resources determines the amount of biomass that an ecosystem can produce (Latham et al., 1998; Lindner et al., 1997).

In conclusion, all these interactions indicate that forest vertical structure is intrinsically related with forest evolution. Thus, the stock of forest biomass is determined by trees vertical and horizontal arrangements and it varies over time due to these numerous interactions and disturbances. An understanding of the relationship between these distributions is of essential importance to improve the AGB estimations and to generate generalized inversion algorithms.

2.2.5 Plot sampling and scale

One crucial aspect in the development of RS algorithms for vegetation, however, is the ground-validation of the RS measurements. Nowadays RS accurately measures, for example, the height of the canopy (Mette, 2007). It would therefore be of interest to compare forest inventory data with results from RS at the same scale. This attempt is especially difficult in tropical forest, but so less in intensively measured temperate regions, like Germany.

The considered horizontal scale has a big impact on the structure characterization and needs to be considered. According to Laar and Akça (2007, chap. 2.2.1), the variability of the study variable, e.g. volume/biomass, tends to decrease with increasing the plot size and this turn reduces the sample size required to obtain a predefined precision of the estimated population, but the coefficient of variation tends to decrease curvilinearly with increasing the plot size. Inventory plot size must be defined in order maximize the accuracy but minimizing the costs.

In a relatively homogenous planation forest, however, the coefficient of variation is less severely affected by plot size than in natural forests. For a given sampling intensity, the required number of plots decreases proportionally to plot size. In order to estimate the volume / biomass of a stand with an area of 15 ha, a sampling intensity of 5%, and sample plots with a radius of 7 m. The optimum plot size is also related with forest type, stand structure, site, and genetic parameters. For example, inventories of multispecies tropical forests with a low density of merchandisable trees require large plots, whereas small plots are adequate in clonal plantations (van Laar and Akça, 2007, chap. 2.2.1).

Concentric circular plots have been successfully used in the inventory of all-aged forests. Three circles with different radii and the same center are super-imposed. All trees with a dbh of more than 7 cm are measured within the inner plot, this with a dbh of more than 20 cm within the second smallest circular plot and the trees with a dbh of more than 40 cm within the outer

circular plot. Volumes and confidence intervals have to be calculated for each of the tree size categories separately. Plot size affects the sampling cost per unit, which increases when decreasing area. Therefore, there three main factors to consider in the decision of the plot size: the size must be optimum to produce the highest precision at a given cost, or the size is optimum to give the lowest cost at a given precision, or the size is associated with the lowest value of variance multiplied by its cost.

At finer spatial scales variability in forest features is large, suggesting that there are forest features visible at a given spatial scale but not at coarser ones (Chave and Levin, 2003). While averaging results from small size plots reduces the variance due to error in the single tree-biomass-estimation procedure, it also masks biomass variability caused by structural variability (Shugart et al., 2010). Forest structure analyses are also highly affected by the considered spatial scale; that is, the inventory scale also influences the overall forest structure and its dynamics in time. At a large scale (close to 1 ha), a forest stand seeks an equilibrium state with a characteristic configuration but at a small scale (the so-called gap scale), the forest ecosystem state is affected by continuously undergoing changes driven by the presence of large trees. The gap size is, according to Shugart (2010), related to the size of the tree canopy dominant trees (10m to 30 m implying a 0.01 to 0.1 ha area).

3 Discussion

In this section the main contributions of this thesis are discussed. Starting from mapping of large-scale areas with satellite missions and continuing with the development of the structure-to-biomass inversion algorithm, firstly developed using forest ground inventory data, and later applied to RS SAR data.

3.1 Large-scale mapping with SAR systems

Measuring biomass from space will not be as precise as measurements on the ground, but satellite data can provide useful information as they allow not only the estimation of the total amount of carbon sources and sinks but also their precise location and distribution. Even a segmentation of forests in different biomass classes would provide essential and valuable information about the spatial distribution of carbon sources and sinks. Due to the structural complexity that makes many forests of the world very challenging for biomass mapping from satellite platforms, the first step of this dissertation was focused on the Boreal region. Nevertheless, and despite the homogenous structure of these forests, the boreal region is a key environment in the global carbon cycle.

In the boreal zone the carbon stock is usually well known at state level (Houghton, 2005) thanks to high precision ground forest inventories. However, forest inventories are designed to deliver average wood volumes for administrative units; they do not provide maps of biomass at a resolution compatible with land use changes, spatial distribution and changes in biomass within forested areas are highly unknown.

Boreal forests are and will be affected by forest fires, intensive logging activities, development on abandoned agricultural areas or a biomass increase by forest growth. There are both, periodically changing carbon sinks and carbon sources whose detection and updating requires regular monitoring intervals. Average values for very large areas will bias the calculated sources and sinks of carbon (Houghton et al., 2009). Therefore, it is needed to have a consistent source of information all over the boreal zone. Due to the vastness and remoteness of this area,

satellite imagery is the only possible source of information to extend and update boreal forest biomass classifications.

The amount of forested land under certification standards like FSC increases rapidly, reaching 150 million ha of tropical, temperate and boreal forests. FSC, for example has been involved in the Transparent Project ("Transparentforests | ESA's ARTES Applications," n.d.), The Transparent Project is a collaboration with the European Space Agency (ESA), investigating the usage of RS to assist and improve the certification process, whose goal is the development of a methodology that can provide an independent source of temporally and spatially accurate data (e.g. land use and land use changes across the auditing period) to support the certification process. They demand that for this purpose high resolution RS data are highly needed.

The changing climatic conditions will introduce higher uncertainties in forest management strategies and may require an update of forest management planning in shorter time intervals. State forest administrations in Central Europe for instance, have started to introduce RS techniques to support their management and information plans and to update their data bases (Schneider et al., 2013). Shorter time intervals for updates and full area coverage of forest management information may accelerate planning modifications to compensate for a changing environment, natural hazards or fast changing socio-economic conditions (Schneider et al., 2013). The main existing RS data are based on optical systems, which are limited to qualitative classifications and generally result in an insufficient number of forest classes (mainly distinguishing between forest and non-forest, or deciduous and coniferous forests). These classifications are generally able to map different stages of forest re-growth, but have limited success in determining biomass in closed canopies and in high biomass forests (Goetz et al., 2009; Houghton et al., 2009), resulting in a low number of forest classes, particularly in high biomass forests.

At European level the main (most important) land cover classification is the Coordination of Information on the Environment (CORINE) ("CORINE Land Cover — European Environment Agency (EEA)," n.d.). CORINE was initiated in 1985 by the European Commission and aimed at gathering environmental information about certain priority topics for the European Union (air, water, soil, land cover, coastal erosion, biotopes, etc.). CORINE is an

inventory of the land cover represented by 44 classes as a cartographic product at a scale of 1:100000. This database is operationally available for most areas of Europe.

The project Global Land Cover 2000 Maps has provided a global harmonized land cover map with an overall classification accuracy of 68.6 % (Mayaux et al., 2006). This project combines data from spaceborne passive optical sensors with different resolutions, such as the Moderate Resolution Imaging Spectral Radiometer (MODIS) (500 x 500 m spatial resolution) on board of the Terra and Aqua platforms and VEGETATION (300 x 300 m spatial resolution) on board of SPOT-4 and SPOT-5. This map classifies forests in seven categories from evergreen to deciduous forests, and different proportions of mixed forests.

Quantitative forest RS data are commonly provided by spaceborne LiDAR systems. Global forest height maps based on the combination of LiDAR with optical (passive) RS systems have been proposed, in the last years, by (Simard et al., 2011), (Lefsky, 2010). The approach shown in (Lefsky, 2010) tries to overcome the limitations in spatial coverage of the spaceborne LiDAR system GLAS using the multispectral data from MODIS. For this a canopy height model derived from GLAS vertical profiles, in combination with uniform land surface patches deduced from MODIS image segmentation, was used to create patches of uniform forest heights. The global forest height map (canopy height) proposed in (Simard et al., 2011) has a spatial resolution of $1km^2$. This map extends the works of (Lefsky, 2010) with validation against field measurements. The overall RMSE is 4.4 m to 6.1 m.

SAR systems, particularly when they are operated at lower frequencies (L-band), offer great potential for mapping forest cover, disturbances and also biomass (Thiel et al., 2009; Wagner et al., 2003). In the SIBERIA project (Wagner et al., 2003), a radar approach, based on ERS/JERS backscattering and ERS interferometric coherence, was used to generate a land cover classification with three forest biomass classes (sensitive up to 81 m3/ha corresponding to 40 Mg/ha) showing the potential of synthetic aperture radar (SAR) to map boreal forest biomass.

Santoro et al. (2011) proposed an algorithm for the estimation of Growing Stock Volume (GSV) using hyper temporal stacks of C-band SAR backscatter data from Envisat ASAR ScanSAR in the boreal region. This algorithm has shown a good sensitivity without saturation up to 300 m^3/ha (~150 Mg/ha) with RMSE's from 47.7 to 96.2 %. Recently, a biomass map for the

entire Northern Hemisphere, ("BIOMASAR.org: About BIOMASAR," n.d.), was produced within the BIOMSAR project using this algorithm, with a spatial resolution of 1 km^2.

The TanDEM-X classification (Toraño et al., 2015a) shows a great potential for forest biomass classification in the boreal regions as shown in our tests sites. It is a classification that with a high resolution (max 16x16 m) can produce biomass maps with four or five classes, up to biomass levels of 250 Mg/ha. This classification uses a standardized methodology that can be applied to large scales, with the potential to provide with constant monitoring and mapping. In comparison with the studies shown above its main advantages lie not only on the high resolution but mainly on the reproducible approach. The performance analysis reported in Toraño (2015a) shows both the limitations and potentials of the biomass classification, with a minimum and a maximum performance limit. This means that the availability of future missions, not only from TanDEM-X but from other single-pass configurations, can improve the classification and add a temporal dimension for forest/land-use change monitoring.

An extension of this methodology, based on improved biomass estimations is the focus of the following studies. A higher understanding of the forest structures will lead to further classifications in the temperate and the tropical regions. Nevertheless a standard classification for the boreal area would already contribute to a reduced uncertainty for a 30% of the total global biomass stock.

3.2 Development of a structure-to-biomass allometry

The definitions of forest structure that are found in the literature change depending on the aim of the considered study. The scale at which the structure is defined also impacts the concept itself and the separation between the horizontal and vertical components of the 3-dimensional structure. Therefore, the first step in a study focused on structure is the careful definition of the components and scales that are going to be analyzed.

A first approach to understand structure can be done by studying single forest variables, and their distribution in the horizontal dimension, being the height-to-biomass allometric relationship a first step in this direction. The improvement of height-to-biomass allometries using parameters of higher complexity like structure or density has been extensively treated in literature, especially in the last decade. From an allometric point of view studies like (Pretzsch

and Biber, 2005) have used horizontal structures, characterized by the Stand Density Index (SDI) to improve biomass/volume estimations. However, the SDI being associated to the dbh cannot be directly estimated with active RS systems. A high number of papers have been published using LiDAR metrics to derive these parameters.

The objective of this allometry was to offer a methodology and an expression that can be used with RS systems that can measured accurately the vertical position of the forest scatterers, that is, height and vertical structure. This methodology has served as a backbone and unifying theory, which can be used a basis for the understanding of the signal response to the forest compartments and also as a first expression that can be modified or adapted to the different frequencies (especially in the case of SAR). The example regarding L-band SAR over the Traunstein forest is reported in the following section.

The most challenging issue in the characterization of structures has been to find a model that can describe the vertical distribution of the forest biomass. Inventory data was first used to access this information. Using the Legendre decomposition as a parameterization tool of the profile frequencies showed a great potential in accordance with the observations presented by (Cloude, 2006). This polynomial basis was conducted with a decomposition using the Fourier transform showing a greater adaptability to biomass profiles. A ratio called S_{rat} (Torano, 2015b) between the dominant frequencies was able to characterize the diversity in the profiles, being able also to distinguish different levels of biomass. The proportionality which was observed between the ratio and the biomass for profiles (stands) with the same dominant height allowed the utilization of this parameter in a biomass allometric relationship. Moreover, further allometric conclusions could be drawn using the structure ratio, e.g. the ratio was sensitive to the gap fraction in a forest stand.

A problem associated with the inventory data was the spatial horizontal scale. The small size of the inventory plots, designed to statistically estimate stand variables, resulted too small to represent characteristic vertical and horizontal structures. As the inventory plots available from the Bavarian sties, Traunstein and Ebersberg, are spaced in a 100x100 m grid and have an area of 0.05 ha with an average dominant height up to 40 m, the gaps size should have an area closer to 0.1 ha (Shugart et al., 2010). Thus, the small area of an inventory plot is indeed too small and introduces statistical noise, which increases the deviation of height-to-biomass relationships.

On the other hand, the bias in the structure estimation increases when reducing the scale. It has been observed that areas of at least 0.5 ha are necessary to have a stable and representable estimation of the forest vertical structure (Shugart et al., 2010). The allometric relationship of forest structure to forest biomass becomes representable at this scale. Therefore, forest inventories with full tree measurements in lager areas (0.5-1ha) would improve the understanding and development of structure allometric relationships.

Different aggregation techniques could be tested in order to access representative structures. In the following, and in order to further prove the allometric relationships that were thoroughly described in this dissertation, some details from a test in larger inventory sites are shown.

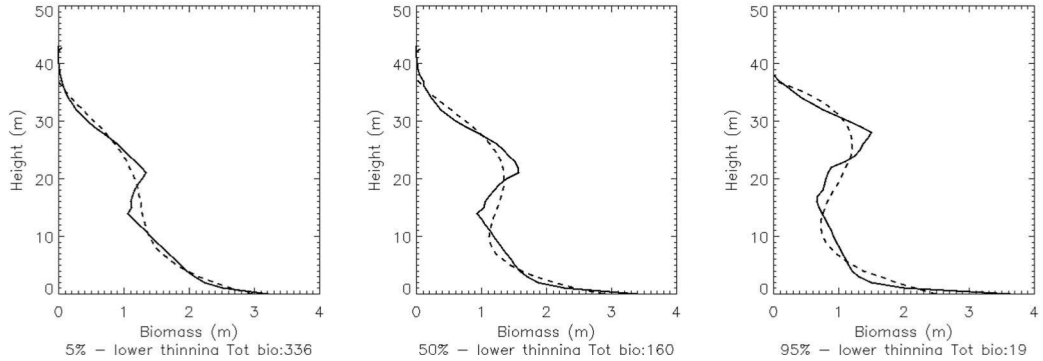

Figure 14: Profile changes under thinning from below management for a 5%, 50%, and 95% basal area removal. The original profile is represented in black and the reconstructed profile with 1–4 polynomials in blue.

The validity of the conclusions extracted from the structure-to-biomass relationships were also tested using modeled scenarios. That is, simulating thinning techniques, both, from below and above, in order to test the impact of biomass removals under controlled conditions. Inventory data from permanent growth research areas of 25 m × 25 m were used to initialize both models. In these areas, all trees were measured and monitored with high precision; hence, they were suitable for detailed modeling analyses. Moreover, these areas were sufficiently large to simulate forest changes solving the problem of the scale influences. Basic assumptions were applied to simulate the thinning processes. For the thinning from below, trees with the smallest diameter were removed in steps of 5% of the total remaining stem basal area. For the thinning from above,

the trees with the largest diameters were removed also in steps of 5% of the total stem basal area. For each step, biomass and the structure ratio S_{rat} were calculated. Height growth was not considered here. The percentage of basal area removed from the original stage is indicative of the intensity of the thinning.

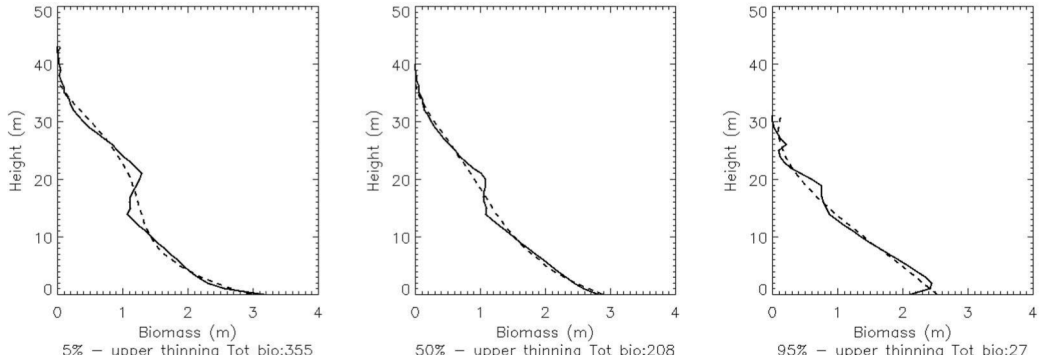

Figure 15: Profile changes under thinning from above management for a 5%, 50%, and 95% basal area removal. The original profile is represented in black and the reconstructed profile with 1–4 polynomials in blue.

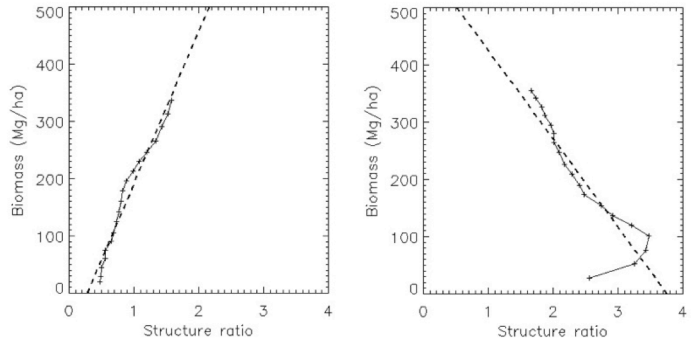

Figure 16: Biomass vs. structure ratio for thinning from below management (right) and from above (left).

By using the simulation scenarios, the direct correlation between structure ratio and biomass was confirmed. However, even if in the case of a thinning from below a direct correlation was observed, an inverse correlation was observed in the case of thinning from above (Figure 16). There was a tendency for thinning from above to contradict the assumptions made in the inversion process: biomass was not directly proportional to the structure ratio. However, we can assume that these processes are rare and do not occur in forests under natural development,

although they can explain part of the error observed in the biomass inversion. Changes in the biomass profile induced by thinning are displayed in Figure 14 (thinning from below) and in Figure 15 (thinning from above). Two main differences between these two thinning processes could be observed. First, there were different height trends, whereas thinning from below the tree height did not reduce the profile height, and thinning from above tree height decreased as the largest trees were removed. Second, although under thinning from below the biomass profile became sharper (crown compartment was dominant), under thinning from above the biomass profile became smoother (stem compartment was dominant). Estimated biomass vs. structure ratio for every thinning step is shown in Figure 16, on the left for thinning from below and on the right for thinning from above.

The analyses done on simulation scenarios over a larger area confirmed other two assumptions. The first one is the sensitivity of the structure ratio based on low frequency Legendre polynomials to changes in biomass at this level of resolution; and the second is the gain in stability of the structure-to-biomass relationship when increasing the stand area.

To conclude, this method is, however, restricted to the empirical estimation of the exponents for each area. A further extension with more test sites especially in different climatic regions will further improve the applicability of the method. For example, as the structure fills in and more layers appear within one height segment, as it would be expected in the tropical regions, the estimation of new exponents would be necessary to compensate for a higher biomass-to-structure dependency.

3.3 From biomass-derived allometric relationships to SAR reflectivity

The main challenge for the transfer of allometric relationships derived for bio-physical systems to remotely sensed variables is to understand the actual connection between the two systems. In the case of SAR a physical interpretation of the vertical distribution of the backscattered power, that is SAR vertical reflectivity profiles, is essential.

RS has tried during the last two decades to extract biomass relations from vertical structure profiles, principally obtained using LiDAR systems, in both space and air-borne platforms. The interpretation of LiDAR approaches offers a first degree in the understanding of the response of short wavelength signals to the forest structures. This can be later used to further study the radar

signal, which is the main application shown in this study. Multiples studies can be commented regarding LiDAR vertical profiles (Dubayah and Drake, 2000; Harding et al., 2001a; Lefsky et al., 2005) .

The main contribution of this thesis has been the development of a structure characterization that can be used to parameterize complex vertical profiles The first similarity and physical variable that remains between the expression developed for biomass profiles and for reflectivity profiles is the height H. The retrieval of forest height, with accuracy above a 10 % allows the estimation of the same physical variable and therefore, it can be used in the structure-to-biomass allometric relationships shown in Toraño (2015b).

In Toraño (2015b) the potential of the structure ratio is shown, but when it is applied to the SAR reflectivity profiles estimated with TomoSAR/Capon the relationship to biomass is changed, and most importantly inverted. This fact points towards the main interpretation of the radar backscatter connection with forest structures at L-Band. The following points need to be considered for the understanding of the interpretation of the radar signal using the structure theory that has been described throughout this thesis.

1) Stem/crown proportion defines the structure ratio: on one hand, low-frequency Legendre components respond to the slow changing components of the profile. In the case of biomass profiles it is shown in Toraño et al. (2015b) that they are strongly connect to the stem compartment. On the other hand, high frequency Legendre components respond to the fast changing components of the profile. In this case, it was shown how these frequencies are strongly connected to the crown compartments.
2) L-band is very sensitive to forest volumes: volumes from a SAR point of view represent in forest (and allometry) the crown compartment. For this reason, the reflectivity profile is almost "blind" to the stem compartment. If a ratio is calculated between the low and high frequencies, an increase of the response coming from the volumes will decrease the value of the ratio.
3) The relationship of the structure ratio to biomass can change between systems: in terms of biomass, in Toraño et al. (2015b) it was proved how according to literature, the ratio is proportional to biomass. That means, an increase of the proportion of the stem compartment (which typically allocates 60% of the biomass), is translated in a higher

filling of the gap structure, which means higher density at a given height, and therefore, higher biomass.

In conclusion, with a profile coming from L-Band SAR, the main contribution coming from the stem decreases to a factor of ~1, which is the low frequency in the numerator of the structure ratio. This however, does not decreases the sensitivity of the ratio to biomass because of the following reasons:

- The low frequency still acts as a measure of the average power of the normalized vertical reflectivity profile.
- An increase of the crown compartments in absence of the stem influence is interpreted as an increase of the Leaf Area Index, which is highly connected with tree density and gap filling and, therefore, is a very good proxy to biomass at a given height.
- Finally, having a low frequency that lies around one, an increase of the high frequencies in the denominator will decrease the ratio when the gap filling increases. That is the value of the ratio is inversely proportional to biomass.

These conclusions have led to a biomass inversion expression similar to what it shown in Toraño et al. (2015b) as introduced in Toraño et al. (2015c) :

$$AGB = 40 S_{rat}^{-0.55} H^{0.85} \tag{28}$$

Furthermore, a sensitivity analysis was carried out to test the performance of the inversion against error sources. In Figure 17 the results of the sensitivity analysis are shown in terms of RMSE and the correlation factor. Starting from the best case scenario shown in Toraño et al. (2015c), i.e. in HH polarization under moist conditions, a relative error has been added independently to the height (read) and S_{rat} (blue). From this analysis, it is concluded that the estimation of height is critical for the biomass estimation degrading to a correlation of 0.2 after adding an extra 10% error. However, the estimation of structure is more robust remaining at 0.5 after adding an extra 10% error.

This methodology, however, is affected by the variability of the vertical reflectivity estimation method and also by the empirical estimation of inversion parameters. The lack of tomographic data sets limits this extension towards other sites and a further generalization.

Nevertheless, the great potential of the vertical profiling techniques will soon allow the continuation of investigation in this direction.

The tomographic methods that were used to derive the vertical reflectivity may also affect the biomass estimation, as each tomographic approach may produce profiles with different relative amplitudes to the ones we have used here (Pardini et al., 2012).

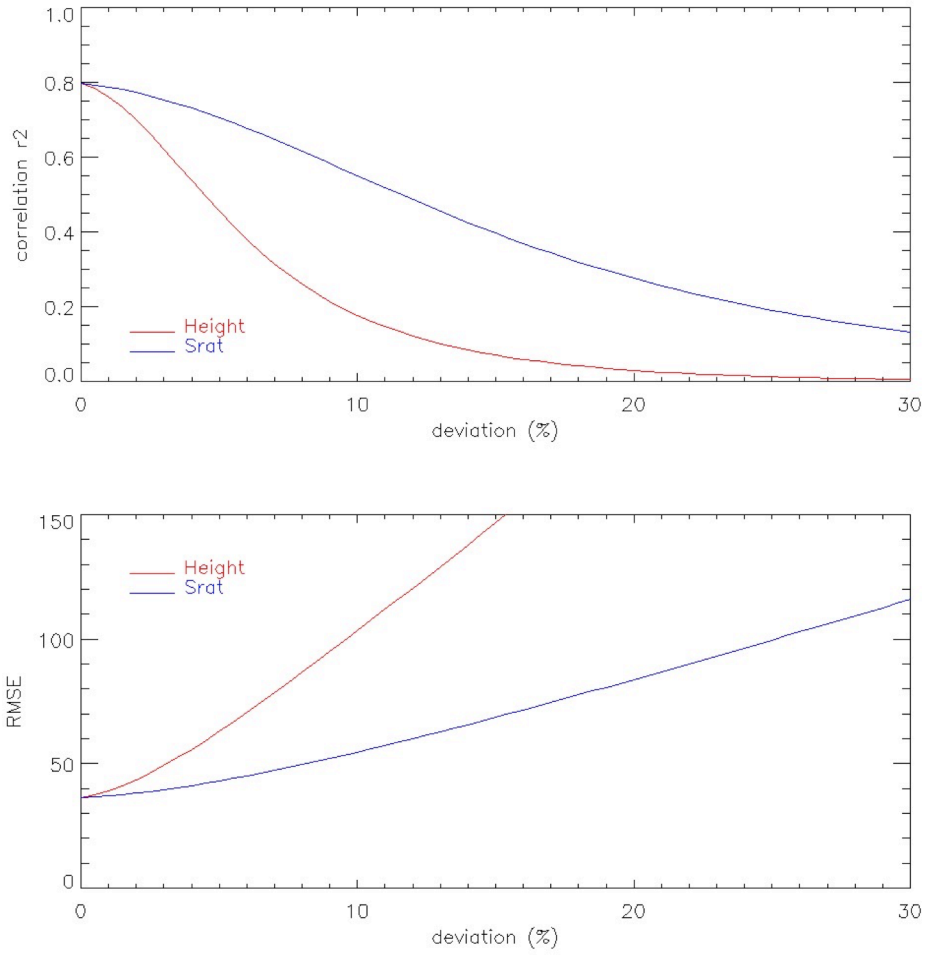

Figure 17: Sensitivity analysis for the biomass inversion with SAR reflectivity profiles in L-Band. The starting point corresponds to the best inversion scenario (HH in moist conditions). A relative error is added to this scenario to the estimation of height (red) and to the estimation of S_{rat}. The results for the correlation factor r^2 are displayed on the top and for the RMSE on the bottom panel.

Preliminary observations using other tomographic data sets from Traunstein in 2009 under different phenological conditions (spring and autumn) support the validity of the biomass

inversion expression and the structure indicator to characterize and improve biomass inversion using vertical reflectivity profiles. Inversion correlations close to 80% (i.e. in the frame of 20% accuracy estimation) in all the tested scenarios and a reduction of the RMSE between the structure and the height-to-biomass inversions are consistently observed. A summary of these results is shown in Figure 18. On the top panel an inversion performed using the height-to-biomass allometric expression ($AGB = 0.9H^{1.58}$) for leaf-on (spring) and leaf-off (autumn) are displayed for HH and HV polarizations. On the bottom panel for the same scenarios an inversion using the structure-to-biomass expression (28) is shown.

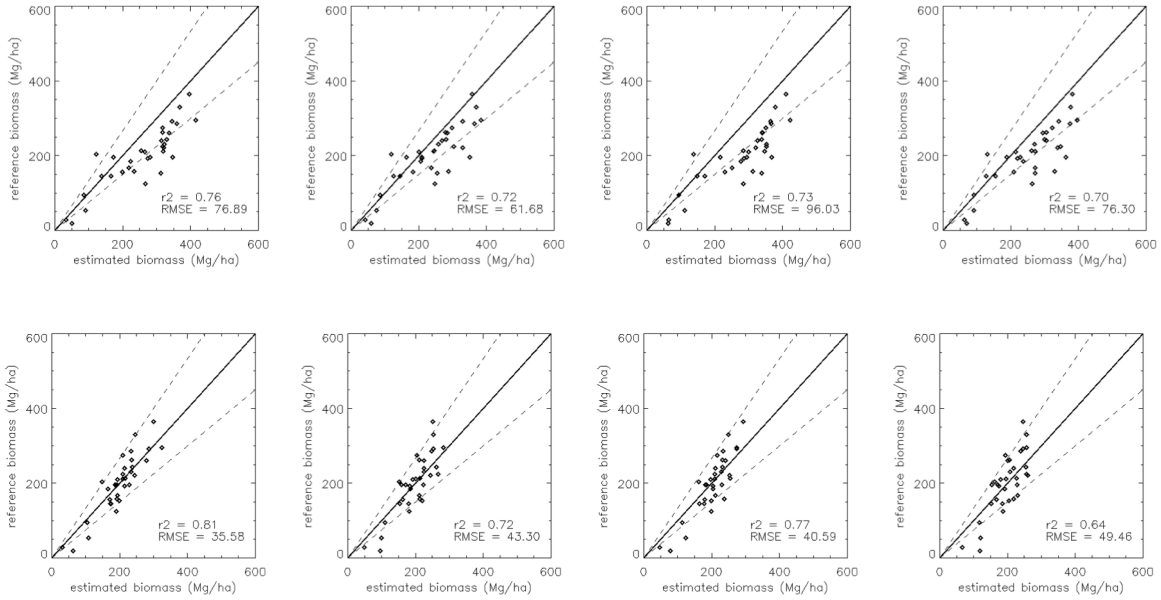

Figure 18: Biomass inversion results for the TempoSAR campaigns over Traunstein in 2009. On The top panel the inversion results using only height ($AGB = 0.9H^{1.58}$) are shown and in the bottom panel the inversion results for the structure and height expression (28) are shown. From left to right the scenarios are displayed as follows: Spring-HH, Spring-HV, Autumn-HH and Autumn-HV.

The main conclusions extracted from these last analyses focused on the height estimation from the reflectivity profiles. The estimation algorithm presented in Toraño et al. (2015c) is estimated from the shape of the vertical profile, which is affected by the structure and weather conditions. Thus, forest height estimation is already affected by structure elements, especially under SAR tomographic configurations that lead to a low vertical resolution. This means, that the detection of forest compartments is mixed and strongly affected by structurally induced changes.

For this reason, the inversion from the height-to-biomass expression using the estimated height from the reflectivity profiles shows an improvement respect to the previous scenarios shown in Toraño et al. (2015b). This structure leakage is worth to be investigated to further improve and understand the radar signal response to biomass.

4 Conclusions and future work

In this thesis, the potential of forest vertical structures to improve the estimation of aboveground biomass (AGB), a key variable in the global carbon cycle, has been investigated and demonstrated. The carbon stored in forest ecosystems, measured as AGB, is the most uncertainty measured variable in the carbon cycle. Therefore, the need of a standardized methodology that can be applied globally thanks to RS systems has been proved to be essential in order to reduce this uncertainty and, as a consequence, to improve the understanding of climate change processes.

The Earth's forest ecosystems comprise several biomes with very different structural properties. Starting from the boreal biome, which presents the most homogenous structures to the tropical regions, general allometric relationships have been studied.

In the boreal region, thanks to this homogenous structure, a biomass classification algorithm could be tested using high radar frequency data (X-band) from the TanDEM-X mission. This showed the potential of height-to-biomass allometric relationships as a first step to quantify/classify biomass in larger regions of the world. The performance analysis that was carried out was not only a measure of the potential of the technique but it also provided with a realistic quantification of the biomass estimation error, in all cases lower than the uncertainties that nowadays exist in these kinds of classifications.

However, as it is often mentioned throughout this thesis, the height-to-biomass allometric relationships loose accuracy when they are applied in highly structure ecosystems, in terms of density, species or layers. For this reason a deeper study, which is the core of the work, was carried out in order to, first, study the allometric properties of the forest vertical structure and second, to find the relationship to AGB.

The structure descriptor S_{rat} is the main contribution of the study. Being able to characterize vertical structures, not only from modeled vertical biomass profiles but also from L-band SAR vertical reflectivity profiles, the ratio offered a new way to understand the connection

between these structures and AGB. In both systems the ratio between low profile frequencies were shown to be the main descriptors of biomass. Due to the different bio-physical information contained in the biomass and the reflectivity profiles, the relation of the ratio in the structure-to-biomass inversion expression needed to be modified. Nevertheless, the transfer from biomass to L-band reflectivity was successful and similar performances were observed. That is, the structure-to-biomass systematically improved the height-to-biomass inversions a 20 %, in both, correlation factor and RMSE, achieving an average estimation error which stays within the 20% accuracy threshold, defined for global carbon estimations. Moreover, useful and interesting biophysical conclusions could be drawn depending on the structure ratio correlation sign and its connections to the forest compartments.

Finally, the use of this structure ratio as a structure characterization parameter based on polynomial based decompositions has been shown, as the lowest frequencies of the vertical structure are strongly correlated to biomass.

The methodologies and conclusions derived during this dissertation have also a great potential for the future development of global biomass estimators. One suitable option would be the expansion of the biomass classification for future continuations of the TerraSAR-X/TanDEM-X mission, in order to have access to the temporal changes of biomass in the boreal biome. New coming and SAR missions like Tandem-L, a single pass L-pass interferometric SAR mission, would even allow the application of structure-to-biomass allometries in denser and highly structure forests allowing the test of the methods developed here. Nevertheless, the extension and validation of the vertical structures analyses performed in Traunstein would be needed, using a higher number of data sets, to advance not only in the characterization interpretation of SAR profiles from different environments, but also under a higher range of weather and seasons.

The direct relationship between the structure ratio and forest density could also help in the improvement of the allometric relationships and the fusion with other remotely sensed data could allow pre-classifications of the structure data, compensating for biases coming from the species composition and reaching biomass inversions with even lower estimation errors.

5 References

Asner, G.P., Powell, G.V.N., Mascaro, J., Knapp, D.E., Clark, J.K., Jacobson, J., Kennedy-Bowdoin, T., Balaji, A., Paez-Acosta, G., Victoria, E., Secada, L., Valqui, M., Hughes, R.F., 2010. High-resolution forest carbon stocks and emissions in the Amazon. Proc. Natl. Acad. Sci. 107, 16738–16742. doi:10.1073/pnas.1004875107

Assmann, E., 1961. Waldertagskunde. Organische Produktion, Struktur, Zuwachs und Ertrag von Waldbeständen. BLV Verlagsgesellschaft, München, Bonn, Wien.

Bamler, R., Hartl, P., 1998. Synthetic aperture radar interferometry. Inverse Probl. 14, R1. doi:10.1088/0266-5611/14/4/001

BIOMASAR.org: About BIOMASAR [WWW Document], n.d. URL http://biomasar.org/ (accessed 5.18.15).

Burschel, P., Huss, J., 1997. Grundriss des Waldbaus. 2. neu bearbeitete und erweiterte Auflage. Berl. Parey S 487.

Cairns, M.A., Brown, S., Helmer, E.H., Baumgardner, G.A., 1997. Root biomass allocation in the world's upland forests. Oecologia 111, 1–11. doi:10.1007/s004420050201

Capon, J., 1969. High-resolution frequency-wavenumber spectrum analysis. Proc. IEEE 57, 1408–1418. doi:10.1109/PROC.1969.7278

Chave, J., Andalo, C., Brown, S., Cairns, M.A., Chambers, J.Q., Eamus, D., Fölster, H., Fromard, F., Higuchi, N., Kira, T., Lescure, J.-P., Nelson, B.W., Ogawa, H., Puig, H., Riéra, B., Yamakura, T., 2005. Tree allometry and improved estimation of carbon stocks and balance in tropical forests. Oecologia 145, 87–99. doi:10.1007/s00442-005-0100-x

Chave, J., Levin, S., 2003. Scale and Scaling in Ecological and Economic Systems. Environ. Resour. Econ. 26, 527–557. doi:10.1023/B:EARE.0000007348.42742.49

Cloude, S.R., 2006. Polarization coherence tomography. Radio Sci. 41, RS4017. doi:10.1029/2005RS003436

CORINE Land Cover — European Environment Agency (EEA) [WWW Document], n.d. URL http://www.eea.europa.eu/publications/COR0-landcover (accessed 5.18.15).

Defries, R.S., Hansen, M.C., Townshend, J.R.G., Janetos, A.C., Loveland, T.R., 2000. A new global 1-km dataset of percentage tree cover derived from remote sensing. Glob. Change Biol. 6, 247–254. doi:10.1046/j.1365-2486.2000.00296.x

Drake, J.B., Dubayah, R.O., Knox, R.G., Clark, D.B., Blair, J.B., 2002. Sensitivity of large-footprint LiDAR to canopy structure and biomass in a neotropical rainforest. Remote Sens. Environ. 81, 378–392. doi:10.1016/S0034-4257(02)00013-5

Dubayah, R.O., Drake, J.B., 2000. LiDAR Remote Sensing for Forestry. J. For. 98, 44–46.

Enquist, B.J., Niklas, K.J., 2001. Invariant scaling relations across tree-dominated communities. Nature 410, 655–660. doi:10.1038/35070500

Enquist, B.J., West, G.B., Brown, J.H., 2009. Extensions and evaluations of a general quantitative theory of forest structure and dynamics. Proc. Natl. Acad. Sci. 106, 7046–7051. doi:10.1073/pnas.0812303106

Fletcher, K., European Space Agency (Eds.), 2012. Report for mission selection: biomass coreh2o premier, ESA SP. ESA Communication Production Off, Noordwijk.

Gehrhardt, E., 1930. Ertragstafeln für reine und gleichartige Hochwaldbetände von Eiche, Buche, Tanne, Fichte, Kiefer, grüner Douglasie und Lärche. Springer, Berlin.

Gibbs, H.K., Brown, S., Niles, J.O., Foley, J.A., 2007. Monitoring and estimating tropical forest carbon stocks: making REDD a reality. Environ. Res. Lett. 2, 045023. doi:10.1088/1748-9326/2/4/045023

Goetz, S.J., Baccini, A., Laporte, N.T., Johns, T., Walker, W., Kellndorfer, J., Houghton, R.A., Sun, M., 2009. Mapping and monitoring carbon stocks with satellite observations: a comparison of methods. Carbon Balance Manag. 4, 2. doi:10.1186/1750-0680-4-2

Hall, S.A., Burke, I.C., Box, D.O., Kaufmann, M.R., Stoker, J.M., 2005. Estimating stand structure using discrete-return LiDAR: an example from low density, fire prone ponderosa pine forests. For. Ecol. Manag. 208, 189–209. doi:10.1016/j.foreco.2004.12.001

Harding, D.J., Lefsky, M.A., Parker, G.G., Blair, J.B., 2001a. Laser altimeter canopy height profiles: methods and validation for closed-canopy, broadleaf forests. Remote Sens. Environ. 76, 283–297. doi:10.1016/S0034-4257(00)00210-8

Hese, S., Lucht, W., Schmullius, C., Barnsley, M., Dubayah, R., Knorr, D., Neumann, K., Riedel, T., Schröter, K., 2005. Global biomass mapping for an improved understanding of the CO2 balance—the Earth observation mission Carbon-3D. Remote Sens. Environ. 94, 94–104. doi:10.1016/j.rse.2004.09.006

Houghton, R.A., 2005. Aboveground Forest Biomass and the Global Carbon Balance. Glob. Change Biol. 11, 945–958. doi:10.1111/j.1365-2486.2005.00955.x

Houghton, R.A., Hall, F., Goetz, S.J., 2009. Importance of biomass in the global carbon cycle. J. Geophys. Res. Biogeosciences 114, G00E03. doi:10.1029/2009JG000935

Hyde, P., Dubayah, R., Peterson, B., Blair, J.B., Hofton, M., Hunsaker, C., Knox, R., Walker, W., 2005. Mapping forest structure for wildlife habitat analysis using waveform LiDAR: Validation of montane ecosystems. Remote Sens. Environ. 96, 427–437. doi:10.1016/j.rse.2005.03.005

Intergovernmental Panel on Climate Change, Stocker, T.F. (Eds.), 2014. Climate change 2013: the physical science basis ; Working Group I contribution to the Fifth Assessment Report of the Intergovernmental Panel on Climate Change. Cambridge Univ. Press, New York, NY.

Koetz, B., Morsdorf, F., Sun, G., Ranson, K.J., Itten, K., Allgower, B., 2006. Inversion of a LiDAR waveform model for forest biophysical parameter estimation. IEEE Geosci. Remote Sens. Lett. 3, 49–53. doi:10.1109/LGRS.2005.856706

Latham, P.A., Zuuring, H.R., Coble, D.W., 1998. A method for quantifying vertical forest structure. For. Ecol. Manag. 104, 157–170. doi:10.1016/S0378-1127(97)00254-5

Lefsky, M.A., 2010. A global forest canopy height map from the Moderate Resolution Imaging Spectroradiometer and the Geoscience Laser Altimeter System. Geophys. Res. Lett. 37, L15401. doi:10.1029/2010GL043622

Lefsky, M.A., Cohen, W.B., Acker, S.A., Parker, G.G., Spies, T.A., Harding, D., 1999. LiDAR Remote Sensing of the Canopy Structure and Biophysical Properties of Douglas-Fir Western Hemlock Forests. Remote Sens. Environ. 70, 339–361. doi:10.1016/S0034-4257(99)00052-8

Lefsky, M.A., Cohen, W.B., Harding, D.J., Parker, G.G., Acker, S.A., Gower, S.T., 2002. LiDAR remote sensing of aboveground biomass in three biomes. Glob. Ecol. Biogeogr. 11, 393–399. doi:10.1046/j.1466-822x.2002.00303.x

Lefsky, M.A., Harding, D.J., Keller, M., Cohen, W.B., Carabajal, C.C., Del Bom Espirito-Santo, F., Hunter, M.O., de Oliveira, R., 2005. Estimates of forest canopy height and aboveground biomass using ICESat. Geophys. Res. Lett. 32, L22S02. doi:10.1029/2005GL023971

Lindner, M., Sievänen, R., Pretzsch, H., 1997. Improving the simulation of stand structure in a forest gap model. For. Ecol. Manag. 95, 183–195. doi:10.1016/S0378-1127(96)03967-9

Mayaux, P., Eva, H., Gallego, J., Strahler, A.H., Herold, M., Agrawal, S., Naumov, S., De Miranda, E.E., Di Bella, C.M., Ordoyne, C., Kopin, Y., Roy, P.S., 2006. Validation of the global land cover 2000 map. IEEE Trans. Geosci. Remote Sens. 44, 1728–1739. doi:10.1109/TGRS.2006.864370

Mette, T., 2007. Forest biomass estiamtion from polarimetric SAR interferometry. Technische Universität München, Freising.

Mette, T., Papathanassiou, K., Hajnsek, I., Zimmermann, R., 2003. Forest biomass estimation using polarimetric SAR interferometry. Presented at the Workshop on PolinSAR, Frascatti, January 2003.

Moreira, A., Prats-Iraola, P., Younis, M., Krieger, G., Hajnsek, I., Papathanassiou, K.P., 2013. A tutorial on synthetic aperture radar. IEEE Geosci. Remote Sens. Mag. 1, 6–43. doi:10.1109/MGRS.2013.2248301

Myneni, R.B., Dong, J., Tucker, C.J., Kaufmann, R.K., Kauppi, P.E., Liski, J., Zhou, L., Alexeyev, V., Hughes, M.K., 2001. A large carbon sink in the woody biomass of Northern forests. Proc. Natl. Acad. Sci. 98, 14784–14789. doi:10.1073/pnas.261555198

Onaindia, M., Dominguez, I., Albizu, I., Garbisu, C., Amezaga, I., 2004. Vegetation diversity and vertical structure as indicators of forest disturbance. For. Ecol. Manag. 195, 341–354. doi:10.1016/j.foreco.2004.02.059

Papathanassiou, K.P., Cloude, S.R., 2001. Single-baseline polarimetric SAR interferometry. IEEE Trans. Geosci. Remote Sens. 39, 2352–2363. doi:10.1109/36.964971

Pardini, M., Cantini, A., Lombardini, F., Papathanassiou, K., 2014. 3-D Structure Of Forests: First Analysis of Tomogram Changes Due to Weather and Seasonal Effects at L-Band, in: EUSAR 2014; 10th European Conference on Synthetic Aperture Radar; Proceedings of. Presented at the EUSAR 2014; 10th European Conference on Synthetic Aperture Radar; Proceedings of, pp. 1–4.

Pardini, M., Torano Caicoya, A., Kugler, F., Lee, S.-K., Hajnsek, I., Papathanassiou, K., 2012. On the estimation of forest vertical structure from multibaseline polarimetric SAR data, in: Geoscience and Remote Sensing Symposium (IGARSS), 2012 IEEE International. Presented at the Geoscience and Remote Sensing Symposium (IGARSS), 2012 IEEE International, pp. 3443–3446. doi:10.1109/IGARSS.2012.6350680

Parker, G.G., Russ, M.E., 2004. The canopy surface and stand development: assessing forest canopy structure and complexity with near-surface altimetry. For. Ecol. Manag. 189, 307–315. doi:10.1016/j.foreco.2003.09.001

Pretzsch, H., 2014. Canopy space filling and tree crown morphology in mixed-species stands compared with monocultures. For. Ecol. Manag. 327, 251–264. doi:10.1016/j.foreco.2014.04.027

Pretzsch, H., 2009. Forest Dynamics, Growth, and Yield, in: Forest Dynamics, Growth and Yield. Springer Berlin Heidelberg, pp. 1–39.

Pretzsch, H., 2006. Species-specific allometric scaling under self-thinning: evidence from long-term plots in forest stands. Oecologia 146, 572–583. doi:10.1007/s00442-005-0126-0

Pretzsch, H., Biber, P., 2005. A Re-Evaluation of Reineke's Rule and Stand Density Index. For. Sci. 51, 304–320.

Reineke, L.H., 1933. Perfecting a stand-density index for even-aged forests. J Agric Res 46, 627–638.

Rötzer, T., Grote, R., Pretzsch, H., 2005. Effects of environmental changes on the vitality of forest stands. Eur. J. For. Res. 124, 349–362. doi:10.1007/s10342-005-0086-2

Saatchi, S.S., Harris, N.L., Brown, S., Lefsky, M., Mitchard, E.T.A., Salas, W., Zutta, B.R., Buermann, W., Lewis, S.L., Hagen, S., Petrova, S., White, L., Silman, M., Morel, A., 2011. Benchmark map of forest carbon stocks in tropical regions across three continents. Proc. Natl. Acad. Sci. 108, 9899–9904. doi:10.1073/pnas.1019576108

Saatchi, S.S., Houghton, R.A., Santos Alvalá, R.C. Dos, Soares, J.V., Yu, Y., 2007. Distribution of aboveground live biomass in the Amazon basin. Glob. Change Biol. 13, 816–837. doi:10.1111/j.1365-2486.2007.01323.x

Santoro, M., Beer, C., Cartus, O., Schmullius, C., Shvidenko, A., McCallum, I., Wegmüller, U., Wiesmann, A., 2011. Retrieval of growing stock volume in boreal forest using hyper-

temporal series of Envisat ASAR ScanSAR backscatter measurements. Remote Sens. Environ. 115, 490–507. doi:10.1016/j.rse.2010.09.018

Schneider, T., Elatawneh, A., Rahlf, J., Kindu, M., Rappl, A., Thiele, A., Boldt, M., Hinz, S., 2013. Parameter Determination by RapidEye and TerraSAR-X Data: A Step Toward a Remote Sensing Based Inventory, Monitoring and Fast Reaction System on Forest Enterprise Level, in: Krisp, J.M., Meng, L., Pail, R., Stilla, U. (Eds.), Earth Observation of Global Changes (EOGC), Lecture Notes in Geoinformation and Cartography. Springer Berlin Heidelberg, pp. 81–107.

Shugart, H.H., Saatchi, S., Hall, F.G., 2010. Importance of structure and its measurement in quantifying function of forest ecosystems. J. Geophys. Res. Biogeosciences 115, G00E13. doi:10.1029/2009JG000993

Simard, M., Pinto, N., Fisher, J.B., Baccini, A., 2011. Mapping forest canopy height globally with spaceborne LiDAR. J. Geophys. Res. Biogeosciences 116, G04021. doi:10.1029/2011JG001708

Solomon, S., Quin, D., Manning, M., Chen, Z., Marquis, M., Averyt, K.B., Tignor, M., Miller, H.L. (Eds.), 2007. Climate change 2007: the physical science basis ; contribution of Working Group I to the Fourth Assessment Report of the Intergovernmental Panel on Climate Change, 1st published. ed. Cambridge Univ. Press, Cambridge.

Spencer, H., 1864. The Principles of Biology. William and Norgate.

Thiel, C.J., Thiel, C., Schmullius, C.C., 2009. Operational Large-Area Forest Monitoring in Siberia Using ALOS PALSAR Summer Intensities and Winter Coherence. IEEE Trans. Geosci. Remote Sens. 47, 3993–4000. doi:10.1109/TGRS.2009.2021469

Thompson, D.W., 1917. On growth and form. Cambridge [Eng.] University press.

Toraño, A.C., Kugler, F., Hajnsek, I., Papathanassiou, K.P., 2016a. Large scale biomass classification in boreal forests with TanDEM-X data. IEEE Trans. Geosci. Remote Sens. (accepted for publication)

Toraño, A.C., Kugler, F., Pretzsch, H., Papathanassiou, K.P., 2015b. Forest vertical structure characterization for estimating aboveground biomass. Can. J. For. Res.

Toraño, A.C., Pardini, M., Hajnsek, I., Papathanassiou, K.P., 2015c. Forest aboveground biomass estimation from vertical reflectivity profiles at L-Band. IEEE Geosci. Remote Sens. Lett.

Transparentforests | ESA's ARTES Applications [WWW Document], n.d. URL https://artes-apps.esa.int/projects/transparentforests (accessed 5.18.15).

Treuhaft, R.N., Gonçalves, F.G., Drake, J.B., Chapman, B.D., Santos, J.R. dos, Dutra, L.V., Graça, P.M.L.A., Purcell, G.H., 2010. Biomass estimation in a tropical wet forest using Fourier transforms of profiles from LiDAR or interferometric SAR. Geophys. Res. Lett. 37, L23403. doi:10.1029/2010GL045608

van Laar, A., Akça, A., 2007. Forest Mensuration, 2nd edition. ed. Springer, Dordrecht.

Wagner, W., Luckman, A., Vietmeier, J., Tansey, K., Balzter, H., Schmullius, C., Davidson, M., Gaveau, D., Gluck, M., Le Toan, T., Quegan, S., Shvidenko, A., Wiesmann, A., Yu, J.J., 2003. Large-scale mapping of boreal forest in SIBERIA using ERS tandem coherence and JERS backscatter data. Remote Sens. Environ. 85, 125–144. doi:10.1016/S0034-4257(02)00198-0

Wardle, D.A., Hörnberg, G., Zackrisson, O., Kalela-Brundin, M., Coomes, D.A., 2003. Long-Term Effects of Wildfire on Ecosystem Properties Across an Island Area Gradient. Science 300, 972–975. doi:10.1126/science.1082709

Yoda, K., Kira, T., Ogawa, H., Hozumi, K., 1963. Yoda K, Kira T, Ogawa H, Hozumi K (1963) Self-thinning in overcrowded pure stands under cultivated and natural conditions. J. Inst. Polytech. Osaka City Univ., D 107–129.

Zenner, E.K., Hibbs, D.E., 2000. A new method for modeling the heterogeneity of forest structure. For. Ecol. Manag. 129, 75–87. doi:10.1016/S0378-1127(99)00140-1

6 Publication summary

6.1 List of original publications

I. Torano Caicoya, A., Kugler, F., Papathanassiou, K., Pretzsch, H., 2015. Forest vertical structure characterization using ground inventory data for the estimation of forest aboveground biomass. Can. J. For. Res. doi:10.1139/cjfr-2015-0052

II. Toraño, A.C., Kugler, F., Hajnsek, I., Papathanassiou, K.P., 2016. Large scale biomass classification in boreal forests with TanDEM-X data. IEEE Trans. Geosci. Remote Sens. (accepted for publication)

III. Toraño, A.C., Pardini, M., Hajnsek, I., Papathanassiou, K.P., 2015. Forest aboveground biomass estimation from vertical reflectivity profiles at L-Band. IEEE Geosci. Remote Sens. Lett. (In Press). doi: 10.1109/LGRS.2015.2477858

6.2 I. Forest vertical structure characterization using ground inventory data for the estimation of forest aboveground biomass

Journal: Canadian Journal of Forest Research (CJFR)

Authors: Astor Torano Caicoya, Florian Kugler, Hans Pretzsch, Konstantinos Papathanassiou

Impact Factor: 1.683 (2014)

Contribution: Most of the writing of this article was carried out by the author. Corrections and the development of the content was achieved with the suggestions of the co-authors. The author was responsible for the processing of the forest inventory databases into variables readable for programing languages and also developed a vertical biomass model under the close supervision of Florian Kugler. The author developed the structure characterization ratio and was responsible for the development, evaluation and validation of a structure-to-biomass allometric expression, which lead to a reduction in the variance of the biomass estimation. This contribution also led to a novel methodology for the calculation of a structure-based allometric level estimator.

Summary: Allometric equations have been commonly used to estimate forest biomass by means of forest height. However, changing forest density or structure heterogeneity biases the allometric relationships that have been studied in the recent times. In this paper, the potential of vertical forest structure allometric relationships for biomass inversions has been investigated from a biophysical perspective. The main objective is the investigation of vertical forest structure as a parameter that can be measured from RS systems such as synthetic aperture radar, which are sensitive to the vertical distribution of forest biomass.

This study was based on inventory data from the Traunstein and Ebersberg test sites. These sites are located in Bavaria (southeast Germany) and were selected to be two typical temperate forests but with very different forest structural conditions in terms of vertical and horizontal heterogeneity. Traunstein being a close-to-nature managed forest presents very heterogeneous conditions, with mixed species (mainly *Picea abies, Fagus sylvatica and Abies alba*) and high

levels of biomass. Ebersberg, which is a productive forest, is managed as a homogenous monoculture of *Picea abies* (Norway spruce).

In order to characterize the vertical structure, vertical biomass profiles were modeled from forest inventory data. However, due to the complexity of the profile curve a characterization based on the Legendre decomposition was performed. For this, a structure ratio, which uses low Legendre frequencies, was proposed as structure descriptor. First, it was observed that the first four polynomials were enough to explain more than the 90% of biomass represented by the profile. Second, after a normalization process which isolates the relative structure information (independent from the total biomass of the profile) it was observed that the ratio between the first Legendre polynomial (lowest frequency) and the following three polynomials (high frequencies) was directly proportional to biomass for a constant dominant (profile) height.

The sensitivity of the structure ratio to biomass was studied, concluding that the numerator of the ratio was proportional to the stem biomass while the denominator was proportional to the crown biomass. Therefore, and according to literature, the connection of the ratio to biomass could be explained.

Finally, a structure-to-biomass inversion expression was developed, which using the structure and the dominant forest height, was able to improve for aboveground biomass estimations. Results from the structure-to-biomass inversion algorithm show a clear improvement with respect to traditional height-to-biomass expressions, with increasing correlation factor (r^2) from 0.52 to 0.75 for Traunstein and from 0.51 to 0.72 for Ebersberg, and reducing the root mean square errors from 75.32 to 47.56 Mg/ha and from 73.25 to 42.13 Mg/ha, respectively. An allometric level calculated from the structure ratio could further adapt the difference in slopes from the two sites, reducing the need of empirical estimations and making the inversion more robust.

6.3 II. Large Scale Biomass Classification in Boreal Forests with TanDEM-X Data

Journal: IEEE Transactions on Remote Sensing (TGRS)

Authors: Astor Torano Caicoya, Florian Kugler, Irena Hajnsek, Konstantinos Papathanassiou

Impact Factor: 3.514 (2014)

Contribution: The author did the most of the writing together with Florian Kugler, who had a greater contribution especially in section IV. The author was responsible for the last stage of processing from the TanDEM-X acquisition using procedures developed from Florian Kugler. Moreover, the author performed the estimation of forest height and biomass for each data set and acquisition and developed a performance analysis procedure to estimate forest biomass classes. Finally, the author was also responsible for the validation of the biomass classification methodology and adaption of the biomass maps for the comparisons against pre-existing classifications like CORINE, together with the estimation of the confusion matrices.

Summary: This paper is focused on the large scale mapping of boreal forests biomass using an approach that can be applied to standard DEM TanDEM-X products, the only mission product with full global coverage. Many biomass estimation and large scale classifications exist in the literature. However, systematic classification approaches are missing. A biomass classification with measureable error and performance amylases in boreal forest environments is proposed here.

Boreal forest ecosystems are characterized by a rather homogenous stand structure, which has the advantage that by means of a single allometric equation the estimation biomass from forest height is possible with sufficient accuracy. Therefore, the performance of one equation, which only needs one variable, can be evaluated for quantitative biomass classifications in the entire boreal region.

The interferometric coherence from TanDEM-X DEM data is used to estimate forest height. The accuracy of the height inversion is evaluated first for single bistatic acquisitions under summer and winter conditions. Due to the lack of observations to estimate all the variables required in the inversion model (Random Volume over Ground-RVoG) the impact of the assumptions of constant values for the extinction and ground-to-volume ratios were evaluated. The availability of dual baseline scenarios allowed the estimation of an extra variable reducing the impact of the assumptions in the height inversion and increasing the estimation performance. In the case of the dual baseline scenario, only acquisitions in different seasons (winter/summer) were able to improve the height inversion. Changes in the volume and ground response due to the seasonality effects produced a phase center height difference, which allowed the estimation of an extra parameter. If both interferograms were acquired under summer conditions no phase difference was observed.

Once forest height is estimated, an allometric equation was used to calculate aboveground biomass. Data from two forest sites, boreal (Krycklan) and hemi-boreal (Remningstorp) in north and southern Sweden, respectively, were investigated. The differences, especially in the winter conditions, from the two sites made the analyses valuable for the characterization of the variability within the boreal region.

The number of biomass classes that can be potentially obtained for all the scenarios considered in this paper was estimated from a performance analysis. Height estimation accuracy was the driver of the performance, therefore varying between single and dual inversion scenarios and seasons. For summer acquisitions, four biomass classes can be obtained, with a maximum biomass class of >200 Mg/ha. For winter acquisitions or when a mixed summer – winter approach is applied, five biomass classes, up to 220 Mg/ha, can be obtained.

The resulting classification for the optimum scenarios in winter conditions was evaluated against a forest/non-forest classification derived from the European thematic land-cover classification CORINE. The forest non-forest boundary was considered for the TanDEM-X classification in 20 Mg/ha while in the case of CORINE the forest class was just done grouping the coniferous, broadleaves and mixed forest classes. The TanDEM-X classification showed a very good agreement with CORINE, and was able improve to further improve the forest class by adding quantitative forest biomass classes with a higher spatial resolution of 16x16 m, in contrast

to the 100x100 of CORINE. Moreover, the higher special accuracy allowed a better characterization of the smallest patches of forest. Using confusion matrices to evaluate both, single and dual baseline scenarios, overall accuracies ~90% were observed for all scenarios.

6.4 III. Forest aboveground biomass estimation from vertical reflectivity profiles at L-Band

Journal: IEEE Geoscience and Remote Sensing Letters (GRSL)

Authors: Astor Torano Caicoya, Matteo Pardini, Irena Hajnsek, Konstantinos Papathanassiou

Impact Factor: 2.095 (2014)

Contribution: The author was responsible for most of the writing of the manuscript with help from Matteo Pardini in section II.B. The main contribution from the author was the bio-physical interpretation of vertical profiles obtained from SAR Tomographic techniques towards their use in a structure-to-biomass allometric expression. The estimation of the original SAR reflectivity profiles was done by Matteo Pardini. The author also developed novel techniques to correct for SAR extinction effects on the SAR reflectivity profiles and adapted a forest height estimation algorithm tested for P-band profiles to the L-band data set. Finally, the author developed and corrected the structure-to-biomass allometric approach to the biomass adapted SAR profiles and generated the final biomass maps from the SAR data set.

Summary: Forest vertical structure parameters can be accessed using Synthetic Aperture Radar (SAR) system configurations thanks to tomographic techniques (TomoSAR). In this manuscript, SAR reflectivity profiles are used to extract structure information in the test site of Traunstein (Southeast Germany) and to evaluate its potential for the improvement of biomass estimations in highly heterogeneous forest environments.

Forest height is the most important parameter for the allometric estimation of aboveground forest biomass (AGB). However, variable forest stand densities and heterogeneity in the vertical structure limit the performance of the allometric estimation of AGB from height measurements alone. However, the use of vertical forest structure information as an indicator for the variation of stand density has been proposed and used to improve the allometric estimation of AGB from height measurements.

In this work, L-band reflectivity profiles reconstructed from data at different polarizations (HH and HV) and acquired under "moist" and "dry" weather conditions, were investigated. A structure ratio, based on a Legendre polynomial decomposition, which was derived for vertical biomass profiles, needs to be now adapted to the vertical reflectivity profiles. A reflectivity profile is not sensitive to all the forest compartments and therefore the relation between the Legendre frequencies changes, impacting the proportionality of the structure ratio to AGB. The main change in the inversion respect to the vertical biomass profiles is the change in sign of the structure ratio, which shows an inverse proportionality. This is explained by the dominance of the crown compartment, which in absence of the stem response mainly affects the structure ratio. For this reason, an increase of the high frequencies (crown) response, which is proportional to the forest density, will decrease the value of the ratio when increasing the biomass.

The proposed allometric AGB estimator increases the correlation factor from 0.60 to 0.81 and reduces the RMSE from 50.25 Mg/ha to 36.30 Mg/ha when compared to the AGB estimation from forest height alone. The best results correspond to the "moist" acquisition using the HH polarization. The influence of the weather conditions and the polarization can impact the estimation, although the inversion results have remained for all cases within a 10 % difference respect to the best-case scenario. For all conditions we observe a constant improvement of ~20% when compared to height-only allometry. The sensitivity of HV to the vertical structure is higher than in HH, a better height estimation in HH (main lobes are closer to top of the canopy) leads to overall better inversion results. This effect also influences the inversions in "dry" conditions: due to the lower extinction, the height estimation performance decreases and the reflectivity becomes less sensitive to the forest volumes affecting the performance of the inversion algorithm.

I

NRC Research Press

ARTICLE

Forest vertical structure characterization using ground inventory data for the estimation of forest aboveground biomass

Astor Toraño Caicoya, Florian Kugler, Hans Pretzsch, and Konstantinos Papathanassiou

Abstract: A common method for estimating forest biomass is to measure forest height and apply allometric equations. However, changing forest density or structure heterogeneity increases the variability of the known allometric relationship. Here, we investigated the potential of allometric relationships based on vertical forest structure for biomass inversions with a global potential. First, vertical biomass profiles, which were calculated from ground forest inventory data, were used to model forest vertical structure. Then, a vertical structure ratio based on Legendre polynomials was proposed as a structural descriptor and its sensitivity to biomass was evaluated. Finally, we developed a structure-to-biomass inversion expression that could be extrapolated for aboveground biomass estimations. This is a case study based on inventory data from the Traunstein and Ebersberg test sites, two temperate forests located in southeastern Germany with different forest structural conditions. Results from the structure-to-biomass inversion algorithm show a clear improvement with respect to traditional height-to-biomass expressions, with increasing correlation factor (r^2) from 0.52 to 0.73 for Traunstein and from 0.51 to 0.76 for Ebersberg and reducing the root mean square errors from 75.32 to 47.56 Mg·ha^{-1} and from 73.25 to 48.31 Mg·ha^{-1}, respectively.

Key words: allometry, self-thinning, temperate forest, stand density, Legendre decomposition, ground inventory data.

Résumé : Une méthode classique pour estimer la biomasse forestière consiste à mesurer la hauteur de la forêt et à appliquer des équations allométriques. Cependant, la variation ou l'hétérogénéité de la structure de la forêt augmente la variabilité de la relation allométrique connue. Nous avons étudié le potentiel des relations allométriques fondées sur la structure verticale de la forêt pour les inversions de la biomasse avec un potentiel global. Premièrement, les profils verticaux de biomasse, qui ont été calculés à partir de données d'inventaire forestier sur le terrain, ont été utilisés pour modéliser la structure verticale de la forêt. Ensuite, un ratio de structure verticale basé sur les fonctions polynomiales de Legendre a été proposé comme descripteur de la structure et sa sensibilité à la biomasse a été évaluée. Finalement, nous avons développé une expression d'inversion de la structure à la biomasse qui pouvait être extrapolée pour estimer la biomasse aérienne. Il s'agit d'une étude de cas supportée par des données d'inventaire provenant des sites d'essai de Traunstein et d'Ebersberg, deux forêts tempérées situées dans le sud-est de l'Allemagne dont la structure diffère. Les résultats de l'algorithme d'inversion de la structure à la biomasse représentent une nette amélioration par rapport aux expressions traditionnelles de hauteur à biomasse avec une augmentation du coefficient de corrélation (r^2) de 0,52 à 0,73 à Traunstein et de 0,51 à 0,76 à Ebersberg et une réduction de l'erreur quadratique moyenne de respectivement 75,32 à 47,56 et 73,25 à 48,31 Mg·ha^{-1}. [Traduit par la Rédaction]

Mots-clés : allométrie, éclaircie naturelle, forêt tempérée, densité du peuplement, décomposition de Legendre, données d'inventaire sur le terrain.

Introduction

Forest biomass is an essential part of the terrestrial carbon pool; therefore, it is a very important contribution in the global carbon cycle (Drake et al. 2002; Houghton et al. 2009). Forest biomass is a main variable for mapping the amount and geographic distribution of forests and its change in time is required to understand the development of carbon fluxes (Brown 2002). However, biomass stock and spatial distributions are still unknown parameters for many forest regions of the world. Thus, the magnitude, location, and cause of terrestrial carbon sinks and sources are not well quantified on a global scale (Houghton et al. 2009). Therefore, methodologies capable of retrieving biomass and forest dynamics at a global scale are highly sought.

Accurate terrestrial biomass measurements are time consuming, expensive, and rare (Houghton 2005). Forestry science aims to reduce the effort of measuring biomass with the help of allometric functions that can estimate biomass from easily measurable tree variables such as diameter at breast height (dbh), basal area, top tree height, and form factor (factor between the volume contained in the real-shaped stem and a cylinder with a section that has a diameter equal to the dbh and same height). However, single-tree measurements are ineffective for large areas and global applications. In contrast, forest stand parameters are an option with great potential as remote sensing (RS) systems can measure them globally. To develop methodologies that use forest stand parameters to estimate aboveground biomass (AGB), new allometric relationships need to be derived and investigated.

Received 4 February 2015. Accepted 17 September 2015.

A. Toraño Caicoya, F. Kugler, and K. Papathanassiou. Radar Concepts Department, Microwaves and Radar Institute, German Aerospace Center (DLR), (DLR-HR), D-82234 Oberpfaffenhofen, Germany.
H. Pretzsch. Chair for Forest Growth and Yield Science, Center of Life and Food Sciences Weihenstephan, Technische Universität München, Hans-Carl-von-Carlowitz-Platz 2, 85354 Freising, Germany.
Corresponding author: Astor Toraño Caicoya (e-mail: astor.toranocaicoya@dlr.de).

Published at www.nrcresearchpress.com/cjfr on 29 September 2015.

A first approach in this direction was introduced in Mette et al. (2003). AGB is estimated using allometric relationships based on forest stand height. This allometric approach used a power law equation that relates biomass to height and uses an empirically derived allometric level (l_a):

$$(1) \qquad B_a = l_a 1.66 H^b$$

where B_a is the stand (aboveground) biomass (Mg·ha^{-1}), H is forest dominant height or $H100$ (height of the 100 thickest trees per hectare (Laar and Akça 2007)), and b is an allometric exponent. This height-to-biomass allometry allowed biomass estimations from methodologies that are capable of resolving forest height. Several techniques, in addition to ground forest inventory data, can estimate forest height, e.g., photogrammetry (Næsset 2002; Schneider et al. 2013), light detection and ranging (LiDAR) (Dubayah and Drake 2000), and polarimetric synthetic aperture radar (SAR) interferometry (Pol-InSAR) (Papathanassiou and Cloude 2001). Height-to-biomass allometric relationships proved to be robust under homogenous forest conditions and able to accurately estimate AGB from forest dominant height for the predominant temperate European tree species. However, the diversity in forest structure can reduce the precision of this allometric relationship (Toraño et al. 2010), thus reducing its accuracy for AGB estimations in forest stands with a heterogeneous structure. Forest structure is then described, in the most general terms, as the distribution of biomass in space, i.e., as a vertical and horizontal spatial arrangement of tree species, tree sizes, or ages (Zenner and Hibbs 2000), which can be measured by distribution of age classes, arrangement of species into different canopy layers, and distribution of individuals among diameter classes.

Studies based on conventional forest yield related stand parameters, e.g., dbh, basal area, or height, have tended to neglect three-dimensional (3-D) stand structures (Onaindia et al. 2004), and there is not a clear understanding regarding the allometric relationship that conditions the vertical and horizontal distribution of forest layers and structures (Köhler and Huth 2010). A study of the horizontal structures characterizing forest stand density (Pretzsch and Biber 2005) showed a strong relationship between AGB and horizontal forest structure.

New RS techniques such as multibaseline Pol-InSAR (Cloude 2006; Dinh et al. 2012; Treuhaft et al. 2010) and full-waveform LiDAR (Harding et al. 2001; Lefsky et al. 2005) enable measurements of variables that in addition to forest height are connected to forest vertical structure. The majority of these methods have attempted to quantify forest vertical structure (Hall et al. 2005; Parker and Russ 2004; Drake et al. 2002), finding good correlations between AGB and height metrics or percentiles that are connected to the vertical organization of the forest stand canopy. However, studies based on structures cannot be directly compared among systems and (or) with ground measurements, as is done in the case of forest height, which is, in fact, a physically derived variable. Structure is a variable of complex definition and each RS system is sensitive to different compartments of the vertical biomass distribution (stems, crowns, leaves, etc.).

Due to this difficulty and the limitations of homogenization of methodologies that account for the different system responses, in this study, we have focused on the vertical biomass distribution obtained from ground data from forest inventories. In this way, vertical biomass profiles (independent from the measuring system) can be used to analyze and (or) quantify the relationships that exist, at a biophysical level, between forest vertical structure and biomass. These can be interpreted not only as a base for RS applications, but also towards silvicultural investigations. Therefore, the allometric relationships between all vertical elements represented by the vertical structure profile and biomass need to be investigated. For this purpose, polynomial series decompositions (Cloude 2006; Toraño et al. 2010) arise as a suitable method that can characterize and preserve these relationships, contrary to single metrics.

Allometric theory: from the single tree to the stand

The connection between allometry and growth is outlined in the theory of dynamic morphology (Bertalanffy 1942). One of the key allometric patterns observed for both plant and animal communities is the inverse relationship between body mass and density. Therefore, the physiological relevance of allometric functions lies in the interpretation that the proportion of the total growth energy received by an organism is proportional to its relative size. This principle can be transferred to the population (stand) using the self-thinning rule, according to which the number of individuals is reduced while they compete for resources, increasing their size until the stand reaches a maximum ecological AGB (carrying capacity) (Luyssaert et al. 2008).

Allometric theory predicts then that the total number of individuals per unit area (N) is proportional to the total body mass (M) per unit area (–3/2 power) (Yoda et al. 1963). Applying these scaling laws to entire communities, organismal interspecific interactions can link larger scaled allometric properties of communities across different ecosystems (Enquist and Niklas 2001). Accordingly, Pretzsch (2009) describes how the first version of Eichhorn's rule identified that the statistical relationship between stand mean height and standing volume is valid for more or less untreated stands. Especially, the interpretation of Eichhorn's rule, according to Assmann (1961), lies on an estimation of total production in relationship with age, height, and yield classes. Extensions of allometric and biomechanical theory predict that the total standing community biomass will not vary with respect to species composition or latitude (Enquist and Niklas 2001).

Allometric principles for quantifying vertical forest structure

Recent studies have started to incorporate forest structure heterogeneity variables that are not only considering 1-D variables, but also a 3-D forest representation with horizontal and vertical components (Lefsky et al. 2005; Zenner and Hibbs 2000). Connections provided by such studies have led to new theories that provide a basis for extrapolation of small-scale and high-resolution measurements, as well as for testing and verifying 3-D measurements (Parker et al. 2004).

To understand the mechanistic essence of allometric relationships such as the self-thinning rule, a thorough understanding of the relationship between spatial interactions among individuals and spatial arrangements of these individuals is needed (Li et al. 2000). The existing forest structures enable trees to influence factors such as light, temperature, and precipitation, which in turn influence growth and determine the competition among trees for resources and the biomass production (Pretzsch 2009). In this way, a 3-D stand structure determines the stability of a forest to a large extent and defines its dynamics (evolution in time) (Onaindia et al. 2004).

The interactions between trees are explained according to Pretzsch (2009) as a process with two feedback loops that proceed at different time scales. In the first feedback loop, the local environmental conditions within the stand are influenced by the structure of the canopy, which provides crucial feedbacks between structure, environment, and growth, drives population dynamics (Pretzsch 2014), and controls the absorption of photosynthetically active radiation (Parker et al. 2004). Because processes modify structures, the resulting structures can assist the interpretation of those processes that are more difficult to measure or observe. The structural relationships of processes and of individual trees also scale-up to generate emergent properties of forests such as size, structure, and spacing relationships (Enquist et al. 2009). Hence, all of these interactions indicate that

Table 1. Characteristics of the two test sites.

	Bürgerwald Traunstein	Ebersberger Forst
Forest type	Temperate forest	Temperate forest
Biomass range (Mg·ha^{-1})	40–450	40–350
Height range (m)	10–45	5–40
Stand density[a] (stems·ha^{-1}) (minimum/mean/maximum)	20/1960/2140	20/1530/8400
Main species (proportion, %)	Norway spruce (29%), European beech (28%), silver fir (18%)	Norway spruce
Management	Close-to-natural silviculture	Intensively managed for timber production
Area (ha)	230	3400
Number of plots	228	3468
Plot size (m^2)	500	400
Spatial grid (m)	100×100	100×100
Average slope (%)	22	5
Location	47°51′32.45″N, 12°39′20″E	48°6′56″N, 11°53′31″E

[a]Stand density is calculated without trees with diameter at breast height (dbh) < 7.5 cm.

forest vertical structure is intrinsically related to forest evolution. In conclusion, the stock of forest biomass is determined by the vertical and horizontal arrangement of trees; it varies over time because of numerous intraspecific stand structural interactions and disturbances and is defined, at the same time, by the site conditions, i.e., climate and soil conditions. An understanding of the relationship between these parameters is essential for improving allometric AGB estimations.

Objectives

The objective of this study is to investigate and describe the relevance of stand structural variables that can be globally connected to estimate AGB. Specifically, this paper is organized as follows: (*i*) we propose an allometric model to derive a forest vertical biomass function from ground forest inventory data; (*ii*) we propose a new methodology to characterize forest vertical structure; (*iii*) we investigate the allometric relevance of the vertical structure characterization; and (*iv*) we develop a structure-to-biomass inversion expression for AGB estimations combining forest height and a vertical structure descriptor.

Materials and methods

Test sites

We investigated inventory data from two different test sites in Bavaria (south of Germany) that represent different stand structures: Bürgerwald Traunstein and Ebersberger Forst. The forest characteristics are summarized in Table 1.

Bürgerwald Traunstein (from now on Traunstein site) is a temperate, mountainous, managed forest with a maximum biomass of 450 Mg·ha^{-1}, maximum forest height of approximately 45 m, and mixed species composition. The main tree species are Norway spruce (*Picea abies* (L.) Karst), European beech (*Fagus sylvatica* L.), and silver fir (*Abies alba* Mill). The forest stand is under "close-to-nature" silvicultural treatments that have produced a highly structured and diverse forest structure. Traunstein has a mean tree density of 1960 stems·ha^{-1}, with 8400 stems·ha^{-1} in the most densely stocked stands and 20 stems·ha^{-1} in the least densely stocked stands. The median density for stands with the highest biomass (B > 400 Mg·ha^{-1}) is 2140 stems·ha^{-1}, which is above the mean tree density.

Ebersberger Forst (from now on Ebersberg site) is an intensively managed forest site formed by a monoculture of Norway spruce on a very flat terrain and is treated using intensive forest management techniques. The inventory plots are generally very homogenous. The biomass range is 40–350 Mg·ha^{-1}, with a maximum forest height of approximately 40 m. Ebersberg has a mean tree density of 1530 stems·ha^{-1}, with 8980 stems·ha^{-1} in the most densely stocked stands and 20 stems·ha^{-1} in the least densely stocked stands. The median density for the stands with highest biomass (B > 400 Mg·ha^{-1}) is 1000 stems·ha^{-1}, which is below the mean tree density.

These investigations relied on inventory data collected in a 10-year cycle by the forest management services. The inventory data for the two Bavarian test sites has been provided according to the inventory system of the Bavarian state forest (Mette et al. 2003). This system is based in three concentric circles in which trees are measured depending on their diameters (Fig. 1): in the inner circle (50 m^2), all trees are measured; in the second circle (150 m^2), trees with a dbh between 10 and 30 cm are measured; and in the largest circle (500 m^2 for Traunstein and 400 m^2 for Ebersberg), only trees with a dbh larger than 30 cm are measured. Depending on each diameter class, expansion factors (×16, ×4, from inside to outside, respectively) are applied to extrapolate the measured trees to the inventory area (largest circle).

3-D structure modeling: vertical biomass profiles

Forest vertical structure is a 3-D variable; therefore, its characterization requires a method that can express this complexity. The solution considered in this study calculated vertical forest biomass profiles, which modeled for each plot the amount of biomass variation with height. To obtain these profiles on a plot level, first the vertical biomass distribution on a tree level is required to be modeled. Adequate models for tree crown and stem forms were required to derive the dry biomass stored in a single tree. These models are introduced in the following sections.

Stem model

Stem radius as function of height was modeled according to the improved Brink's function from von Gadow and Hui (2001) (Appendix A). This function shows good agreement with a theoretical stem shape as the lower section is modeled as a neiolid frustum, the middle section is modeled as a paraboloid frustum, and the upper section is modeled as a cone. Finally, we calculated the biomass enclosed in this volume using species-specific wood densities (World Agroforestry Centre 2011).

Crown model

Crown measurements are very intensive and time consuming; therefore, they are not commonly available in inventory data (Nadkarni et al. 2004). A precise model of the crown layer is required to achieve an accurate representation of the vertical biomass distribution because the forest canopy is a key structural component for understanding and characterizing forest vertical structure, and it has been shown in the past that it is essential for deriving allometric relationships (Lefsky et al. 1999).

We selected a model that describes the species-specific crown shape based on the parameters dbh and tree height. This crown model is based on the investigations of Pretzsch (2009) and is explained below. The model particularly fits the requirements of

Fig. 1. Field inventory plot scheme. For each circle, different diameter at breast height (dbh) classes are measured. Inner circle, 50 m² (dbh < 10 cm); middle circle, 150 m² (10 cm < dbh < 30 cm); outer circle, 500 m² for Traunstein and 400 m² for Ebersberg (dbh > 30 cm).

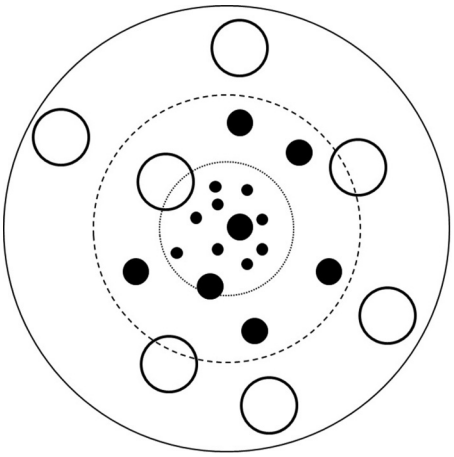

this study because it allows the calculation of average species-specific crown shapes in forested conditions. A representation of the crown model with the required parameters is shown in Fig. 2.

The biometric reproduction of crown perimeter was performed for different species in a standard calculation procedure describing the change in crown radius (r) with increasing distance (dist) from the tree tip. The crown model splits the crown into a sunlit crown and a shaded crown. The sunlit crown is exposed to direct sunlight and its crown radii (r_0) are calculated according to eq. 2:

$$r_0 = a \times \text{dist}^b \quad (2)$$

where the species-specific tree parameter is a and the species-specific exponent is b. The radii in the shaded crown (r_u) were calculated using a linear equation with the species-specific parameters c and d:

$$r_u = c + d \times \text{dist} \quad (3)$$

Values for the parameters a, b, c, and d are species dependent and can be found for the major European tree species as a function of the maximum crown radius (Pretzsch 2009). Using tree height, crown base height, mean crown radius, and the species-specific crown shape parameter, we estimated the spatial expansion of the crown, crown volume, and crown surface area.

For estimating the biomass enclosed by tree crowns, we used a set of allometric equations that were estimated for the Central and Northern European regions (Zianis et al. 2005). These allometric equations were species dependent and were chosen to fit the growing conditions found at the test site. They described crown biomass as a function of dbh and (or) tree height. The equations used are presented in Table 2.

Plot representation

A vertical biomass profile on a plot basis was obtained by summing the vertical distribution of biomass in stems and crowns for every measured tree in the inventory plot. Biomass distribution along the height gives a characteristic profile for each plot. For this, a vertical biomass profile was subsequently generated by summing the biomass of all trees within a measured plot area (0.05 ha) (Fig. 3). Here, 1 m sampling was chosen, which gave a biomass value per metre of height.

Fig. 2. Modeling of the tree volume. Tree stem is described using the Brink function from Klaus von Gadow (Appendix A), where H is the tree height and dbh is the diameter at breast height. The radius of the sunlit crown l_0 is described by the function $r_0 = a \times \text{dist}\ b$ with species-specific parameters a and b. The shaded crown l_u is modeled by the linear equation dist × d. The parameters and variables are as follows: r, crown radius; l, crown length; r_0, sunlit crown radius; l_0, length of the sunlit crown; r_u, shaded crown radius; l_u, length of the shaded crown; r_{max}, largest crown radius; r_{cb}, crown radius at crown base; dist, distance from the tip of the tree; and a, b, c, d, species-specific shape parameters (Pretzsch 2009).

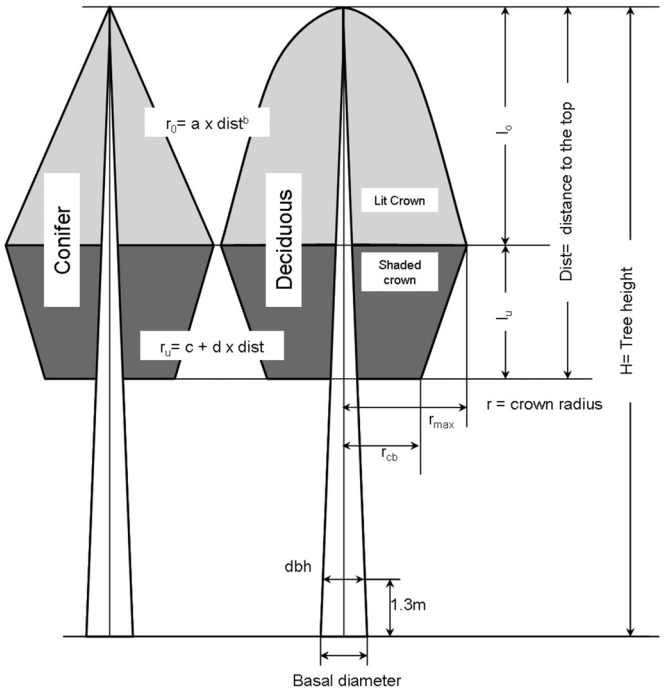

Vertical structure characterization at plot level

Vertical biomass profiles represent the distribution of biomass with forest height; however, the resulting profile is too complex to be applied in an allometric relationship. To evaluate and understand the vertical biomass profiles and the role of vertical structure on biomass at a stand level, we conducted the following: (*i*) decomposed each vertical biomass profile into a set of profiles with variable spatial frequency (Legendre series); (*ii*) analyzed the correlation of each vertical component to biomass; (*iii*) normalized each profile to study the relative vertical structure independently from the total biomass; and (*iv*) combined the low-frequency coefficients into a structure ratio that is sensitive to biomass.

The Legendre decomposition: structure descriptor

The Legendre series were investigated to characterize forest biomass profiles. An evaluation was conducted on multiple inventory plots. The Legendre polynomials ($P(z)$) are solutions of the Legendre's differential equation and can be defined as the coefficients in a Taylor series expansion (Arfken and Weber 2005). The Legendre series ($B(z)$) are described as

$$B(z) = \sum_n a_n P_n(z)$$
$$a_n = \frac{2n+1}{2} \int_{-1}^{1} B(z) P_n(z) \mathrm{d}z \quad (4)$$

where a_n is the Legendre coefficient, $P_n(z)$ is the Legendre polynomial, and n stands for the order of the polynomial. Equation 5

Table 2. Allometric equations selected for deriving crown biomass (Zianis et al. 2005) as a function of tree diameter.

Species	Equation	R^2	dbh[a] range (cm)
Norway spruce (*Picea abies* (L.) Karst.)	Ln(*B*)(Mg) = −0.2804 + 8.5242(0.01 × dbh)/(0.01 × dbh + 13)	0.945	0–50
European beech (*Fagus sylvatica* L.)	B(Mg) = 0.0031 × dbh$^{3.161}$	0.924	—
Silver fir (*Abies alba* Mill.)	B(kg) = 0.0060722 + 9.58 × 10^{-6} × dbh$^{2.5578}$	—	—
Scots pine (*Pinus sylvestris* L.)	Ln(*B*)(Mg) = −2.8604 + 9.1015 × dbh/(dbh + 10)	0.922	0–45
Sessile oak (*Quercus petrea* (Matt.) Liebl.)	B(kg) = 2.1612 × 10^{-4} × dbh^2	—	—

[a]Diameter at breast height, dbh (cm).

Fig. 3. Vertical biomass profile sample obtained from the sum of the biomass of all modeled trees inside an inventory plot in 1 m height samples.

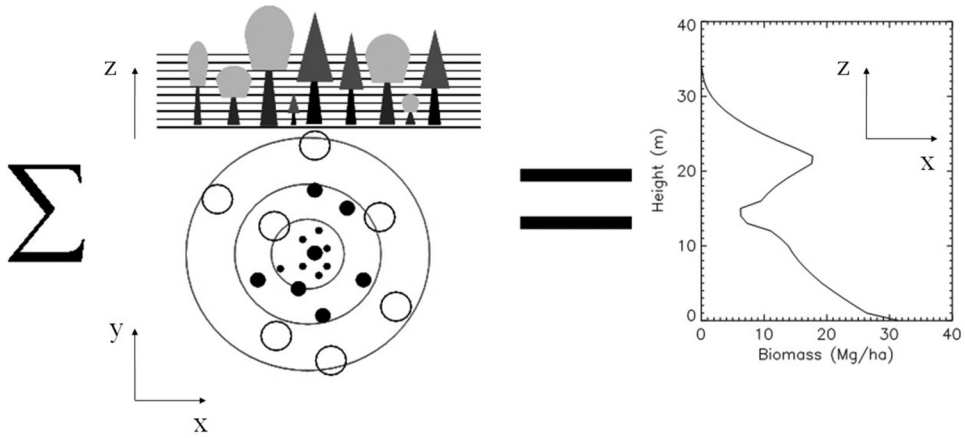

shows the Legendre polynomial up to $n = 4$ as a function of height. Figure 4 shows a vertical representation of these Legendre polynomials.

$$
\begin{aligned}
P_0(z) &= 1 \\
P_1(z) &= z \\
P_2(z) &= \frac{1}{2}(3z^2 - 1) \\
P_3(z) &= \frac{1}{2}(5z^2 - 3z) \\
P_4(z) &= \frac{1}{8}(35z^2 - 30z + 3)
\end{aligned}
\tag{5}
$$

As profile (forest) height is known, the resulting coefficients for the Legendre decompositions are stretched to their correspondent height during the reconstruction of the profile. An example is shown in Fig. 5. A biomass profile was reconstructed using different number of frequencies obtained from the Legendre decomposition (blue).

The number of vertical frequencies that are needed to reconstruct a profile depend on the vertical resolution. The Legendre polynomials tend to reconstruct the original profile with few frequencies and adopt the main features of the profile more easily, particularly in the bottom and the top of the curve.

The Legendre decomposition provides a set of Legendre coefficients (a_0–a_n) for every biomass profile. A Legendre coefficient represents the degree of adjustment between a characteristic polynomial and the biomass profile. The combination of Legendre polynomials allows reconstruction of the corresponding profile: $B_n = a_n P_n(z)$ so that a higher number of polynomials results in a better reconstruction of the original profile. The relationship between the Legendre components (B_n) and the results from the single component profile reconstruction and total biomass are studied in the following sections.

After applying the Legendre decomposition, the Legendre coefficients (a_1–a_n) depend on the total biomass of the profile. Thus, we normalized the biomass profiles to focus the information contained in the biomass profiles to pure structural information. This normalization process allowed a direct comparison between the

Fig. 4. Vertical representation of the Legendre polynomials until order 5 (P_0–$P_4(z)$).

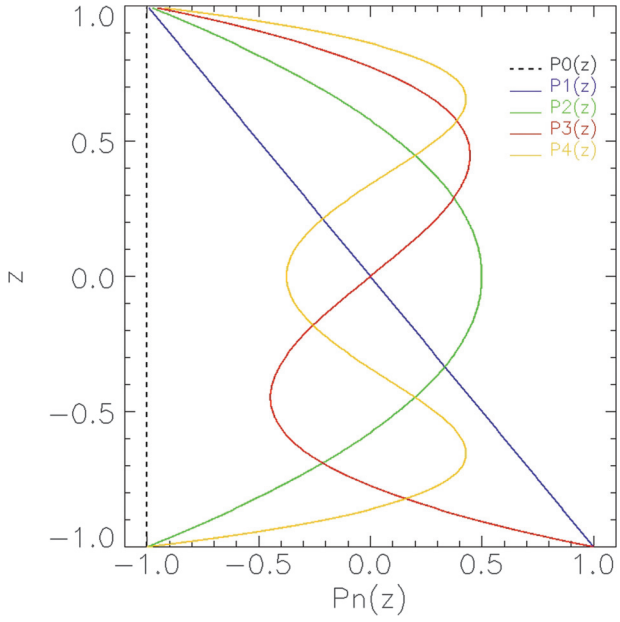

vertical biomass profiles and other normalized vertical profiles. In accordance with the normalization conducted for the polarization coherence tomography profiles (Cloude 2006), each Legendre coefficient (a_n) was normalized using a_0, which contains the total biomass of the profile ($a_{0n} = H/B$). The normalization is done using eq. 6:

$$
a_{0n} = \frac{a_n}{(1 + a_n)} \tag{6}
$$

However, the normalization step, using the Legendre coefficient a_0, decorrelates the structure to a biomass relationship. At

Fig. 5. Biomass profile reconstruction using different number of frequencies obtained from the Legendre decomposition (red). On the right, four polynomials were used, and on the left, 11 polynomials were used.

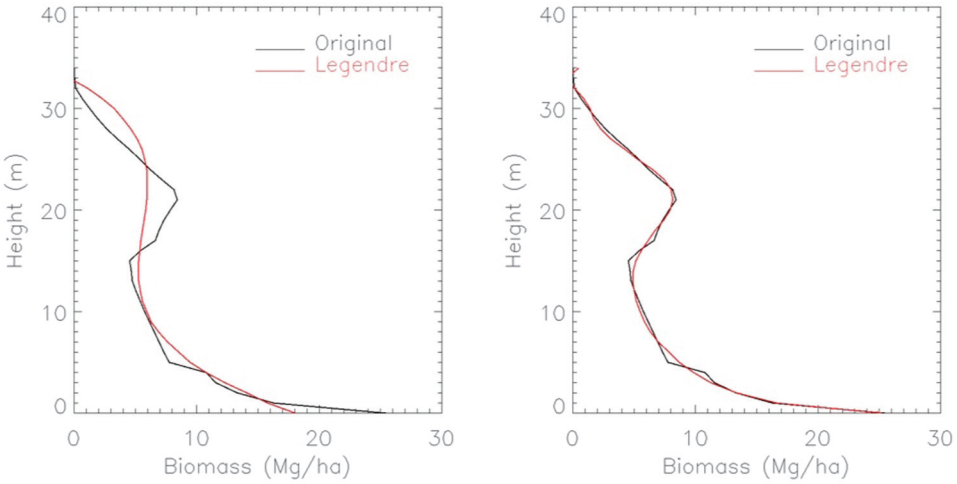

this point, we could not use the direct relationship between the Legendre components and the biomass and were required to find a new descriptor. Therefore, to exploit the relative dependencies between the profile frequencies characterized by the Legendre coefficients, we combined the first four Legendre coefficients into a structure ratio. This ratio, from now on, is called the structure ratio (S_{rat}) and was calculated as the fraction between low- (a_{01}) and high-frequency (a_{02}, a_{03}, a_{04}) Legendre coefficients:

$$S_{rat} = \frac{|a_{01}|}{|a_{02}| + |a_{03}| + |a_{04}|} \quad (7)$$

where a_{0n} are the normalized coefficients. To demonstrate the potential of the structure ratio for interpreting the allometric relationships between the vertical structure and biomass, we calculated the correlation of the structure ratio with the ratio of stem biomass over tree crown biomass.

Structure and scale dependency

Before analyzing the potential of the new structural descriptor, we considered the impact of the stand size on the structure-to-biomass relationship. A small stand size may present limitations to characterize the heterogeneity of the forest structures (Shugart et al. 2010). One solution to this problem was to combine neighboring plots, according to a distance radius criterion, to simulate larger integration areas. However, if only a distance criterion is used, plots that represent differently structured stands (mainly because of forest management) may be erroneously combined. Thus, the relationship of vertical structure to biomass could be lost. Therefore, a structure and height difference criteria between plots was used.

The integration was conducted in the following manner. First, S_{rat} and profile height were calculated for every plot. Then, using a moving window of 150 m (to ensure that the eight closest points were included), S_{rat} and height differences between the central plot and every other plot in the group were calculated. Those plots with differences below certain thresholds were averaged. For S_{rat}, a threshold $S_{rat} > 0.5$ was used, which corresponded to a quarter of the structure range. A height (H) < 15 m threshold was selected for the height difference because this distance would typically avoid the combination of forest stands in different age classes. Finally, a new profile was generated using the data from the combined inventory plots, and new heights and S_{rat} were estimated.

Biomass inversion

The structure-to-biomass inversion expression was developed from the combined height and structure ratio based on the following principle. Those inventory plots that followed the height-to-biomass allometric curve corresponded to forest stands with ideal allometric conditions, which meant a steady state in terms of resources and demographic conditions (Enquist et al. 2009) and also a vertical structure that represented those conditions. Using the relationship observed between forest vertical structure descriptor S_{rat} and the forest biomass, it was possible to compensate for the deviations of the plots that were not representing the expected structural conditions that the height-to-biomass allometric equation predicts. An empirical estimation of the parameters a, b, and c yielded an optimized expression of the structure-to-biomass, thereby determining the structure ratio S_{rat} as a weighting factor (eq. 8):

$$B = aS_{rat}^{b}H^{c} \quad (8)$$

where H is the profile height, which is equivalent to the dominant forest height or $H100$.

Results

From height-to-biomass relationships to a structure allometry

The first application of the Legendre decomposition as a vertical structure indicator of biomass is shown in Fig. 6.

The correlation between biomass and the Legendre components of an order > 4 (B_4) was very low and in all cases < 0.2. This shows that the first four frequencies explain the highest proportion of biomass, and for this reason, they were the ones considered to be studied. The importance of each frequency is detailed below.

The highest correlation coefficient was observed for component B_1 followed by B_3. The slope of the fitting line represented the proportion of the total biomass that was explained by each Legendre component. At both sites, the largest proportion of biomass was explained by component B_3, followed by component B_1, and then component B_2. From component B_4 and upwards, the explained proportion of biomass was negligible. Moreover, a low number of Legendre polynomials (eq. 5) was sufficient to distinguish between different levels of biomass. The importance of these first four polynomials was also illustrated by examining

Fig. 6. Correlation between Legendre components (B_1–B_4, from left to right) and total biomass: (top) Traunstein site; (bottom) Ebersberg site.

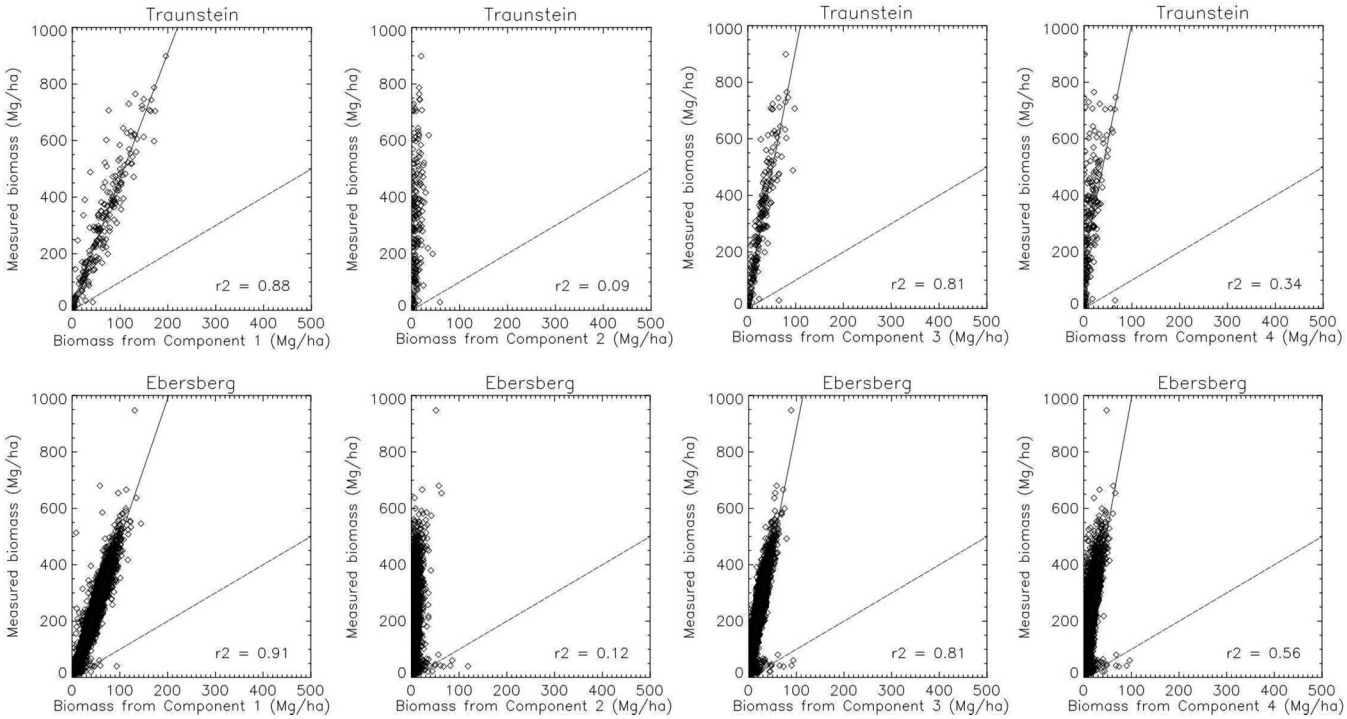

Fig. 7. Maximum (solid) and minimum (dashed) biomass profile reconstruction at 35 m at the test site Traunstein. Four Legendre polynomials are sufficient to detect differences in the profile.

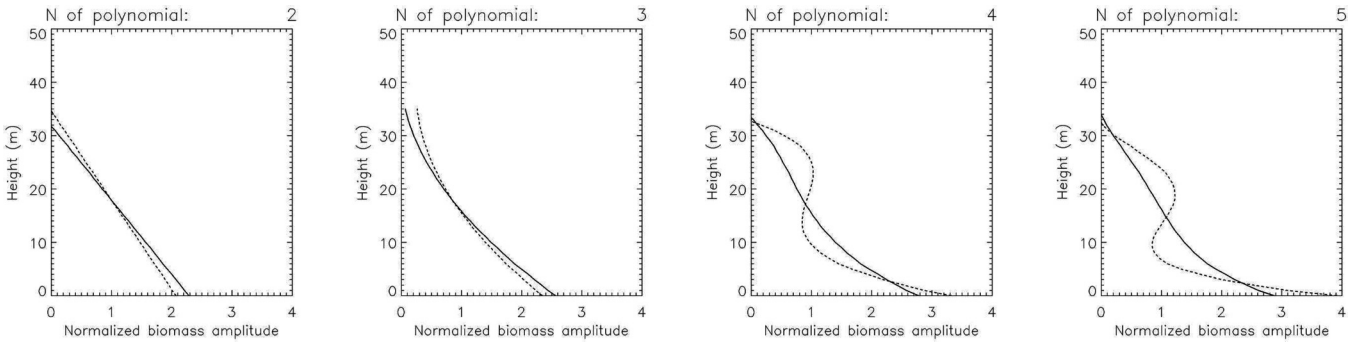

single profiles (Fig. 7). Profiles of 33 m height, with high biomass (dashed) and low biomass (solid), were displayed for reconstructions with five Legendre polynomials. When four or more polynomials were used, it was possible to identify two levels of biomass: the high biomass profile presented with a smoothed shape, which could be interpreted as a higher proportion of the stem compartment biomass; and the low biomass profile presented with a sharper shape, which could be interpreted as a higher proportion of the crown compartment biomass. In Fig. 8, we showed the amplitude of the four Legendre polynomials (a_{01}–a_{04}) for the high and low biomass inventory plots to illustrate the effects of frequency change in the structure ratio. In the profile with a lower biomass (left), even if the amplitude of the first Legendre component (blue) was higher than in the high biomass profile (right), the higher frequencies (components 2, 3, and 4) were dominant, and in total, they were higher than the low-frequency (component 1), which resulted in a reduced structure ratio.

The height-to-biomass equation (eq. 1) was applied to each of the test sites (Fig. 9). The results for the two test sites were similar when we used a common allometric exponent b of 1.58 and an allometric level l_a of 0.78. They resulted in correlation coefficients of 0.34 for Traunstein and 0.48 for Ebersberg and root mean square errors (RMSEs) of 110.59 Mg·ha^{-1} and 88.68 Mg·ha^{-1}, respectively. Traunstein, being a very diverse forest, was characterized by a lower correlation coefficient because a single allometric level could not describe the high variation in stand density. On the other hand, lower stand diversities resulted in slightly higher correlations as seen for the Ebersberg site. The values for biomass were more extreme than expected because of the small size of the inventory plot that was particularly visible in the higher biomass range: mean biomass of ~200 Mg·ha^{-1} for Traunstein and ~151 Mg·ha^{-1} for Ebersberg, and a maximum biomass of 685 Mg·ha^{-1} and 720 Mg·ha^{-1}, respectively (Fig. 9).

The height-to-biomass allometric relationship after the aggregation process is shown in Fig. 10 for Traunstein (right) and Ebersberg (left). The correlation coefficients were 0.52 for Traunstein and 0.55 for Ebersberg and the RMSEs were 75.32 Mg·ha^{-1} and 68.20 Mg·ha^{-1}, respectively. The deviation was reduced with respect to the nonaggregated case; however, the height value range was retained. The mean values for biomass were now ~190 Mg·ha^{-1} for Traunstein and ~154 Mg·ha^{-1} for Ebersberg, with a maximum biomass of 370 Mg·ha^{-1} and 590 Mg·ha^{-1}, respectively. A clear

Fig. 8. Relative amplitude of each of the first five Legendre polynomials for the low biomass profile (left) and the high biomass profile (right).

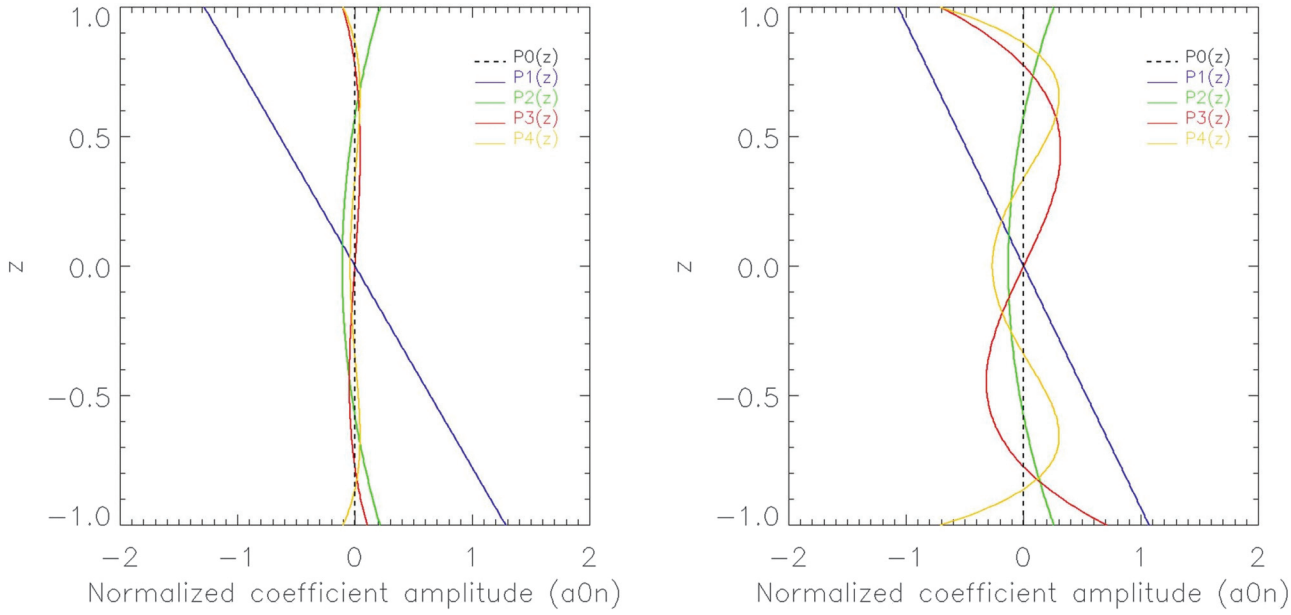

Fig. 9. Height-to-biomass allometry for Traunstein (left) and Ebersberg (right) test sites. Dashed curves correspond to the allometric equation $b = 1.3H^{0.58}$. Both plots are color-coded according to the value of the structure ratio from 0 (blue) to 3 (red).

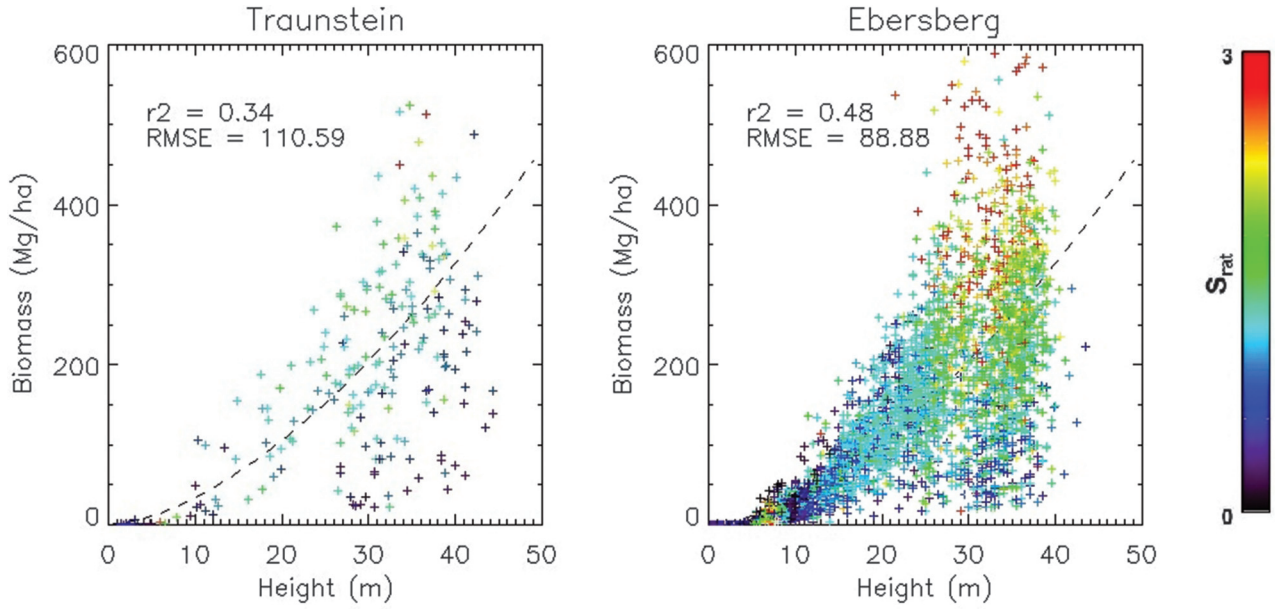

stratification of the structure ratio according to height was observed in both Traunstein and Ebersberg.

In Fig. 10, we show the relationship between the structure ratio, biomass, and height. Every point is color coded according to the value of S_{rat} (from 0 to 3); hence, blue colors indicate a low ratio (0.5), whereas red indicates a high ratio (2.5). For a fixed height, points with low biomass (dark blue) present a lower value of S_{rat} than points with high biomass (red). Plots with an intermediate ratio value (green) tended to follow the allometric curve. This became more obvious in Fig. 11, where biomass was plotted against the structure ratio for plots with the same height, for Traunstein and Ebersberg. A high correlation between the structure ratio and biomass was observed. It was particularly visible in Ebersberg because of the higher number of plots available. The slope of the fitting lines for Ebersberg was lower than for Traunstein.

Biomass inversion and allometric level correction

After applying eq. 8 to both test sites, we realized that a constant bias was still present for site with respect to one another when using the same parameters (a, b, and c). This bias originated because of the very different forest management plans for Traunstein and Ebersberg that resulted in differences in the allometric levels. An approach based on the inventory plots that are placed in the upper side of the height-to-biomass allometry (red plots in Fig. 10) was used to correct for these effects (Pretzsch 2006). These plots corresponded to stands that were not treated or were abandoned by management; hence, they present a common structure

Fig. 10. Height-to-biomass relationship for Traunstein (left) and Ebersberg (right) sites after plot aggregation process. Dashed curves correspond to the allometric equation $b = 1.3H^{0.58}$. Both plots are color-coded according to the value of the structure ratio from 0 (blue) to 3 (red).

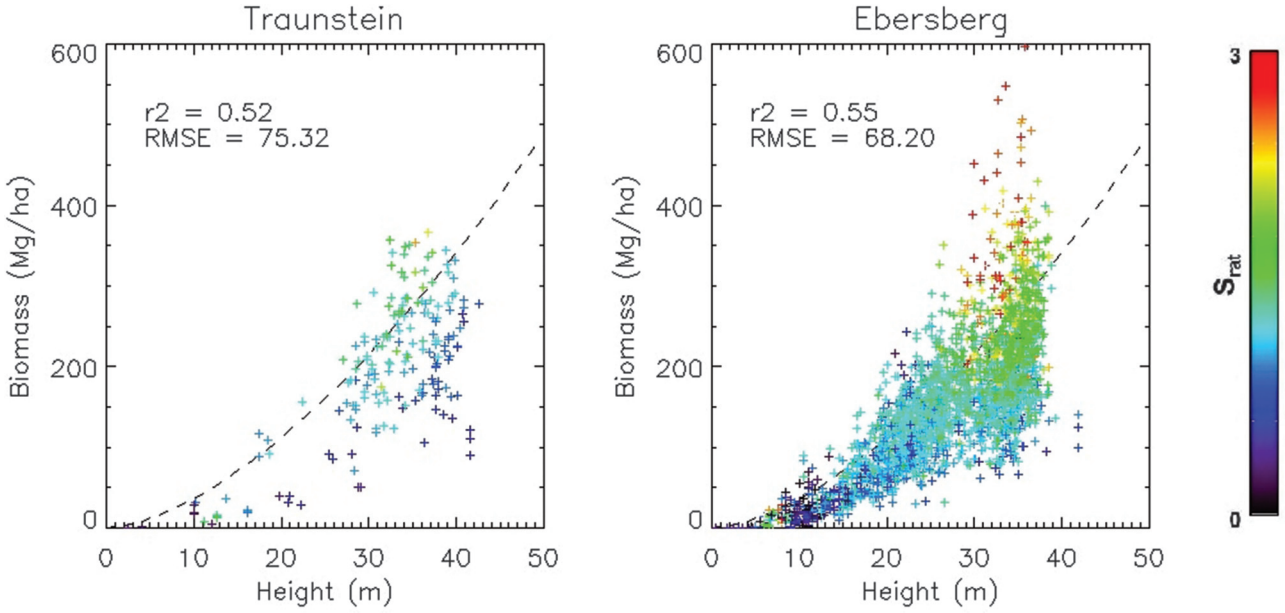

Fig. 11. Relationship between biomass and the structure ratio for profiles with the same height (30 m, right; 36 m, left): (top) Traunstein site; (bottom) Ebersberg site.

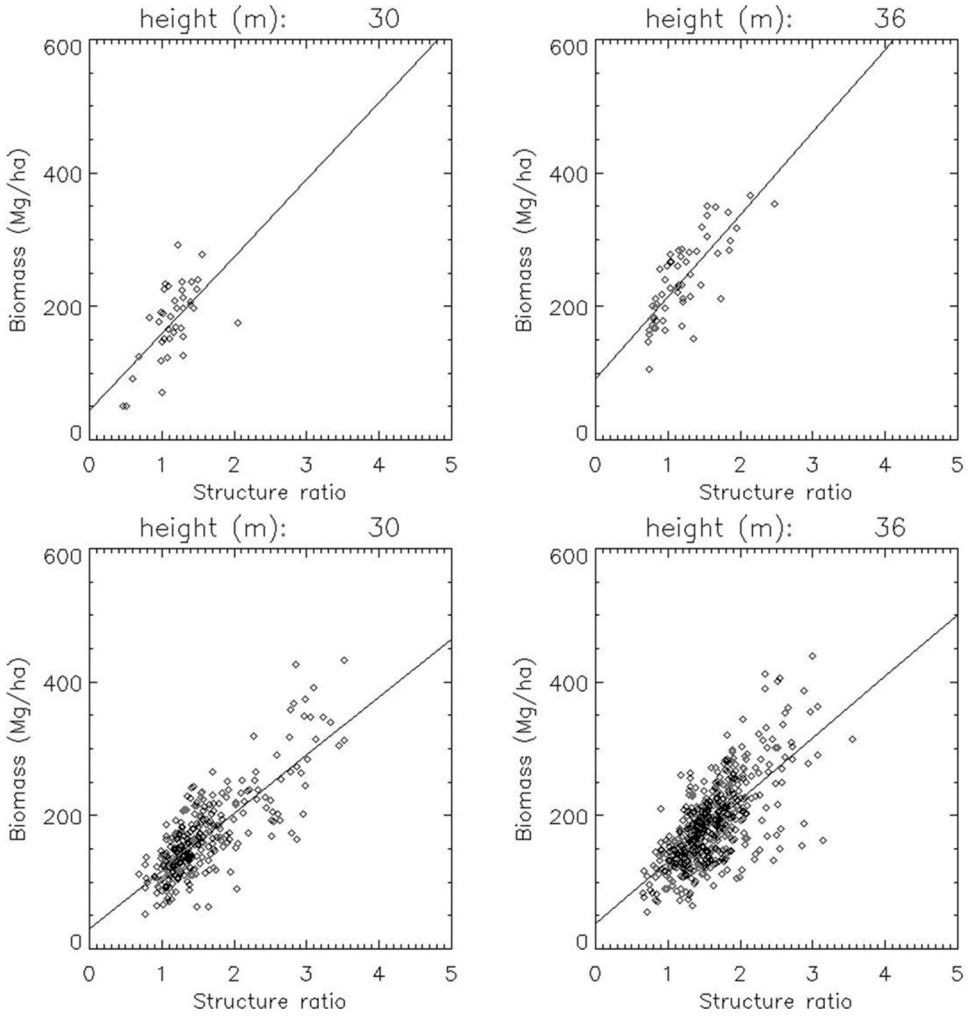

Fig. 12. Height-to-biomass relationship and biomass inversion for Traunstein site (left) and Ebersberg site (right). The values of the coefficients from eq. 10 are as follows: $a = 16$; $b = 0.8$; $c = 0.85$. The values of l_a are 0.61 for the Traunstein site and 0.43 for the Ebersberg site. Both plots are color-coded according to the value of the structure ratio from 0 (blue) to 3 (red).

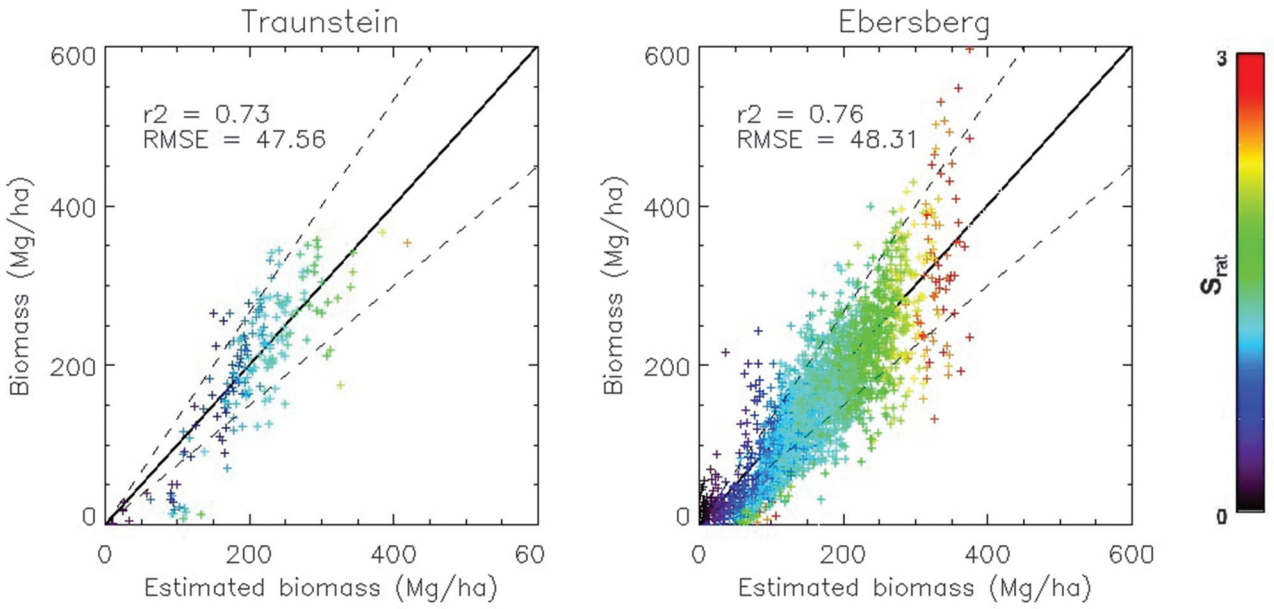

that is also independent from the management for the same region and growth conditions (characterized by the allometric exponent). The bias in structure between the inventory plots placed in the upper side of the height-to-biomass allometry and the mean S_{rat} of the site could be used to estimate the allometric level l_a and thus to correct for deviations between stands. This was calculated as the ratio between the mean S_{rat} of the site (which was expected to follow the allometric curve) and the mean S_{rat} of the 10% highest value for the stands above 20 m (which represents the extreme cases out of management). Thus l_a is calculated using eq. 9:

$$(9) \qquad l_a = \frac{\overline{S_{rat90}}}{\overline{S_{rat}}},\ S_{rat} \in \{S_{rat}, H \geq 20\},\ S_{rat90} \in \{S_{rat}, S_{rat} \geq 0.9\max(S_{rat})\}$$

Therefore, keeping the empirical parameters a, b, and c constant for both test sites, the value of l_a was site dependent and estimated directly from the structural information. l_a was a multiplicative term added to eq. 8, which resulted in eq. 10:

$$(10) \qquad B = l_a \cdot a S_{rat}^{b} H^{c}$$

The parameter with an optimum value for both sites resulted in $a = 3.8$, $b = 0.8$, and $c = 0.85$; and the value of l_a, calculated using eq. 9, was 1.75 for the Traunstein site and 1.89 for the Ebersberg site. The allometric level correction was able to compensate for the slope changes between Traunstein and Ebersberg with comparable levels of performance. The inversion results, shown in Fig. 12, presented a correlation coefficient of 0.73 for Traunstein and 0.76 for Ebersberg, with a RMSE of 47.56 Mg·ha^{-1} and 48.31 Mg·ha^{-1}, respectively. After the inversion, the values for the structure ratio, indicated by the color of each point, were now aligned and directly proportional to the biomass. This indicates that deviations from the height-to-biomass allometric curve can be measured using the values of S_{rat}. Therefore, keeping the empirical parameters a, b, and c constant for both test sites, the value of l_a was site dependent and estimated from the structural information.

Discussion

Forest vertical structure was modeled based on vertical biomass profiles using precisely measured ground forest inventory data as opposed to other techniques such as LiDAR or multibaseline SAR. This structure was measured and parameterized using a novel technique in forestry: the decomposition of forest vertical biomass profiles in Legendre polynomial series. The Legendre polynomials showed great agreement with the natural distribution of biomass. This approach offered a characterization of the profiles that uses all of the vertical forest compartments, without rejecting the lower components as other techniques (mainly applied on LiDAR) based on profile metrics may do (Drake et al. 2002).

The horizontal scale had a big impact on structure characterization and required further consideration. At finer spatial scales, the variability in forest features was large, suggesting that there are forest features visible at a given spatial scale but not at coarser ones (Chave and Levin 2003). Although averaging results from small-sized plots reduced the variance due to error in the single-tree biomass-estimation procedure, it also masked biomass variability caused by structural variability (Shugart et al. 2010). Forest structure analyses were also highly affected by the considered spatial scale in that the inventory scale influenced the overall forest structure and its dynamics over time. At a large scale (close to 1 ha), a forest stand acquired an equilibrium state with a characteristic configuration; however, at a small scale (the so-called gap scale), the forest ecosystem state is affected by continuous changes driven by the presence of large trees. The sensitivity to the gaps has been a major factor in the structure characterization and the S_{rat} sensitivity and will influence the further discussion.

The behavior of the Legendre coefficients indicates that AGB was primarily related to low-frequency Legendre components, which strongly indicates that Legendre coefficients up to the fourth order were sufficient to describe vertical forest structure for biomass estimations. They followed a linear relationship for both test sites and showed that an average of a third of the total biomass was explained by these structural components and was sufficient for AGB estimations, which is indicated by correlations to biomass $r^2 > 0.8$ between the first four Legendre coefficients. However, normalization is necessary to focus only on the struc-

tural information contained in the biomass profiles. This process has shown a loss in the direct relationship between the Legendre coefficients and biomass. Nevertheless, the combination of the coefficients in S_{rat} was able to characterize the allometric relationships between tree structures and biomass, which can be used to improve the biomass inversions.

Biophysical interpretation of the structure ratio

The potential of the Legendre decomposition expressed in S_{rat} to characterize vertical biomass distribution is collected in the trends shown in Fig. 10. These are the basis for the structure characterization developed in this study and correspond with basic allometric (biophysical) principles, which are explained in detail in the following.

High biomass profiles were characterized by low-frequency components (Legendre coefficient a_{01}), as a mature stand approached a homogeneous biomass distribution and a high crown filling (Pretzsch 2014). However, for the same dominant height ($H100$), it is expected that for the sites studied in this paper, a stand with less biomass presented more gaps with a higher heterogeneity; therefore, the proportion of higher frequency components increased (Legendre coefficients a_{02}, a_{03}, and a_{04}). Hence, the structure ratio could detect this change in frequency, and it was sensitive to the biomass explained by the vertical structure profile, which already points out the capacity of the ratio to identify biomass-related changes in the gap fraction, as shown in studies such as Lefsky et al (1999). The S_{rat} trends displayed in Fig. 10, where the value of the ratio increased from bottom to top (proportional to biomass) and from left to right (proportional to height), were even more evident when forest height was kept constant. In this case, there was a clear and direct correlation between the values of the ratio and biomass (Fig. 11). The correlation appears to be linear, although some residual effects from the relationship between height and biomass may induce some curvilinear trends, especially on the higher biomass range. Both trends are accounted for by the parameters a and b in the inversion equation (eq. 10).

The next analysis was to interpret the structure ratio, which was based on the allometric relationships that exist between the crown and the stem compartments and their impact on the vertical structure. Canopy structures have been previously studied repeatedly (Bealde et al. 1982; Lefsky et al 1999; Parker and Russ 2004). However, studies such as Niinemets et al. (2006) state that up to 70%–80% of the AGB is invested in support structures (woody compartments and stems), and the trade-off between the investments in stem and crown-leaf support significantly affects the possible combinations of crown structural design and strategies for light capture and biomass generation. In this study, accounting for the biomass proportion between stems and crowns has therefore introduced a new possibility to estimate the connection between the vertical structure and biomass.

Accordingly, in this study, we have observed that when biomass increased, the ratio of stem to crown increased as the structure ratio increased (Fig. 11), showing that the proportion of stem wood increased in relation to foliage and branches (Petersson et al. 2012). In other words, when the stem proportion was larger with respect to the crown proportion, vertical structure profiles presented a smoother surface for a constant profile height. Thus, considering a constant height, a higher proportion of the crown compartment was translated into sharper profiles, which indicated an increase in the lower frequency components of the profile. At both tests sites, Traunstein and Ebersberg, we found that S_{rat} was highly correlated with the proportion of biomass in the stem compartment and the biomass in the crown compartment (Fig. 13). Moreover, in accordance with Niklas et al. (2003), this trend was independent of the plot profile species composition. Although some residual variations may be the result of local growth conditions, similar slopes in the fitting lines were observed at both test sites. The same effects as discussed above for Fig. 11 are observed here. Nevertheless, the linear trend was chosen as a matter of simplicity to illustrate the direct proportionality observed between the structure ratio and the stem–crown biomass proportion and to allow a direct comparison between the two sites.

The filling of canopy gap structure is still a main driver in the vertical biomass distribution resulting profile, and it is also driven by the species composition. Species with complementary light ecology with an interlocking crown enabled a more complete light interception of mixed stands compared with that of pure stands (Pretzsch 2014), where species are widely distributed along the canopy (Parker et al. 2004). When comparing different levels of biomass, this was translated into profiles with a higher structure ratio value (smoother vertical biomass profiles) because of a lower gap proportion (Parker and Russ 2004). Higher biomass can be explained in terms of higher light interception. The relationship between photosynthetic absorption and crown size is reported in studies such as Canham et al. (1990) or Parker et al. (2004), whether it is quantified in terms of leaf area, crown surface and projection area, or crown length or width. This is further indicated by studies showing that when trees increase their leaf area, they often seem to simultaneously increase crown length or width rather than increase leaf area density (Pretzsch 2014).

Aboveground biomass inversion

The biomass inversion using the structure information contained in S_{rat} improved the inversion results from a height-to-biomass allometry by 20% in the correlation factor and significantly reduced the RMSE (ca. 25 Mg·ha^{-1}) without the need for predelineating homogenous forest stands.

Differences between the two sites were induced by their very different management plans, i.e., mixed close-to-natural for Traunstein and intense monoculture in Ebersberg. These can be detected by the estimation of a structure-based allometric level, therefore showing sensitivity to competitive relationships and disturbances (Latham et al. 1998). An allometric level estimation and subsequent correction could then be conducted using structural information to access the structure-to-biomass relationships of the most densely stocked plots for each site. The considerable changes in the relationships between stand density and biomass were addressed by the structural changes, as seen between pure and mixed stands (Pretzsch 2014). In pure stands such as Ebersberg, a higher correcting value of the allometric level is explained by a narrow saddle in the relationship of maximum growth close to the maximum stand density and a progressive decrease in stand growth with a reduction in stand density. In mixed stands such as Traunstein, with species that are complementary in light ecology and canopy space occupation, the relationship between stand density and biomass can have a much broader saddle, with higher presence of new recruitment in the lower layers after senescence of the upper layer (Luyssaert et al. 2008), resulting in a higher carrying capacity. This translates into a lower slope in the allometric level correction.

Conclusions

This paper proposes a methodology using vertical biomass profiles modeled from ground forest inventory data to improve biomass estimations. This has shown potential applications in forests with complex structures and with biomass that cannot be estimated with sufficient precision using forest stand height. The structure-to-biomass relationships proposed here can be applied to any system that is able to profile forest vertical structure. The structure characterization can be used to detect changes in vertical structure for uses other than biomass estimations because it is particularly sensitive to changes in crown filling and changes in the gap structure.

Fig. 13. Relationship between crown–stem biomass ratio and the structure ratio for profiles with the same height (30 m, right; 36 m, left): (top) Traunstein site; (bottom) Ebersberg site.

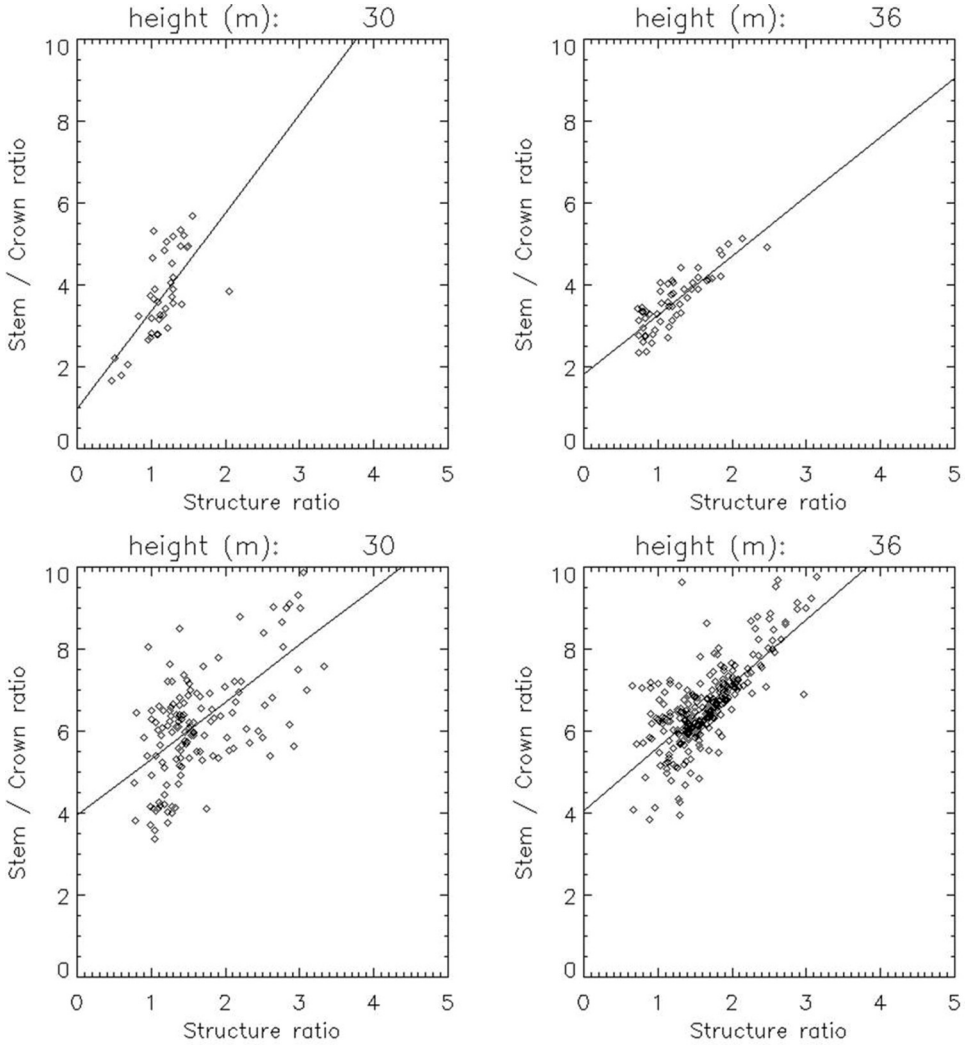

The relationship between vertical structure and biomass, as well as the physical interpretation of structure changes, would be able to enhance the interpretation of reflectivity profiles obtained from RS systems such as SAR or LiDAR. The usage of ground inventory data to generate the vertical biomass profiles that have been investigated here allowed the characterziation of all forest compartments that are potentially detectable by active RS systems, from airborne, ground, or spaceborne systems. Because each system, from the highest frequency (e.g., LiDAR, Xband SAR) to the longest (e.g., P-band SAR), detects different biomass compartments, a methodology that is able to connect allometric relationships for a complete vertical structure with AG biomass can potentially be adapted and implemented with either RS system.

In this paper, we found that traditional height-to-biomass relationships were not accurate enough to estimate AGB in diverse forest systems, which represent a large proportion of the world forest ecosystems (~50%). However, the high variance produced by this allometric relationship can be corrected with the inclusion of second-order parameters such as structure, as we have seen in two forest stands that represent typical structural conditions in Central Europe.

The structure ratio proposed here shows a direct relationship to biomass, and it can be explained by forest biophysical properties, which were tested using ground forest inventory data and modeled scenarios. The noise introduced because of the small inventory plot size was taken into account and corrected using an aggregation algorithm that discriminated between structural discrepancies based on structure ratio and profile height thresholds. The structural differences present at both test sites due to different management treatments could be accessed using the structure descriptor S_{rat} and corrected with the allometric level l_a to obtain similar biomass inversion performances. We have experienced that areas of at least 0.5 ha are necessary to have a stable and representative estimation of the forest vertical structure (Shugart et al. 2010). The allometric relationship of forest structure to forest biomass becomes representative at this scale. Therefore, forest inventories with full tree measurements in larger areas (0.5–1 ha) would improve the understanding and development of structure allometric relationships.

This method is restricted to the empirical estimation of the exponents for each area. A further extension with more test sites, particularly in different climatic regions, would improve the applicability of the method.

Acknowledgements

We thank the Bavarian State Forest (Bayersiche Staatsforsten) for the high-quality data provided in the forest inventories. We

also thank Peter Biber from Chair for Forest Growth and Yield Science at Munich's University of Technology (TUM) for his useful suggestions and collaboration. This work has been partially supported by the HGF – Helmholtz Alliance "Remote Sensing & Earth System Dynamics".

References

Arfken, G.B., and Weber, H.J. 2005. Mathematical methods for physicists. 7th ed. Elsevier Academic Press, London, UK.

Assmann, E. 1961. Waldertragskunde. Organische Produktion, Struktur, Zuwachs und Ertrag von Waldbeständen. BLV Verlgasgesellschaft, München, Bonn, Wien. pp. 161–168.

Bealde, C.L., Talbot, H., and Jarvis, P.G. 1982. Canopy structure and leaf area index in a mature Scots pine forest. Forestry, **55**: 105–123. doi:10.1093/forestry/55.2.105.

Bertalanffy, L.V. 1942. Theoretische Biologie; Zweiter Band: Stoffwechsel und Wachstum. Borntraeger. Berlin.

Brown, S. 2002. Measuring carbon in forests: current status and future challenges. Environ. Pollut. **116**(3): 363–372. doi:10.1016/S0269-7491(01)00212-3.

Canham, C.D., Denslow, J.S., Platt, W.J., Runkle, J.R., Spies, T.A., and White, P.S. 1990. Light regimes beneath closed canopies and tree-fall gaps in temperate and tropical forests. Can. J. For. Res. **20**(5): 620–631. doi:10.1139/x90-084.

Chave, J., and Levin, S. 2003. Scale and scaling in ecological and economic systems. Environ. Resour. Econ. **26**(4): 527–557. doi:10.1023/B:EARE.0000007348.42742.49.

Cloude, S.R. 2006. Polarization coherence tomography. Radio Sci. **41**(4): RS4017. doi:10.1029/2005RS003436.

Dinh, H.T.M., Rocca, F., Tebaldini, S., d'Alessandro, M.M., and Le Toan, T. 2012. Linear and circular polarization P band SAR tomography for tropical forest biomass study. *In* Proceedings of the 9th European Conference on Synthetic Aperture Radar, 2012. EUSAR. pp. 489–492.

Drake, J.B., Dubayah, R.O., Knox, R.G., Clark, D.B., and Blair, J.B. 2002. Sensitivity of large-footprint lidar to canopy structure and biomass in a neotropical rainforest. Remote Sens. Environ. **81**(2–3): 378–392. doi:10.1016/S0034-4257(02)00013-5.

Dubayah, R.O., and Drake, J.B. 2000. Lidar remote sensing for forestry. J. For. **98**: 44–46.

Enquist, B.J., and Niklas, K.J. 2001. Invariant scaling relations across tree-dominated communities. Nature, **410**(6829): 655–660. doi:10.1038/35070500.

Enquist, B.J., West, G.B., and Brown, J.H. 2009. Extensions and evaluations of a general quantitative theory of forest structure and dynamics. Proc. Natl. Acad. Sci. U.S.A. **106**(17): 7046–7051. doi:10.1073/pnas.0812303106.

Hall, S.A., Burke, I.C., Box, D.O., Kaufmann, M.R., and Stoker, J.M. 2005. Estimating stand structure using discrete-return lidar: an example from low density, fire prone ponderosa pine forests. For. Ecol. Manage. **208**(1–3): 189–209. doi:10.1016/j.foreco.2004.12.001.

Harding, D.J., Lefsky, M.A., Parker, G.G., and Blair, J.B. 2001. Laser altimeter canopy height profiles: methods and validation for closed-canopy, broadleaf forests. Remote Sens. Environ. **76**(3): 283–297. doi:10.1016/S0034-4257(00)00210-8.

Houghton, R.A. 2005. Aboveground forest biomass and the global carbon balance. Glob. Change Biol. **11**(6): 945–958. doi:10.1111/j.1365-2486.2005.00955.x.

Houghton, R.A., Hall, F., and Goetz, S.J. 2009. Importance of biomass in the global carbon cycle. J. Geophys. Res. **114**(G2). G00E03. doi:10.1029/2009JG000935.

Köhler, P., and Huth, A. 2010. Towards ground-truthing of spaceborne estimates of above-ground life biomass and leaf area index in tropical rain forests. Biogeosciences, **7**: 2531–2543. doi:10.5194/bg-7-2531-2010.

Laar, A. van, and Akça, A. 2007. Forest mensuration. 2nd ed. Springer, Dordrecht.

Latham, P.A., Zuuring, H.R., and Coble, D.W. 1998. A method for quantifying vertical forest structure. Forest Ecology and Management, **104**: 157–170. doi:10.1016/S0378-1127(97)00254-5.

Lefsky, M.A., Cohen, W.B., Acker, S.A., Parker, G.G., Spies, T.A., and Harding, D. 1999. Lidar remote sensing of the canopy structure and biophysical properties of Douglas-fir western hemlock forests. Remote Sens. Environ. **70**(3): 339–361. doi:10.1016/S0034-4257(99)00052-8.

Lefsky, M.A., Harding, D.J., Keller, M., Cohen, W.B., Carabajal, C.C., Del Bom Espirito-Santo, F., Hunter, M.O., and de Oliveira, R. 2005. Estimates of forest canopy height and aboveground biomass using ICESat. Geophys. Res. Lett. **32**: L22S02. doi:10.1029/2005GL023971.

Li, B.-L., Wu, H., and Zou, G. 2000. Self-thinning rule: a causal interpretation from ecological field theory. Ecol. Model. **132**: 167–173. doi:10.1016/S0304-3800(00)00313-6.

Luyssaert, S., Schulze, E.-D., Börner, A., Knohl, A., Hessenmöller, D., Law, B.E., Ciais, P., and Grace, J. 2008. Old-growth forests as global carbon sinks. Nature, **455**: 213–215. doi:10.1038/nature07276.

Mette, T., Papathanassiou, K., Hajnsek, I., and Zimmermann, R. 2003. Forest biomass estimation using polarimetric SAR interferometry. *In* Proceedings of the Workshop on PolinSAR, Frascatti, January 2003.

Nadkarni, N.M., Parker, G.G., Rinker, H.B., and Jarzen, D.M. 2004. The nature of forest canopies. *In* Forest canopies. 2nd ed. Elsevier Academic Press, California, U.S.A. pp. 3–23.

Næsset, E. 2002. Determination of mean tree height of forest stands by digital photogrammetry. Scand. J. For. Res. **17**: 446–459. doi:10.1080/028275802320435469.

Niinemets, Ü., Portsmuth, A., and Tobias, M. 2006. Leaf size modifies support biomass distribution among stems, petioles and mid-ribs in temperate plants. New Phytol. **171**: 91–104. doi:10.1111/j.1469-8137.2006.01741.x.

Niklas, K.J., Midgley, J.J., and Enquist, B.J. 2003. A general model for mass–growth–density relations across tree-dominated communities. Evol. Ecol. Res. **5**: 459–468.

Onaindia, M., Dominguez, I., Albizu, I., Garbisu, C., and Amezaga, I. 2004. Vegetation diversity and vertical structure as indicators of forest disturbance. For. Ecol. Manage. **195**(3): 341–354. doi:10.1016/j.foreco.2004.02.059.

Papathanassiou, K.P., and Cloude, S.R. 2001. Single-baseline polarimetric SAR interferometry. IEEE Trans. Geosci. Remote. Sens. **39**(11): 2352–2363. doi:10.1109/36.964971.

Parker, G.G., and Russ, M.E. 2004. The canopy surface and stand development: assessing forest canopy structure and complexity with near-surface altimetry. For. Ecol. Manage. **189**(2004): 307–315. doi:10.1016/j.foreco.2003.09.001.

Parker, G.G., Harmon, M.E., Lefsky, M.A., Chen, J., Pelt, R.V., Weis, S.B., Thomas, S.C., Winner, W.E., Shaw, D.C., and Frankling, J.F. 2004. Three-dimensional structure of an old-growth *Pseudotsuga–Tsuga* canopy and its implications for radiation balance, microclimate, and gas exchange. Ecosystems, **7**: 440–453. doi:10.1007/s10021-004-0136-5.

Petersson, H., Holm, S., Ståhl, G., Alger, D., Fridman, J., Lehtonen, A., Lundström, A., and Mäkipää, R. 2012. Individual tree biomass equations or biomass expansion factors for assessment of carbon stock changes in living biomass — a comparative study. For. Ecol. Manage. **270**: 78–84. doi:10.1016/j.foreco.2012.01.004.

Pretzsch, H. 2006. Species-specific allometric scaling under self-thinning: evidence from long-term plots in forest stands. Oecologia, **146**(4): 572–583. doi:10.1007/s00442-005-0126-0.

Pretzsch, H. 2009. Forest dynamics, growth, and yield. *In* Forest dynamics, growth and yield. Springer, Heidelberg, Berlin. pp. 1–39.

Pretzsch, H. 2014. Canopy space filling and tree crown morphology in mixed-species stands compared with monocultures. For. Ecol. Manage. **327**: 251–264. doi:10.1016/j.foreco.2014.04.027.

Pretzsch, H., and Biber, P. 2005. A re-evaluation of Reineke's rule and stand density index. For. Sci. **51**(4): 304–320.

Schneider, T., Elatawneh, A., Rahlf, J., Kindu, M., Rappl, A., Thiele, A., Boldt, M., and Hinz, S. 2013. Parameter determination by RapidEye and TerraSAR-X data: a step toward a remote sensing based inventory, monitoring and fast reaction system on forest enterprise level. *In* Earth Observation of Global Changes (EOGC), Lecture Notes in Geoinformation and Cartography. *Edited by* J.M. Krisp, L. Meng, R. Pail, and U. Stilla. Springer, Berlin, Heidelberg. pp. 81–107.

Shugart, H.H., Saatchi, S., and Hall, F.G. 2010. Importance of structure and its measurement in quantifying function of forest ecosystems. J. Geophys. Res. **115**(G2): G00E13. doi:10.1029/2009JG000993.

Toraño, A.C., Kugler, F., Papathanassiou, K., Biber, P., and Pretzsch, H. 2010. Biomass estimation as a function of vertical forest structure and forest height — potential and limitations for radar remote sensing. *In* 8th European Conference on Synthetic Aperture Radar (EUSAR), 7 to 10 June 2010, Eurogress, Aachen, Germany. VDE Verlag GmbH, Berlin. pp. 1–4.

Treuhaft, R.N., Gonçalves, F.G., Drake, J.B., Chapman, B.D., dos Santos, J.R., Dutra, L.V., Graça, P.M.L.A., and Purcell, G.H. 2010. Biomass estimation in a tropical wet forest using Fourier transforms of profiles from lidar or interferometric SAR. Geophys. Res. Lett. **37**(23): L23403. doi:10.1029/2010GL045608.

von Gadow, K., and Hui, G. 2001. Modelling forest development. Springer Science & Business Media, Berlin.

World Agroforestry Centre. 2011. Citing online sources: advice on online citation formats [online]. Available from http://worldagroforestrycentre.org/regions/southeast_asia/resources/wood-density-database [accessed 3 February 2015].

Yoda, K., Kira, T., Ogawa, H., and Hozumi, K. 1963. Self-thinning in overcrowded pure stands under cultivated and natural conditions. J. Biol. Osaka City Univ. **14**: 107–129.

Zenner, E.K., and Hibbs, D.E. 2000. A new method for modeling the heterogeneity of forest structure. For. Ecol. Manage. **129**(1–3): 75–87. doi:10.1016/S0378-1127(99)00140-1.

Zianis, D., Muukkonen, P., Mäkipää, R., and Manuccini, M. 2005. Biomass and stem volume equations for tree species in Europe. *In* Silva Fennica monographs 4. The Finish Society of Forest Science, the Finish Forest Research Institute.

Appendix A

Brink's function

The Brink functions defined in von Gadow and Hui (2001) models the tree stem as following:

$$
\begin{aligned}
r(h) &= u + v\mathrm{e}^{-ph} - w\mathrm{e}^{qh} \\
u &= \frac{i}{1 - \mathrm{e}^{q(1.3-h)}} + (\mathrm{dbh} - i)\left(1 - \frac{1}{1 - \mathrm{e}^{p(1.3-h)}}\right) \\
v &= \frac{(\mathrm{dbh} - i)\mathrm{e}^{1.3p}}{1 - \mathrm{e}^{p(1.3-h)}} \\
w &= \frac{i\mathrm{e}^{-qh}}{1 - \mathrm{e}^{q(1.3-h)}}
\end{aligned} \tag{1}
$$

where $r(h)$ is the tree radius as a function altitude h, u, v, and w are the parameters of the expression $r(h)$, dbh is the diameter at breast height, i is a species-specific asymptote parameter, p is a species-specific parameter describing the lower part of the stem, and q is a species-specific parameter describing the upper part of the stem.

Reference

von Gadow, K., and Hui, G. 2001. Modelling forest development. Springer Science & Business Media, Berlin.

II

Large Scale Biomass Classification in Boreal Forests with TanDEM-X Data

Astor Toraño Caicoya, Florian Kugler, Irena Hanjsek, *Fellow, IEEE* and Kostantinos Papathanassiou, *Fellow, IEEE*

***Abstract*— Boreal forests are characterized by a rather homogenous stand structure which allows by means of a single allometric equation to estimate biomass from forest height with sufficient accuracy and, therefore, to use this equation for quantitative biomass classifications. In this paper, interferometric TanDEM-X DEM data is used to estimate forest height over boreal forest systems. The accuracy of the height inversion is evaluated for single and also dual baseline scenarios, under summer and winter conditions. Then, an allometric equation is used to transfer forest height to biomass. For this, two forest sites, boreal (Krycklan) and hemi-boreal (Remningstorp) in north and southern Sweden, respectively, are investigated. A performance analysis is carried out in order to estimate the maximum number of biomass classes obtained, depending on the height estimation accuracy. For summer acquisitions, four biomass classes can be obtained, with a maximum biomass class of >200 Mg/ha. For winter acquisitions or when a mixed summer – winter approach is applied, five biomass classes, up to 220 Mg/ha, can be obtained. This classification shows a good agreement with CORINE, an existing land cover classification, and can improve it by adding quantitative forest biomass classes with a high spatial resolution of 16x16 m..**

***Index Terms*— Above-ground biomass, boreal forest, forest structure, forest height, land cover, TanDEM-X, bistatic, SAR**

I. INTRODUCTION

BOREAL forests contain roughly 1/3 of the global forest biomass [1]. Carbon stock is, for many countries, well known at state level thanks to ground forest inventories [2]. However, forest inventories are designed to estimate average wood volumes for administrative units and are less effective to provide information at the spatial resolution required for mapping of land use changes [1].

Measurements of boreal forest resources are often outdated because they are affected by forest fires, intensive logging activities and natural reforestation on abandoned agricultural areas or forest regrowth [1]. Changes in the forest coverage can act as both periodically changing carbon sinks and carbon sources [3]. Accurate large-scale biomass classifications (according to [1], on the order of 10-20%) are, therefore, essential for a better characterization of forest resources, which in fact influence directly the carbon fluxes [5]. Remote sensing configurations are predestinated to provide information of the required spatial and temporal resolutions [5].

Optical remote sensing system configurations are able to provide accurate stand classifications, although rather limited when it comes to quantitative biomass estimations, mainly distinguishing between forest and non-forest, or deciduous and coniferous forests. In this way, they are able to map different stages of forest re-growth, but have limited success in determining biomass in closed canopies or in high biomass forests [6], [7].

The most homogenous European-wide land cover classification is the Coordination of Information on the Environment (CORINE). CORINE is an inventory of the land cover represented by 44 classes (3 forest classes) as a cartographic product at a scale of 1:100000, with a maximum spatial resolution of 100x100 m [8]. This product has been developed combining multiple optical remote sensing data sources, like Landsat and Spot, with existing national land cover maps. Constrains are due to the lack of temporal resolution and the intense non-systematic methodology.

In a more systematic approach, the Global Land Cover 2000 Maps project provides a global harmonized land cover map with an overall classification accuracy of 68.6% [9] . Data from optical spaceborne (passive) sensors at different resolutions, 500x500m for the MODIS and 300x300 m for SPOT 4-5, are combined and forests are classified in seven classes from evergreen to deciduous, and different proportions of mixed forests.

LIDAR configurations made important contributions [10]. Global forest height maps based on the combination of spaceborne LIDAR (GLAS) with optical (passive) remote sensing systems (MODIS) have been proposed by [11], [12] with a spatial resolution of 1km^2. The discontinuous coverage of the LIDAR system is compensated extrapolating the data with the help of the optical data.

Synthetic Aperture Radar (SAR), offers great potential for quantitative and qualitative global forest cover mapping [13], [14], [15], thanks to the wall to wall coverage capability, combined with a high spatial resolution. In the SIBERIA project [13], a radar approach, based on ERS(C-band)/JERS(L-band) data was used to generate a land cover

Manuscript received March xx, 2015; revised month xx, 201x, Current Version published month xx, 201x. This work has been partially supported by the HGF - Helmholtz Alliance "Remote Sensing & Earth System Dynamics".
Astor Toraño Caicoya, Florian Kugler and Konstantinos Papathanassiou are with the Radar Concepts Department, Microwaves and Radar Institute, German Aerospace Center (DLR), (DLR-HR), D-82234 Oberpfaffenhofen, Germany. (e-mail: astor.toranocaicoya@dlr.de, florian.kugler@dlr.de, kostas.papathanassiou@dlr.de).

classification with a spatial resolution of 50x50 m and three forest biomass classes (only sensitive up to 81 m^3/ha corresponding to ~40 Mg/ha of biomass).

In [1] an algorithm for the estimation of Growing Stock Volume (GSV) using stacks of C-band SAR images acquired from Envisat ASAR ScanSAR for the boreal region is proposed. The algorithm shows a performance up to 300 m³/ha (~150 Mg/ha) with RMSE's from 47.7 to 96.2%. Recently, a biomass map for the entire Northern Hemisphere was produced within the BIOMASAR project, but still with a spatial resolution of 1 km^2 [16].

TanDEM-X, is the first bistatic spaceborne SAR mission and with a global single-pass interferometric measurements, offers a unique contribution [17], [18]. The primary mission objective is the generation of a consistent global digital elevation mode (DEM), mapping, in the standard DEM mode, the total globe twice between 2011 and 2013 [17]. The potential to use interferometric measurements to derive forest height [19], [20], [21], [22], combined with a high spatial resolution (12x12 m), motivates the utilization of this global data set for updating, extending and/or improving the thematic forest classifications and biomass mapping as seeing in works like [23], [24], [25], [26], [27].

The main objective of this paper is to develop and validate a methodology for (unsupervised) large scale boreal forest biomass classification. Forest biomass is allometrically derived from forest height which is estimated from TanDEM-X data. Since boreal forests (mainly taiga) are characterized by a rather homogenous structure, one single allometric equation can be used for the entire boreal zone.

The methodology developed here comprises the following steps: first, a sensitivity analysis was carried out in order to define the number of independent biomass classes which can be distinguished. This was done by taking into account the accuracy of the selected allometric relationship and the accuracy of forest height estimation, for different acquisition scenarios (single and dual baseline scenarios). Second, the height inversion algorithms were validated against reference LIDAR data. Third, the biomass classification results were evaluated with the help of confusion matrices and contrasted through maps of differences. Finally, the biomass classification was evaluated against the CORINE classification.

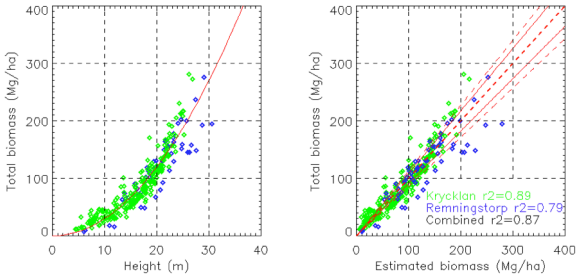

Fig. 1. Height (H100) to biomass allometry for the ground plots of Krycklan (green) and Remningstorp (blue). Left: height (H100) obtained from LIDAR vs. biomass obtained from LIDAR. Red line represents (2). Right: Reference biomass (from LIDAR) against biomass estimated from (2). Full red lines indicated the standard deviation and the dashed lines indicate the boundaries for a 90% of confidence interval.

II. Height-to-Biomass Allometry

A. Structure and height- to- biomass allometry

Aboveground forest biomass is the dry matter content of the trees in a forest stand and therefore, is a measure of the carbon stored in the forest stand. It can be derived from forest parameters such as forest dominant height-H100, using allometric equations [28], [29], [30]. The H100 is a standard parameter in forest mensuration which is defined as the mean height of those 100 trees per hectare with the largest diameter [31]). The allometric approach proposed in [30], uses a power law equation to relate biomass to (stand) height for a given empirically derived allometric level l_a. In this sense, l_a is the scaling factor between the allometric exponent (b) and the stand density (or basal area) that shows a low variability among tree species and is mainly connected to forest management (stand characteristics):

$$B = l_a 1.66 h_v^b, \quad (1)$$

where B (Mg/ha) is the biomass, h_v (m) forest height and b an allometric exponent. The height-to-biomass allometric relation has been proven to be stable and able to be estimate accurately (r^2 ~ 0.7) above ground forest biomass (AGB) from forest height [30] for homogenous forest conditions. However, variability in forest structure and stand density may bias this allometric relationship and limits its applicability [32].

In the taiga, main forest environment in the boreal region, forest conditions are homogenous in structure as well as in species composition for managed as well as for natural forest conditions. This minimizes the error of using one single allometric equation for biomass estimations all over the boreal zone.

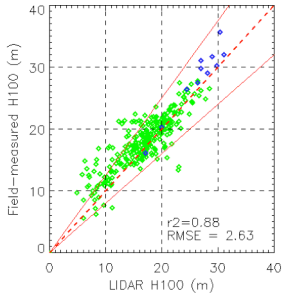

Fig. 2. Height (H100) estimated from field inventory data vs. height (H100) estimated from LIDAR. The solid red lines represent 20% height error intervals. Inventory plots from Krycklan are represented in green and from Remningstorp in blue.

Figure 1, on the left, shows a plot of the LIDAR reference height (H100) against LIDAR forest biomass on stand level for Krycklan in green and Remningstorp in blue (these two sites are presented in detail in section III). An estimate of the forest H100 is obtained as the maximum height within a 10x10 m window of the LIDAR vegetation height [31], [33]. This method was successfully used for small footprint airborne LIDAR systems, with 1 to 4 hits/m^2 [20] in both sites. In Figure 2 the correlation between H100 estimated from field inventory plots and the corresponding H100 estimated in the same area from LIDAR data is shown. Despite the noise

introduced by geolocation errors coming from the small size of the inventory plots in Krycklan (10 m radius), the overall correlation is close to a 90% ($r^2 = 0.88, \mathrm{RMSE} = 2.63$ m), demonstrating the capability of LIDAR data for the estimation of H100. Only 11 plots with field data were available for Remningstorp, so a correlation factor cannot be estimated for Remningstorp independently.

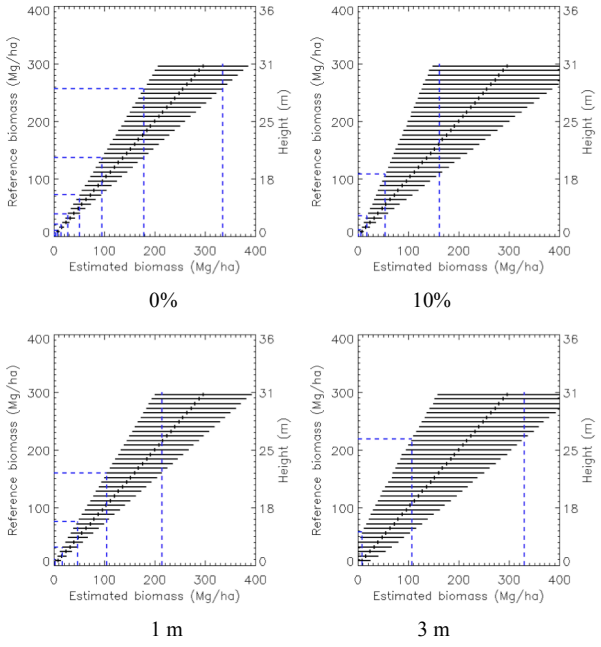

Fig. 3. Classification performance based on (4) for a 90% confidence interval, with relative height errors on the top panel and absolute height errors on the bottom panel. The real biomass is plotted on the y- axis, the estimated biomass, for this confidence interval, is plotted on the x- axis in 10 Mg/ha biomass steps. The blue dashed lines indicate the class boundaries, estimated at the point in which two biomass intervals do not overlap.

Both sites can be characterized by the same allometric relationship (red line in Figure 1 on the left) with a high correlation. The best fitting equation, estimated by the Swedish National Forest Service Inventory (SLU) [34], is described by:

$$B = 0.18 * 1.66{h_v}^2. \quad (2)$$

In Figure 1 on the right, biomass estimated by using the reference LIDAR H100 heights in (2) is plotted against the reference biomass. The overall correlation coefficient is $r^2 = 0.87$ and the standard deviation is ~10%. The high correlation and low standard deviation indicate that one allometric equation can be accurately applied to both sites. The correlation is higher for Krycklan than for Remningstorp. The reason for this, is that Remningstorp lies on the edge of the boreal region and therefore would need a different l_a. At the same time, forest management is more developed at Remningstorp, introducing a higher variation from stand to stand. The impact of using a single equation for the estimation of biomass is assessed with a classification performance analysis.

B. Biomass estimation accuracy

In order to perform a biomass classification, the sources of error in the biomass estimation need to be quantified to define the amplitude and maximum number of classes.

A biomass map is obtained in two steps: first by estimating forest height from interferometric TanDEM-X and second by estimating biomass from height using the allometric relation described in (2). Thus, the accuracy of the estimated biomass depends on two error sources: the accuracy of the estimated height-to-biomass relationship (ΔB) and the accuracy of the forest height estimates (Δh_v). ΔB is defined by the forest stand properties and can only be improved when additional forest parameter(s) (like forest density, structural parameters, etc.) are included in the allometric estimation process [30]. Under the assumption of homogenous stand conditions across the boreal region, ΔB can be assumed constant and it is estimated from the bias observed in the height-to-biomass relationship applied to the reference data (Figure 1).

Δh_v depends on the forest height estimation methodology. Airborne LIDAR measurements provide height estimates with sub-meter accuracy and are therefore used as a reference. For forest heights obtained from TanDEM-X data, Δh_v depends, in general, on the acquisition mode (single-pol, dual-pol, dual-baseline) the amount of available acquisitions (see section IV) and the baseline (reflected by the vertical wavenumber κ_z) of the acquisitions [35] and the forest type.

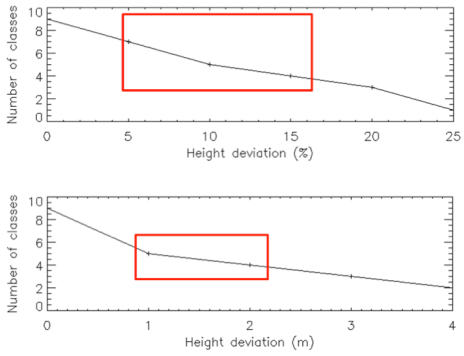

Fig. 4. Number of classes as a function of height error. On the top: relative height error. On the bottom: absolute height error. The red rectangles mark the expected error quantities.

Accordingly, the total biomass estimation sensitivity (ΔB_{tot}) can be expressed as shown in (3).

$$\Delta B_{tot} = \frac{\partial B}{\partial h_v}\Delta h_v + \Delta B. \quad (3)$$

Introducing the deviation of (2) in (3) results in:

$$\Delta B_{tot} = 0.6 h_v \Delta h_v + \Delta B, \quad (4)$$

Δh_v and ΔB determine the number of independent biomass classes which can be identified. However, since the allometric relation and therefore ΔB is assumed constant, the change in number of biomass classes is driven by Δh_v only.

Figure 3 shows the 90% confidence interval, predicted by (4), for a 0% and 10%, relative height error, and 1 and 3 m absolute errors, in 10 Mg/ha steps. The blue dashed lines indicate the boundaries between independent classes, defined

TABLE I
BIOMASS CLASSES FOR RELATIVE HEIGHT ERRORS (UPPER BOUNDARY - MG/HA).

Class	1	2	3	4	5	6	7	8	9
0%	<2	5	10	20	38	72	136	256	>256
5%	<2	6	14	31	68	147	>147		
10%	<3	11	35	107	>107				
15%	<4	24	125	>125					
20%	<9	115	<115						
25%	2	>2							

TABLE 2
BIOMASS CLASSES FOR ABSOLUTE HEIGHT ERRORS (UPPER BOUNDARY - MG/HA).

Class	1	2	3	4	5
1m	<9	31	75	159	>159
2m	<20	98	245	>245	
3m	<57	218	>218		
4m	<95	95			

by the point in which two classes do not overlap each other, for a 90% confidence interval. The black horizontal lines represent, therefore, the total ΔB_{tot} estimated using (4) in biomass intervals of 10 Mg/ha. The number of classes as a function of Δh_v is displayed in Figure 4, on the top, for a relative height error and, on the bottom, for an absolute height error. Assuming a perfect height measurement ($\Delta h_v = 0$), 9 biomass independent classes can be identified. This is the maximum performance that can be achieved, due to the residual bias contained in ΔB. In [36] a mean standard deviation of ~2 m across all prevailing heights is reported which allows distinguishing between 4 biomass classes. In case of a 10% height error five classes can be distinguished. For height errors larger than 20% or 3 m only two biomass classes can be identified reducing the classification to a forest/non forest classification. Table 1 summarizes the upper class boundaries for the relative height errors and Table 2 for the absolute height errors.

III. TANDEM-X DEM DATA

A. Test sites

Two sites were evaluated in this study: Krycklan and Remningstorp both located in Sweden.

Krycklan is located in middle Sweden (64°10'N and 20°01'E), a typical boreal forest placed in a hilly topography. Mean forest height is about 18 m with a mean biomass level of 90 Mg/ha. Maximum forest height measured is 30 m with a biomass of 220 Mg/ha. The dominant forest type is a mixed coniferous forest of Norway spruce, Scots pine and Birch. Topography varies between 20 m and 400 m above mean sea level (amsl). The airborne LIDAR data set was acquired in August 2008 and covers ~6700 ha, together with 298 ground-inventory plots. For validation 252 homogeneous stands have been lined out on the LIDAR height map with a mean size of 3.8 ± 2.7 ha (minimum size of 0.3 and maximum of 16.1 ha).

Remningstorp is located in southern Sweden (58°25'N, 13°14'E), a hemi-boreal forest over a rather flat terrain. Prevailing tree species are Norway spruce, Scots pine, Birch and small fractions of Oak and Beech. Maximum forest height

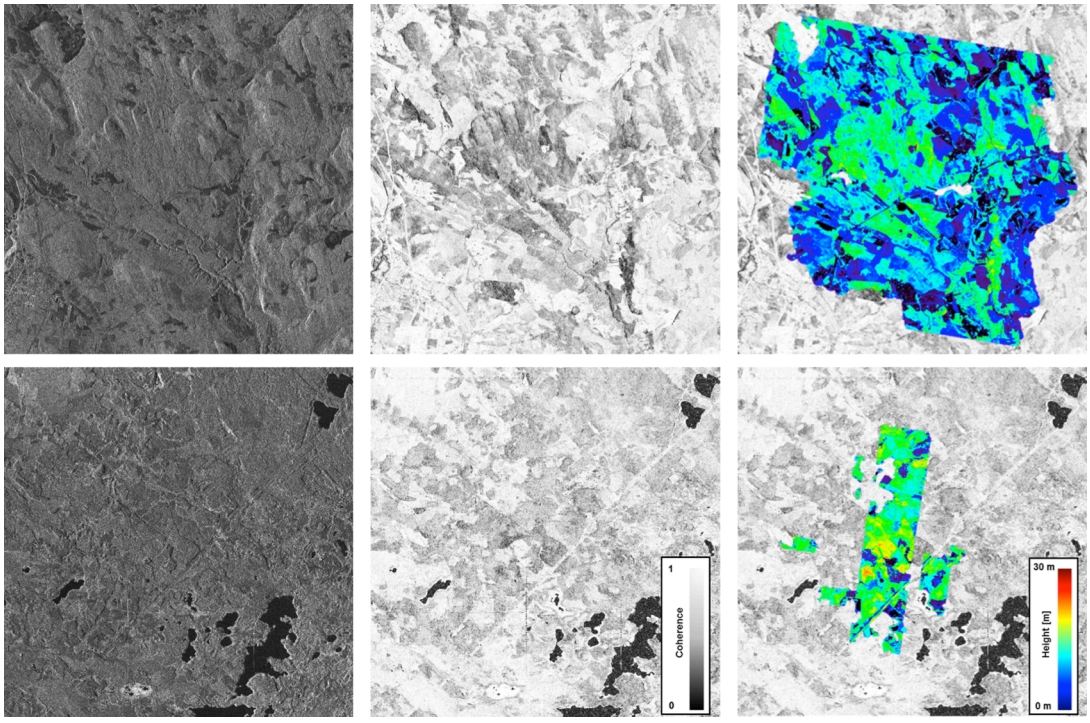

Fig. 5. TanDEM-X data subsets for Krycklan 2011/02/27, 13.5 x 18.8 km, (above) and Remningstorp, 9.3 x 11.3 km, 2011/12/30 (below) From left for right: single look complex amplitude, coherence scaled from 0 (black) to 1 (white), and LIDAR height validation map scaled from 0 to 40, over the coherence image.

is 35 m with a maximum biomass of about 300 Mg/ha. Mean forest height is around 20 m and the mean biomass level on the order of 130 Mg/ha. The topography ranges between 120 m and 145 m amsl. The reference airborne LIDAR data was acquired in April 2007, covering ~1200 ha, together with 11 ground measurement plots. For validation 58 homogeneous forest stands are also delineated on the LIDAR data with a mean size of 2.0 ± 1.8 ha (minimum size of 0.5 and maximum of 9.3 ha).

Validations for both sites were done against LIDAR derived forest top height H100 [28] and biomass [39]. The reference biomass was then estimated by combining LIDAR height with ground inventory data, which corrects for stand densities, defining specific allometries for each site [39], [40].

All TanDEM-X used data were acquired either in 2011 or in 2012 which means a time span of 3 to 5 years with respect to the LIDAR reference data, so forest conditions like stand height can change in this period due to tree growth. Growth for a stand of Norway Spruce (which is the most productive tree species in this region) is taken as reference [20]. For the validation of the model based forest height estimates, three growth periods were considered: short (~0.4 m/year), medium (~0.3 m/year) and tall (~0.1 m/year) forest. Therefore height estimates from the TanDEM-X data are expected to be in the order of ~2 – 2.4 m higher than in the LIDAR ground truth in the low forest stands, ~1.3 – 1.5 m in the middle stands and to slightly increase in the tall stands (below or ~0.5 m). Drastic changes in the forest cover due to clear-cuts can be easily detected by a strong decrease in height. However, changes due to other harvesting activities are unknown and add therefore randomly to the validation plots.

B. DEM data acquisition

The primary objective of the TanDEM-X mission is to generate a global DEM, with a horizontal resolution of 12 m, an absolute height accuracy of 10m and a relative height accuracy of 2 m. The DEM data acquisitions are performed in a bistatic InSAR stripmap mode in HH polarization [17]. The incidence angle for the DEM acquisitions varies between 30° and 48°. For each scene two acquisitions with different baselines are foreseen; the first acquisition has a minimum height of ambiguity of 45 m (κ_z = 0.14) for the small baseline and the second of 35 m (κ_z =0.18) for the large baseline [41]. Acquisitions of the same area are, in general, planned independently from each other and are therefore not necessarily performed within the same season [17].

The largest difference in the boreal region is expected between summer and winter acquisitions. As the backscattering of forests changes according to the seasonal status [20], [36], seasonal differences, which are not accounted in the DEM generation, need to be considered for forest height inversions.

C. List of used data

The TanDEM-X data used in this paper, including maximum and minimum temperatures, for each acquisition day and for both sites, are summarized in Table 3. For each site two DEM mode acquisitions were performed: a first one in winter conditions and a second one (large baseline) in summer conditions.

TABLE 3
SUMMARY OF USED TANDEM-X AND AUXILIARY DATA. POL STANDS FOR POLARIZATION, θ IS THE INCIDENCE ANGLE, κ_z THE VERTICAL WAVE NUMBER, T_{MAX} THE MAXIMUM TEMPERATURE AND T_{MIN} THE MINIMUM TEMPERATURE IN °C OF THE ACQUISITION DAY. ALL DATA ARE ACQUIRED IN ASCENDING AND STRIPMAP MODE.

Test site	Date	θ [°]	κ_z[rad/ m]	Pol.	T_{max}/ T_{min}[°C]
Krycklan	2011/02/27	39	0.14	HH	-5/-13
Krycklan	2012/07/28	40	0.17	HH	13/8
Krycklan	2012/08/19	41	0.16	VV	14/6
Krycklan	2011/07/20	40	0.12	VV	15/12
Remningstorp	2011/12/30	39	0.10	HH	3/-6
Remningstorp	2012/06/23	40	0.19	HH	12/5
Remningstorp	2011/08/20	40	0.12	VV	15/5
Remningstorp	2012/08/28	41	0.17	VV	15/13

In order to evaluate the effect of seasonality on both, the height estimation and the biomass classification performance, four experimental summer acquisitions (two for Krycklan and two for Remningstorp) were additionally used. Unfortunately, experimental acquisitions for the two sites in an acquisition mode similar to the DEM mode acquisitions (single-pol, bistatic, stripmap) were only available in VV polarization. Nevertheless, according to [31] the effect of the polarization (VV instead of HH) has minor effects in the height inversion and therefore the results are comparable. The baselines have also been chosen to be as similar as possible to the standard DEM mode.

Amplitude images, coherence images and the corresponding LIDAR height maps for the winter DEM acquisitions are shown in Figure 5.

Weather data from historical weather records of the Swedish weather stations of Skövde (Remningstorp) and Umeå (Krycklan) [43] were used to assess the weather conditions during the acquisitions.

IV. HEIGHT INVERSION

The main observable of a single TanDEM-X acquisition is the interferometric coherence in a certain polarization [44].

$$\tilde{\gamma}(pol) = \frac{<s_1^{pol} s_2^{pol^*}>}{\sqrt{<s_1^{pol} s_1^{pol^*}><s_2^{pol} s_2^{pol^*}>}}, \quad (5)$$

where S_1^{pol} and S_2^{pol} are the complex signals received at each end of the baseline formed by the two satellites of the

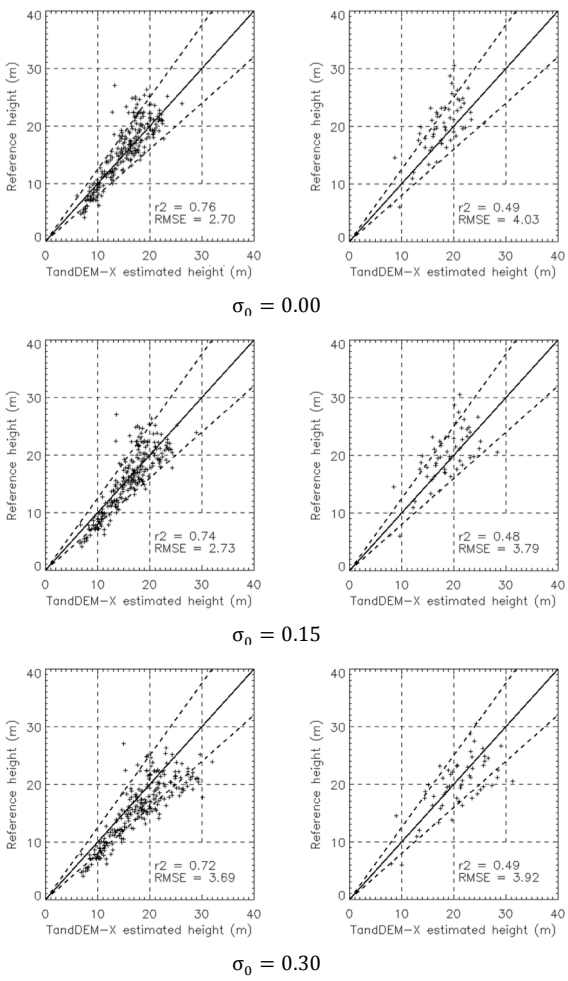

Fig. 6. Height validation plots for the DEM summer acquisition from the Krycklan 2012/07/28 (left panel) and Remningstorp 2012/06/23 (right panel) for different extinction factors σ0. The dashed lines mark the 20% height error intervals.

TanDEM-X mission. "pol" stands for the used polarization which is, in the case of TanDEM-X, HV, VH, HH or VV.

In this work, a 9 x 9 window has been used to estimate the interferometric coherence, which corresponds to about 30 independent looks. Keeping in mind the rather high coherence levels in the data, this number is considered sufficient to compensate estimation's bias [37] and variance [38].

The performance of quantitative interferometric techniques critically depends on the effective spatial baseline used for the interferometric acquisition(s) [20]. The parameter commonly used to account for the phase-to-height scaling induced by the effective baseline is the vertical wavenumber κ_z, expressed by (6):

$$\kappa_z = \mathrm{m}\frac{2\pi\Delta\theta}{\lambda \sin(\theta)} \approx \mathrm{m}\frac{2\pi B_\perp}{\lambda \sin(\theta) R} \quad , \tag{6}$$

where $\Delta\theta$ is the angular separation of the two acquisitions in the direction of the resolution cell, $B_\perp$ is the effective perpendicular baseline, θ the local incidence angle, λ the used wavelength, R the slant range distance and m accounts for the acquisition mode ($m = 1$ for monostatic acquisitions and $m = 2$ for bistatic acquisitions).

Volume decorrelation ($\tilde{\gamma}_{\mathrm{Vol}}$) is the remaining decorrelation contribution that modulates the interferometric coherence [17], [36], after the compensation of all other decorrelation contributions that affect the measured interferometric coherence $\tilde{\gamma}(\mathrm{pol})$. In the case of TanDEM-X, additive noise decorrelation is identified as the main non-volumetric decorrelation contribution, which has to be compensated. A detailed description of the compensation of non-volumetric decorrelation for data of each satellite is given in [20].

The volume decorrelation contribution is directly linked to the vertical distribution of scatterers and can be modeled by a vertical backscatter function f(z) over a dirac-like ground scattering component [42]:

$$\tilde{\gamma}_{\mathrm{Vol}}\left(\mathrm{h}_V, \sigma, \kappa_\mathrm{Z}, \mathrm{m}_{pol}\right) = \exp(\mathrm{i}\,\varphi_0)\frac{\tilde{\gamma}_\mathrm{V} + \mathrm{m}(pol)}{1 + \mathrm{m}(pol)},$$

$$\text{with} \quad \tilde{\gamma}_\mathrm{V} = \frac{\int_0^{\mathrm{h_V}} \mathrm{f(z)} \exp(\mathrm{I}\,\kappa_\mathrm{Z}\,\mathrm{z}')\,\mathrm{dz}'}{\int_0^{\mathrm{h_V}} \mathrm{f(z)}\,\mathrm{dz}'} \tag{7}$$

$$\text{and} \quad \mathrm{f(z)} = \exp\left(\frac{2\sigma z}{\cos(\theta_0)}\right)$$

where $\mathrm{m}(pol)$ is the polarization dependent ground-to-volume power ratio, φ_0 the phase related to the ground topography, θ_0 the local incidence angle, $\mathrm{h_V}$ the height of the volume (which corresponds to forest height), κ_Z the vertical wavenumber and σ the form factor of the exponential backscatter function f(z). In this case, σ can be taken as a mean extinction factor accounting for the attenuation rate of the vegetation layer.

A. Single-pol inversion

TanDEM-X DEM mode acquisitions provide only one complex coherence in a single polarization (HH). In this case, and in the absence of a ground elevation model, there is no reference which can be used to interpret the interferometric phase $\arg(\tilde{\gamma}(\mathrm{pol}))$. Therefore, the only way to enforce a balanced inversion problem is to consider only the coherence amplitudes $|\tilde{\gamma}(\mathrm{pol})|$ and to fix $\mathrm{m(pol)}$ and σ [33]:

$$\min_{\mathrm{h_v}} \left\| |\tilde{\gamma}| - \left|\tilde{\gamma}_{\mathrm{v_0}}(\mathrm{h_v}|\kappa_\mathrm{z}, \sigma = \sigma_0, \mathrm{m} = \mathrm{m}_0)\right| \right\|. \tag{8}$$

In the TanDEM-X DEM mode each site was acquired once in summer and once in winter. In [20] the strong seasonal dependency (summer/winter) of X-band scattering over forested areas has been discussed. As a consequence assumptions about m and σ may differ for summer and winter data. For this single baseline, height inversion scenarios by means of (8) were analyzed in order to define or derive the values for σ_0 and m_0.

1) Summer Scenario

In [20] $\mathrm{m} = 0$ is suggested for summer acquisitions in boreal forests. The best value for σ was here obtained by using several σ values ($\sigma \in [0.00, \ldots, 0.30]$) in (8) and choosing the σ value that provides on average the best height estimates for

both sites (correlation coefficient and root mean square error (RMSE) were used as main statistical performance criteria). Several values of m were also tested for each σ, but are not reported as they have not showed any improvement in the inversion results.

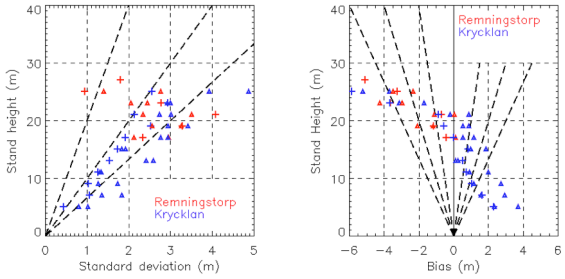

Fig. 7. Accuracy evaluation of the summer acquisitions with σ = 0.1 and m = 0; on the left side: standard deviation vs. forest height, the black lines represent the height error from left to right 5%, 10% and 15%. On the right side: bias vs. forest height, the black lines represent the height error, from inside to outside 5%, 10%, 15%. Triangles: the two experimental acquisitions. Crosses: the DEM acquisition.

Validation plots for the Krycklan DEM mode summer acquisition (2012/07/28) are shown in Figure 6 (left panel) and for the Remningstorp DEM mode summer acquisition (2012/0623/) in Figure 6 (right panel). Low σ values (i.e. σ <0.1) tend to underestimate especially taller forest stands while too large σ values (i.e. σ >0.3) overestimate tall forest stands in both sites. For shorter forest stands similar trends can be observed but less pronounced. σ = 0.1 seems to fit best, also accounting for the expected growth in both sites, and was therefore used to invert the single baseline summer scenarios. Some underestimations occurring above an estimated height of 13m may be caused by unknown harvesting/thinning activities. The experimental mode summer acquisitions confirm the results obtained for the DEM mode acquisitions.

Figure 7 shows for both sites the standard deviation (on the left) and the bias (on the right) of the estimated forest heights as a function of forest height from all summer acquisitions, obtained using (8) with σ_0 = 0.1 and m_0 = 0. In order to estimate the standard deviation and bias, the forest plots were grouped according to the reference height H100 in 2 m height (H100) intervals (sufficient to include enough samples). Standard deviation and bias is then calculated for each group individually. The standard deviation is independent of forest height, varying between 10% and 15% (second and third dashed line from the left in Figure 7 – left side). The bias plot shows an almost linear trend from short to tall forest stands. Short forest stands tend to be overestimated while tall forest stands tend to be underestimated. The larger bias still observed below 10-12 can be a consequence of the height inversion limitations. Indeed, the invertible height range is defined by the effective baseline (κ_Z). Shorter baselines are more sensitive to higher heights and less sensitive to lower heights [36]. While all baselines are sensitive to the tallest trees in both sites (<40 m), this may be especially critical for the experimental acquisitions which with a κ_Z = 0.10 have an optimum height inversion range above 12 m.

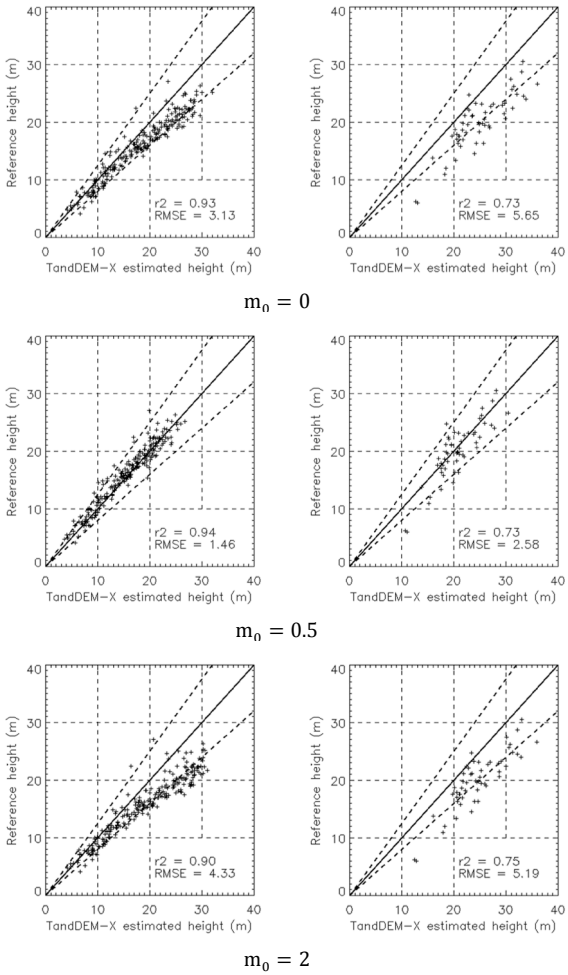

Fig. 8. Height validation plots for the DEM winter acquisition from the Krycklan 2011/02/27 (left panel) and Remningstorp 2011/12/30 (right panel) for σ=0.1 and different m. The dashed lines mark the 20% height error intervals.

The limitation of the proposed single baseline inversion scenario lies on the rather strong assumptions of σ and m, that is, σ and m are kept constant across all forest heights and independent of forest conditions. Probably σ increases with increasing forest height. In addition to the baseline sensitivity, this may also explain the linear trend observed in the bias. An inversion with a fixed mean σ value will cause an underestimation of the tall stands and an overestimation of the short stands. Only average forest heights are estimated without bias (Figure 7, left side).

2) Winter scenario

The inversion scenario of (8) with m = 0 is applied now to the winter data of both sites for different σ values ($\sigma \in [0.00, 0.10, 0.20]$). Here, it has been observed that, when m = 0, for both sites, tall forest stands are severely overestimated while short and young forest stands seem to be estimated well and the performance does not improve by changing σ values. This fact points towards changes in the ground contribution. For this reason, the inversion was repeated applying different m values ($m \in [0.00, \ldots, 2.00]$). The height validation plots for σ = 0.1, for Krycklan, are

shown in Figure 8 (left panel) and for Remningstorp in Figure 8 (right panel).

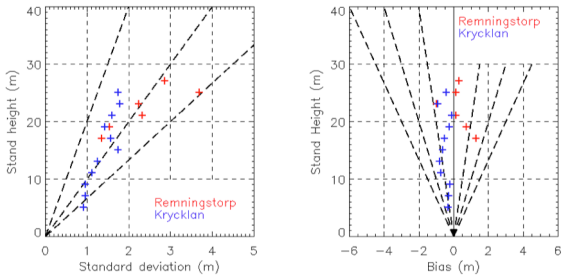

Fig. 9. Accuracy evaluation winter acquisition with σ = 0.1 and m = 0.5. On the left side: standard deviation vs. forest height, the black lines represent the height error from left to right 5%, 10% and 15%. On the right side: bias vs. forest height, the black lines represent the height error, from inside to outside 5%, 10%, 15%.

Figure 9 shows the standard deviation (on the left) and the bias (on the right) of the forest heights estimated using σ_0 = 0.1 and m_0= 0.5 for both sites. Similarly to the summer scenario, the single plots were grouped in 2 m height intervals to calculate standard deviation and bias.

The mean standard deviation is around 10%. Compared to the estimates obtained from the summer acquisitions, the standard deviation is reduced by ~5%. The bias appears independent of forest height on the order of 1m. Accounting for forest growth in Krycklan a general underestimation is observed in short and medium stands (~1.6 and ~1 m). In Remmingstorp the bias is low if the described forest growth is considered (especially noticeable for stands below 20 m).

For the winter acquisitions the assumptions of constant σ and m seem to be less disturbing. The optimal σ and m fluctuate less in the image and the height inversion is therefore more stable.

B. Dual baseline phase difference

The availability of a second complex coherence may improve the accuracy of the height estimates, may reduce the assumptions necessary to invert (7) and probably allows exploiting the phase information.

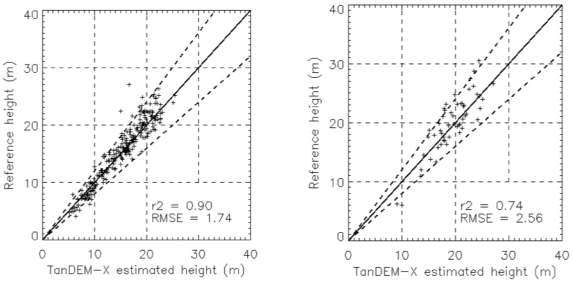

Fig. 10. Height validation plots for the dual baseline inversion scenario using the mean between the summer-winter acquisitions. On the left side: Krycklan (2012/07/28, 2011/02/27). On the right side: Remningstorp (2012/06/23, 2011/12).The dashed lines mark the 20% height error intervals.

A first combination approach was used calculating the mean between the two baselines in order to get an extra look. The results, which for the best case scenario (summer – winter) are shown in Figure 10, do not show an improvement for Krycklan, and a very minor improvement for Remningstorp. Therefore, the exploitation of the phase information can be especially useful.

Of course the backscattering properties change between the two acquisitions [35]. According to (7) changes in σ and m affect the location of the scattering center h_c which is calculated using expression (9):

$$h_c = \frac{h_v}{1-\frac{1}{e^{2\sigma h_v/\cos\theta_0}}} - \frac{\cos\theta_0}{2\sigma}. \qquad (9)$$

Changes in the scattering center height can be used to evaluate changes of backscattering behavior. The height difference of the interferometric phase centers (Δh) can be used as a proxy to estimate the scattering center height difference, and calculated as:

$$\Delta h = (\arg(\tilde{\gamma}_1)/\kappa_{Z1}) - (\arg(\tilde{\gamma}_2)/\kappa_{Z2}). \qquad 10)$$

Δh is estimated for the two experimental mode summer acquisitions, in VV polarization for both sites (Krycklan: 2011/07/20 - 2012/08/19, Remningstorp: 2011/08/20 - 2012/08/28) and for the two DEM mode acquisitions (summer and winter) for each site (Krycklan: 2012/07/28 - 2011/02/27 , Remningstorp: 2012/06/23 - 2011/12/30).

A 2-D histogram of Δh versus forest height is shown in Figure 11 for the experimental mode summer acquisitions, in VV polarization, and in Figure 12 for the summer and winter DEM acquisitions in HH polarization for both sites. For the summer acquisition, a Δh of approximately 0 (see Figure 11) indicates that the extinction factor σ and ground-to-volume ratio m are rather stable between the acquisitions.

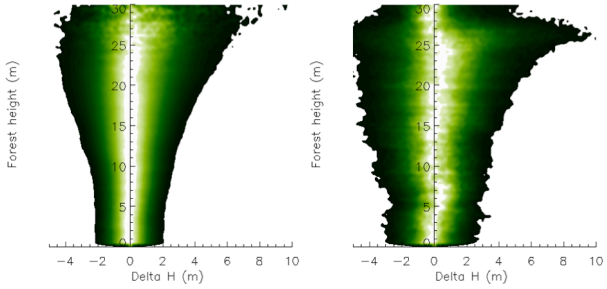

Fig. 11. Summer – summer phase difference: 2-D histogram of Interferometric height difference (VV) vs. forest height. Color scale ranges from dark green (low values) to white (high values). On the left side: Krycklan (2011/07/20 - 2012/08/19). On the right side: Remningstorp (2011/08/20 - 2012/08/28)

For the winter acquisitions, the height of the scattering phase center is usually lower than for summer acquisition [20]. This is reflected in the phase center difference between the summer and winter acquisitions shown in Figure 12 with a positive Δh. This can be interpreted by an increased m in the winter (with respect to the level in summer) and/or a decrease of σ in the winter (respect to summer σ).

For Krycklan, Δh increases almost linearly with increasing forest height. It is worthy noticing that this may be indicating that winter conditions affect all forest height classes in the same way, which argues for a uniform forest structure.

The linear trend between forest height and Δh, as found for Krycklan, could not be confirmed on Remningstorp. There is no clear trend of Δh along forest height. This site has less pronounced winter conditions (mean temperature in winter can be around 0°), so changes in the height of the phase center are mainly induced by the fall of leaves and changing weather conditions.

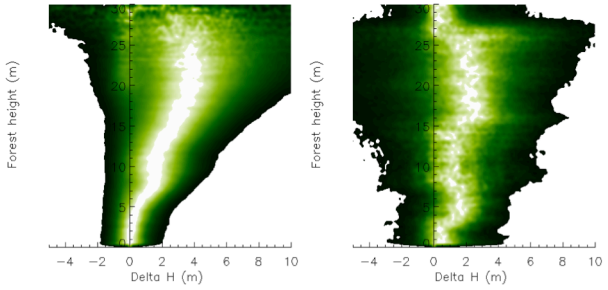

Fig. 12. Summer – winter phase difference summer – winter: 2-D histogram of Interferometric height difference (HH) vs. forest height. Color scale ranges from dark green (low values) to white (high values). On the left side: Krycklan (2011/02/27 - 2012/07/28). On the right side: Remningstorp (2011/12/30 - 2012/06/23).

1) Dual baseline inversion

An additional baseline provides a second estimate of the interferometric coherence. If $\Delta h \approx 0$ then it can be assumed that $m_{s1} = m_{s2} = m$ and $\sigma_{s1} = \sigma_{s2} = \sigma$. Now, the two interferometric coherence amplitudes, $\left|\tilde{\gamma}\left(\text{pol}, \kappa_{z_{s1}}\right)\right|$ and $\left|\tilde{\gamma}\left(\text{pol}, \kappa_{z_{s2}}\right)\right|$, can be used for the inversion. The interferometric phases, $\left(\arg\left(\tilde{\gamma}\left(\text{pol}, \kappa_{z_{s1}}\right)\right)\right.$ and $\left.\arg\left(\tilde{\gamma}\left(\text{pol}, \kappa_{z_{s2}}\right)\right)\right)$, do not provide additional information if both refer to the same scattering center. Hence, a summer – summer inversion scenario allows the estimation of an additional parameter, the volume extinctions factor σ if m = 0 is assumed. h_V and σ are estimated by (11):

$$\min_{h_V,\sigma}\left\|\begin{bmatrix}\left|\tilde{\gamma}\left(\text{pol}, \kappa_{z_{s1}}\right)\right| \\ \left|\tilde{\gamma}\left(\text{pol}, \kappa_{z_{s2}}\right)\right|\end{bmatrix} - \begin{bmatrix}\left|\tilde{\gamma}_{\text{Vol}}\left(h_V, \sigma\middle|\kappa_{z_{s1}}, m = 0\right)\right| \\ \left|\tilde{\gamma}_{\text{Vol}}\left(h_V, \sigma\middle|\kappa_{z_{s2}}, m = 0\right)\right|\end{bmatrix}\right\|. \quad (11)$$

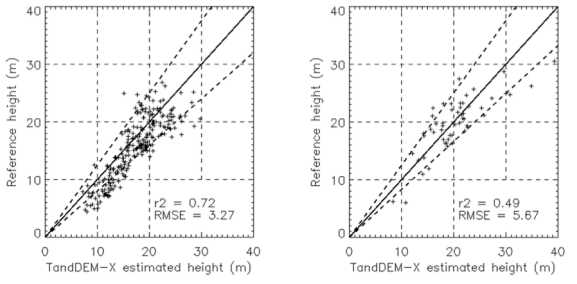

Fig. 13. Height validation plots for the dual baseline inversion scenario described in (11) using the experimental summer acquisitions. On the left side: Krycklan (2011/07/20 - 2012/08/19). On the right side: Remningstorp (2011/08/20 - 2012/08/28). The dashed lines mark the 20% height error intervals.

Allowing σ to be a free parameter, rather than fixed, biases the height estimation. However, this inversion scenario requires for a successful implementation a sufficiently large difference between the two baselines. The smaller the difference between κ_{z_1} and κ_{z_2}, and the difference between $\left|\tilde{\gamma}\left(\text{pol}, \kappa_{z_{s1}}\right)\right|$ and $\left|\tilde{\gamma}\left(\text{pol}, \kappa_{z_{s2}}\right)\right|$, the less stable becomes the inversion.

The results obtained when applying (11) on the summer-summer data are shown in Figure 13 for Krycklan from 2011/07/20 and 2012/08/19 (on the left) and of Remningstorp from 2011/08/20 and 2012/08/28 (on the right). Areas of low coherence (0.2) have been masked out in the dual baseline inversion as the information is no longer reliable there (for the given number of looks).

The presented results do not improve compared to the single baseline summer acquisitions, neither for Krycklan nor for Remningstorp. Probably the assumption $\sigma_{s1} = \sigma_{s2} = \sigma$ is too strong and does not hold on single resolution cell level. As there is an approximate one year difference between the two acquisitions, the temporal changes could be too strong to be used in a common inversion. Due to the poorer performance, this inversion scenario will not be considered for the following analyses.

2) Dual baseline inversion – different phase height

In case of relevant Δh, as found between the DEM summer and winter acquisitions, the assumptions $m_s = m_w$ and/or $\sigma_s = \sigma_w$ (where the suffix s stands for summer acquisitions and the suffix w stands for winter acquisitions) are not anymore valid. With Δh, an additional observable is provided exploiting the phase information of the two interferometric observations and allowing to resolve for an additional unknown parameter, with a total of five unknowns (σ_s, σ_w, m_s, m_w and h_v stand against three observables ($\left|\tilde{\gamma}\left(\text{pol}, \kappa_{z_s}\right)\right|$, $\left|\tilde{\gamma}\left(\text{pol}, \kappa_{z_w}\right)\right|$ and Δh).

In a next step the two unknowns with the largest impact on Δh need to be identified. Results from the single baseline inversion scenario showed that, in the summer and the winter, scenario, $\sigma_0 = 0.1$ seems to apply well and can be assumed as a constant ($\sigma_s = \sigma_w = 0.1$). The variance in the single baseline winter scenario seems to be mainly induced by a changing ground contribution ($m_s \neq m_w$), leading to the following inversion scenario:

$$\min_{H_V,m_w}\left\|\begin{bmatrix}\left|\tilde{\gamma}\left(\text{pol}, \kappa_{z_s}\right)\right| \\ \left|\tilde{\gamma}\left(\text{pol}, \kappa_{z_w}\right)\right| \\ \Delta h\end{bmatrix} - \begin{bmatrix}\left|\tilde{\gamma}_{\text{Vol}_s}\left(h_V,\ m_s\middle|\kappa_{z_s}, \sigma_s = 0.1\right)\right| \\ \left|\tilde{\gamma}_{\text{Vol}_w}\left(h_V, m_w\middle|\kappa_{z_w}, \sigma_w = 0.1\right)\right| \\ \left(\arg\left(\tilde{\gamma}_{\text{Vol}_s}\right)/\kappa_s\right) - \left(\arg\left(\tilde{\gamma}_{\text{Vol}_w}\right)/\kappa_{z_w}\right)\end{bmatrix}\right\|. \quad (12)$$

An alternative inversion scenario follows from the assumption that changes in the height of the scattering center between the summer and the winter acquisition arise from different extinction factors $\sigma_s \neq \sigma_w$ (i.e. differential extinction).

Taking over the assumptions on m from the single baseline inversion scenarios with the best results (see Section IV), $m_s = 0$ and $m_w = 0.5$ lead to the following dual baseline inversion scenario:

$$\min_{H_V,\sigma_s}\left\|\begin{bmatrix}|\tilde{\gamma}(\mathrm{pol},\kappa_{z_s})|\\ |\tilde{\gamma}(\mathrm{pol},\kappa_{z_w})|\\ \Delta h\end{bmatrix}-\begin{bmatrix}|\tilde{\gamma}_{\mathrm{Vol}_s}(h_V,\sigma_s|\kappa_{z_s},m_s=0)|\\ |\tilde{\gamma}_{\mathrm{Vol}_w}(h_V,\sigma_w|\kappa_{\kappa_{z_w}},m_w=0.5)|\\ (\arg(\tilde{\gamma}_{\mathrm{Vol}_s})/\kappa_{z_s})-(\arg(\tilde{\gamma}_{\mathrm{Vol}_w})/\kappa_{z_w})\end{bmatrix}\right\| \quad (13)$$

The results obtained when applying (12) to the winter-summer data are shown in Figure 14. Krycklan is placed on the left side and Remningstorp on the right side. For Krycklan, the inversion results are improved compared to the single baseline inversion and the averaged dual baseline. Moreover, the height estimates from short, middle and tall stands deviate from the 1:1 line in accordance to the expected trend caused by growth effects. For Remningstorp, an inversion according to (12) tends to overestimate forest height. Especially in the taller forest stands, a bias of ~2 m to ~5 m can be observed. Here, changes in the phase center heights Δh seem to be more driven by changes of the extinction σ than by changes of the ground-to-volume ratios m.

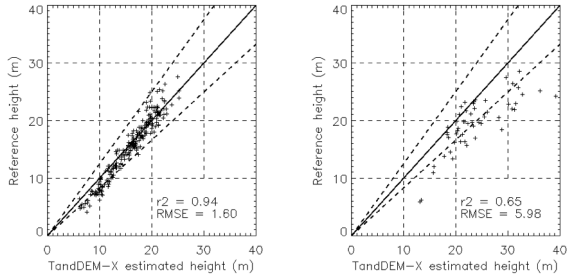

Fig. 14. Height validation plots for the dual baseline inversion scenario described by (12) using the summer and winter DEM acquisitions. On the left side: Krycklan (2012/07/28, 2011/02/27). On the right side: Remningstorp (2012/06/23, 2011/12). The dashed lines mark the 20% height error intervals.

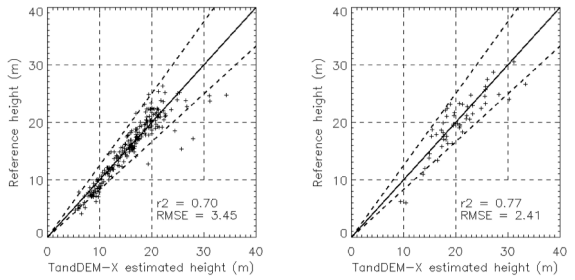

Fig. 15. Height validation plots for the dual baseline inversion scenario described by. (13) using the summer and winter DEM acquisitions. On the left side: Krycklan (2012/07/28, 2011/02/27). On the right side: Remningstorp (2012/06/23, 2011/12). The dashed lines mark 20% height error intervals.

The results obtained when applying (13) on the summer-winter data are shown in Figure 15. Krycklan is placed on the left side and Remningstorp on the right side. For Krycklan the inversion shows a decreased performance using (13). Strong overestimations are observed in some of the taller stands, probably due to wrong assumptions about σ; moreover, the clear growth trend seen in the inversion with (13) is no more visible. For Remningstorp the inversion results are clearly

TABLE 4
FOREST MANAGEMENT STAGES ACCORDING TO A FOUR CLASSES BIOMASS CLASSIFICATION.

Class (Mg/ha)	Forest development stage
0-20	Non forested, regrowth
20-65	Young forest, beginning of thinning
65-200	Mature forest, thinning to harvesting
> 200	Old forest, harvesting, senescence

TABLE 5
FOREST MANAGEMENT STAGES ACCORDING TO A FIVE CLASSES BIOMASS CLASSIFICATION.

Class (Mg/ha)	Forest development stage
0-20	Non forested, regrowth
20-50	Young forest, beginning of thinning
50-100	Thinning processes
100-220	Mature forest, harvest
> 220	Old forest, senescence

improved compared to the single baseline inversion results and also to the averaged dual baseline result. Moreover, the growth effect is clearly visible for short and middle stands.
Figure 16 shows the standard deviation and the bias of the dual baseline forest height estimates as a function of forest height. The triangles represent the inversion without Δh (4), the crosses the inversion with Δh (12) for Krycklan and (13) for Remningstorp. The bias and the standard deviation of the inversion without Δh are comparable to the results of the single baseline inversion, for both sites. In the case of the dual baseline inversion with Δh, the standard deviation improves for Krycklan compared to the winter scenario of this site. A bias of 2 m for the short forest stands is more realistic than in the winter scenario as it accounts for the expected forest growth between the acquisition of the validation data and the acquisition of the TanDEM-X data. Nevertheless, errors introduced by the limitation of the height range inversion due to the short baselines, as seen for the single baseline summer case, may be biasing the height inversion results below 12 m. In the case of Remningstorp, the standard deviation remains close or below 5% and performs better than in the case of the single baseline inversion

.

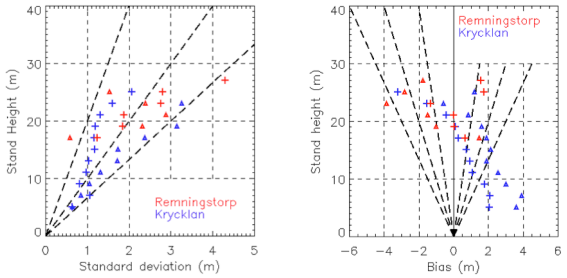

Fig. 16. Accuracy evaluation for the dual baseline inversion. On the left side: standard deviation vs. forest height, the black lines represent the height error from left to right 5%, 10% and 15%. On the right side: bias vs. forest height, the black lines represent the height error, from inside to outside 5%, 10%, 15%. Triangles: dual baseline inversion without Δh (4). Crosses: dual baseline inversion with Δh (12) for Krycklan and (13) for Remningstorp.

Fig. 17. Krycklan biomass classification maps. From left to right: single baseline summer (2012/07/28) with four classes (0-20, 20-65, 65-200, >200 Mg/ha), single baseline winter (2011/02/27) with five classes and dual baseline summer-winter with five classes (0-20, 20-50, 50-100, 100-220, >220). Biomass classes are colored from light to dark green according to the mean biomass (center value) of each class.

V. Biomass Classification

A. Biomass estimation

Biomass is derived from the inverted forest height estimated from TanDEM-X data applying (2), as described in section IV, for both sites. In what follows, only forest heights obtained from all single baseline acquisitions (using (8)) and from the dual baseline summer – winter acquisitions (using (12) for Krycklan and (13) for Remningstorp site) were considered. For the summer acquisitions σ_0 was set to 0.1 and m_0 to 0 and for the winter acquisitions $\sigma_0 = 0.1$ and $m_0 = 0.5$ were used.

B. Biomass classification results.

Based on the classification analysis in section II.B and the estimation accuracy of forest height in section IV, the number of classes and the optimum class boundaries can be deduced.
The estimation of forest heights below 10 m (corresponding to a biomass of 30 Mg/ha), shows a constant error, generally, larger than 20% with a bias typically around 2 m (see Figure 7, Figure 9 and Figure 16). As this trend is generally observed in all scenarios (independently from the overall error), instead of using only relative error boundaries, we define the first class with the boundaries obtained for a 2 m absolute error (Table 2) and for heights larger than 10 m, we estimate the class boundaries applying a relative error. Therefore, the relative error defines the final number of biomass classes, which results in four classes for a 10% error and five classes for a 5% error.
The single baseline summer acquisitions, of both sites, show a relative error of approximately 10% for heights larger than 10 m, allowing a total of four biomass classes: 0 – 20, 20 – 65, 65 – 200 and > 200 Mg/ha (Table 4). For the single baseline winter acquisitions and the dual baseline inversion winter - summer the height error reduces to levels close to 5%, which allows the separation of a five biomass classes, in total: 0 – 20, 20 – 50, 50 – 100, 100 – 220 and > 220 Mg/ha (Table 5). The boundaries of the biomass classes were adjusted to fit defined stages of forest development used in forest management or for the characterization of forest growth stages [31]. The class 0 – 20 Mg/ha corresponds to non-forested areas. In the case of four classes, the class 20 – 65 Mg/ha corresponds to the first stage of a young forest under growth. The beginning of thinning processes mark the next class (65-200 Mg/ha) where the forest stand achieves a mature state and the last thinnings and the harvesting processes will take place. The last class (> 200 Mg/ha) corresponds to an old forest stand. Five classes allow a better distinction within the previous mature forest class, into a forest during the consolidation phase, typically under thinning treatments (50-100 Mg/ha) from an established forest in the last thinning phase or ready for harvesting (100-220 Mg/ha).
The corresponding biomass classification maps are shown for Krycklan in Figure 17: on the left side, the map obtained from the single baseline DEM mode summer acquisition (2012/07/28) with four biomass classes, in the middle, the map obtained from the single baseline DEM mode winter acquisition with five biomass classes (2011/02/27) and on the right side, the map obtained for the dual baseline DEM mode acquisition with five biomass classes. The maps for Remningstorp are shown in Figure 18: on the left, the map obtained for the single baseline DEM mode summer

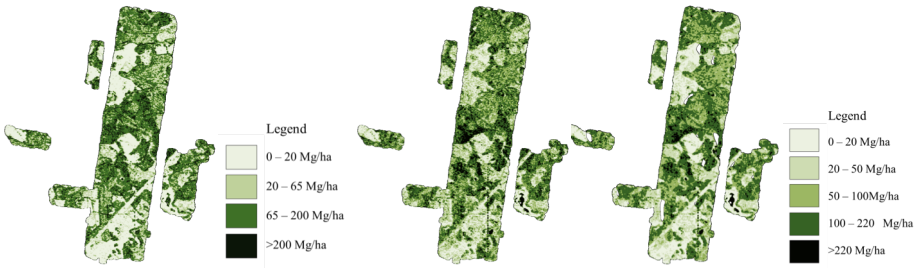

Fig. 18. Remmingstorp biomass classification. From left to right: summer (2012/06/23) with four classes (0-20, 20-65, 65-200, >200 Mg/ha), winter (2011/12/30) and dual baseline summer-winter with five classes (0-20, 20-50, 50-100, 100-220,>220). Biomass classes are colored from light to dark green according to the mean biomass (center value) of each class.

acquisition (2012/06/23) with four biomass classes, in the middle, the map obtained for the single baseline DEM mode winter acquisition with five biomass classes (2011/12/30), and on the right, the map obtained for the dual baseline DEM mode acquisition with five biomass classes.

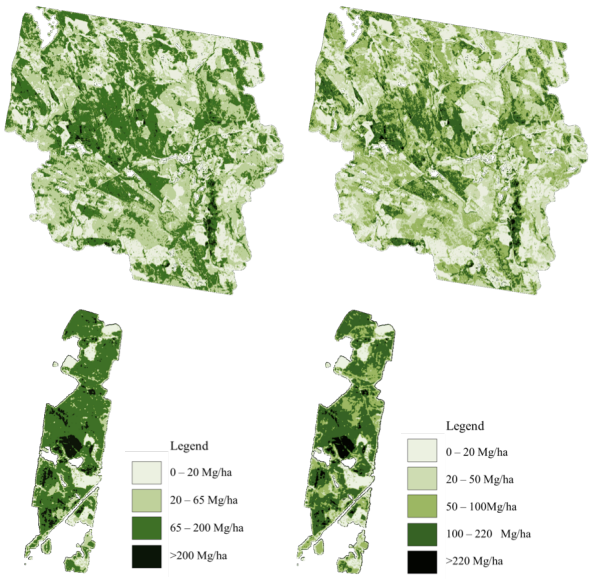

Fig. 19. Biomass classification for the LIDAR-derived reference biomass data. On the left panel: four classes' classification. On the right panel: five classes' classification. On the top panel: Krycklan. On the bottom panel: Remmingstorp. Biomass classes are colored from light to dark green according to the mean biomass (center value) of each class.

The four and five class biomass maps have similar stand boundaries. The winter and the dual baseline acquisitions have a more detailed structure with five classes (mainly visible in Krycklan, due to the larger range of forest heights).

The largest discrepancies between the five classes single baseline winter scenario and the dual baseline scenarios appear in the lowest biomass class < 20 Mg/ha. As forest growth is fastest in this regrowth stage (up to ~10 m tall trees) a general overestimation can mean a higher accuracy in the estimation of those forested areas that still have not reached a higher biomass. In Remmingstorp it is possible to appreciate larger class areas with sharper boundaries, especially in the class 0 – 20 Mg/ha and 50 – 100 Mg/ha.

In Figure 19, the biomass classification maps obtained from the reference LIDAR biomass are displayed for both sites with four and five biomass classes (note that for Remmingstorp the area of the reference biomass data is smaller than the area of the reference H100).

The maps of differences between the biomass classification obtained from TanDEM-X and the equivalent classification obtained from the reference data are shown in Figure 20 for Krycklan and in Figure 21 for Remningstorp. The summer scenario is shown on the left side, the winter scenario in the middle and the dual scenario on the right. Classes that were equal in both scenarios are in green, classes of higher biomass in the TanDEM-X classification scenario are in blue and classes of lower biomass in the TanDEM-X classification are in yellow. The good agreement between the TanDEM-X and the reference classification was somehow expected although specific differences between the acquisitions and the sites were noted. The agreement in Krycklan is in general higher than in Remningstorp. Moreover, it was observed in both sites that the dual baseline scenario allows a better classification, less affected by noise patterns than the winter acquisitions, and was able to compensate the overestimation visible in the other scenarios. In both sites overestimation (blue) is more dominant than underestimation (yellow), especially visible in the winter scenario, where this effect is stronger in the high biomass areas. The summer scenario also shows a very good agreement, favored by the lower class variability (4 biomass classes). Here, an underestimation tendency is more dominant. It is important to note that the area in the center of Remningstorp corresponds to a harvested stand between the LIDAR and the TanDEM-X acquisitions. More comments and conclusions are drawn in the following section.

C. Confusion matrices

The confusion matrix is a commonly used tool for assessing the classification accuracy [44] and it is obtained by counting the correspondence between the reference biomass and the estimated biomass classifications maps. Here, the confusion matrix term will refer, for reasons of simplicity and to allow a faster comparison between the scenarios, to results normalized to the total each column (user accuracy i.e. percentage or right classified pixels). The two sites were combined for the calculation of the confusion matrix.

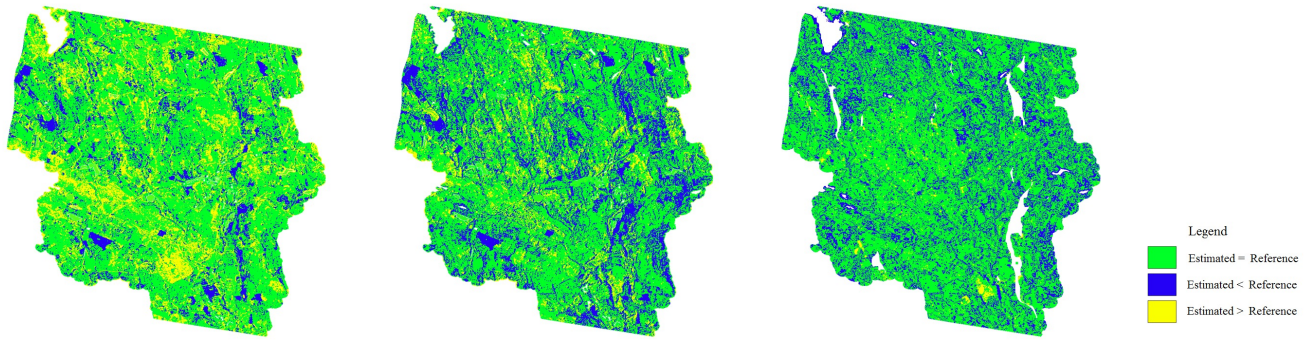

Figure 20: Maps of the differences between the TanDEM-X classification and the equivalent classification obtained from the LIDAR reference data for Krycklan test site. From left to right: summer (2012/07/28) with four classes, winter (2011/02/27) and dual baseline summer-winter with five classes. Classes that are equal in both scenarios are displayed in green, classes of higher biomass in the TanDEM-X classification scenario are displayed in blue and classes of lower biomass in the TanDEM-X classification are displayed in yellow.

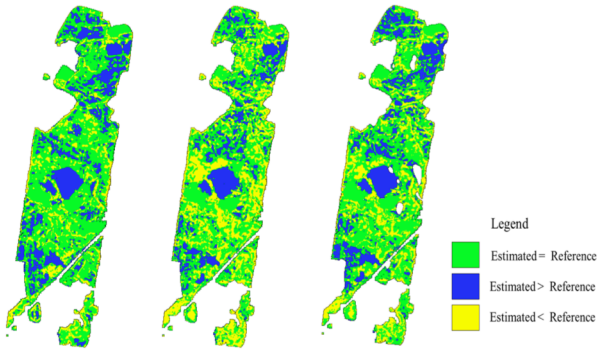

Fig. 21. Maps of the differences between the TanDEM-X classification and the equivalent classification obtained from the LIDAR reference data for Remningstorp test site. From left to right: summer (2012/06/23) with four classes, winter (2011/12/30) and dual baseline summer-winter with five classes. Classes that are equal in both scenarios are displayed in green, classes of higher biomass in the TanDEM-X classification scenario are displayed in blue and classes of lower biomass in the TanDEM-X classification are displayed in yellow.

TABLE 6
CONFUSION MATRIX FOR SINGLE BASELINE SUMMER DEM WINTER ACQUISITIONS SCENARIO (KRYCKLAN 2012/07/28 AND REMNINGSTORP 2012/06/23). OVERALL ACCURACY 88.0%.

Summer, four classes	**Reference classes (Mg/ha)**			
TanDEM-X classification (Mg/ha)	0-20	20-65	65-200	>200
0-20	**0.95**	0.01	0.00	0.00
20-65	0.05	**0.59**	0.09	0.06
65-200	0.00	0.37	**0.90**	0.93
> 200	0.00	0.03	0.01	**0.01**

TABLE 7
CONFUSION MATRIX FOR SINGLE BASELINE WINTER DEM SCENARIO. (KRYCKLAN 2011/02/27 AND REMNINGSTORP 2011/12/30). OVERALL ACCURACY 87.6%.

Winter, five classes	**Reference classes (Mg/ha)**				
TanDEM-X classification (Mg/ha)	0-20	20-50	50-100	100-220	>220
0-20	**0.98**	0.15	0.00	0.00	0.04
20-50	0.02	**0.64**	0.14	0.00	0.06
50-100	0.00	0.20	**0.66**	0.22	0.07
100-220	0.00	0.01	0.20	**0.73**	0.55
>220	0.00	0.00	0.00	0.05	**0.28**

1) Single baseline

One confusion matrix is calculated for the biomass map obtained from the DEM summer acquisitions with four biomass classes (Table 6
) including both sites. The overall accuracy for the highest success rate in both inversion scenarios is found for the lowest biomass class (0 – 20 Mg/ha), with more than 95% right classified pixels.
The 65 – 200 Mg/ha forest class shows a success rate of 90% (for the summer acquisition). In the class >200 Mg/ha practically all pixels are underestimated. This result has to be carefully interpreted as this forest class covers only a small fraction of the image (~2% of the combined reference biomass map), so small displacements between the LIDAR and the TanDEM-X, can strongly influence the accuracy measurement.
The classification of the winter scenario (Table 7) resulted in a mean classification success rate between 64% and 73% for the three biomass classes between 20 and 220 Mg/ha. The worst results were obtained for the highest biomass class >220 Mg/ha with only 28% success rate and the biomass tends to be underestimated.

2) Dual baseline

Classification results for the dual baseline (summer - winter) inversion scenario with five biomass classes have an overall success rate of 86.0% (Table 8). The classification results are comparable with the five classes obtained from the single baseline winter data. Only class >220 Mg/ha improved to a success rate of 37%.
The five years interval between the acquisition of the LIDAR reference data and the TanDEM-X acquisitions (see section II.A) may result in a general overestimation for all biomass classes and may reduce the apparent overall accuracy. Wrong classified pixels tend rather to be overestimated, due to forest growth, than underestimated (except for the highest class, where thinning effects may be reflected in a decrease of the H100). In conclusion, a constant decrease in accuracy in the classes 20 – 50, 50 – 100 and 100 – 220 Mg/ha is observed. In the class >220 Mg/ha the accuracy increases as no forest growth is expected.

TABLE 8
CONFUSION MATRIX FOR DUAL BASELINE SCENARIO WINTER/SUMMER CASE. (KRYCKLAN 2012/07/28 -2011/02/27 AND REMNINGSTORP 2012/06/23-2011/12/30). OVERALL ACCURACY 86.0%.

Dual, five classes	**Reference classes (Mg/ha)**				
TanDEM-X classification (Mg/ha)	0-20	20-50	50-100	100-220	>220
0-20	**0.96**	0.01	0.00	0.00	0.02
20-50	0.04	**0.60**	0.04	0.00	0.11
50-100	0.00	0.37	**0.69**	0.23	0.07
100-220	0.00	0.01	0.25	**0.66**	0.43
>220	0.00	0.01	0.02	0.11	**0.37**

D. Comparison with CORINE

The resulting biomass classification maps from the single baseline scenario of the DEM winter acquisitions (Krycklan 2012/07/28 and Remningstorp 2011/12/30) have been compared with the European thematic classification CORINE.
CORINE has a spatial resolution of 100x100 m. The TanDEM-X classification has a spatial resolution, after multi-looking, of 16x16 m. An image of the overlay between CORINE and the TanDEM-X biomass classification is displayed, for both sites, in Figure 22. Non-forested areas, i.e. grasslands and agriculture, are superimposed in white on the TanDEM-X classification results. As CORINE is a thematic classifier non forested areas from CORINE correspond to the lowest biomass class (<20 Mg/ha) in the TanDEM-X biomass maps which is the case for most of the area in both acquisitions. Forested areas, classified in CORINE as forests (coniferous forest in the rest of the Krycklan site, or mixed

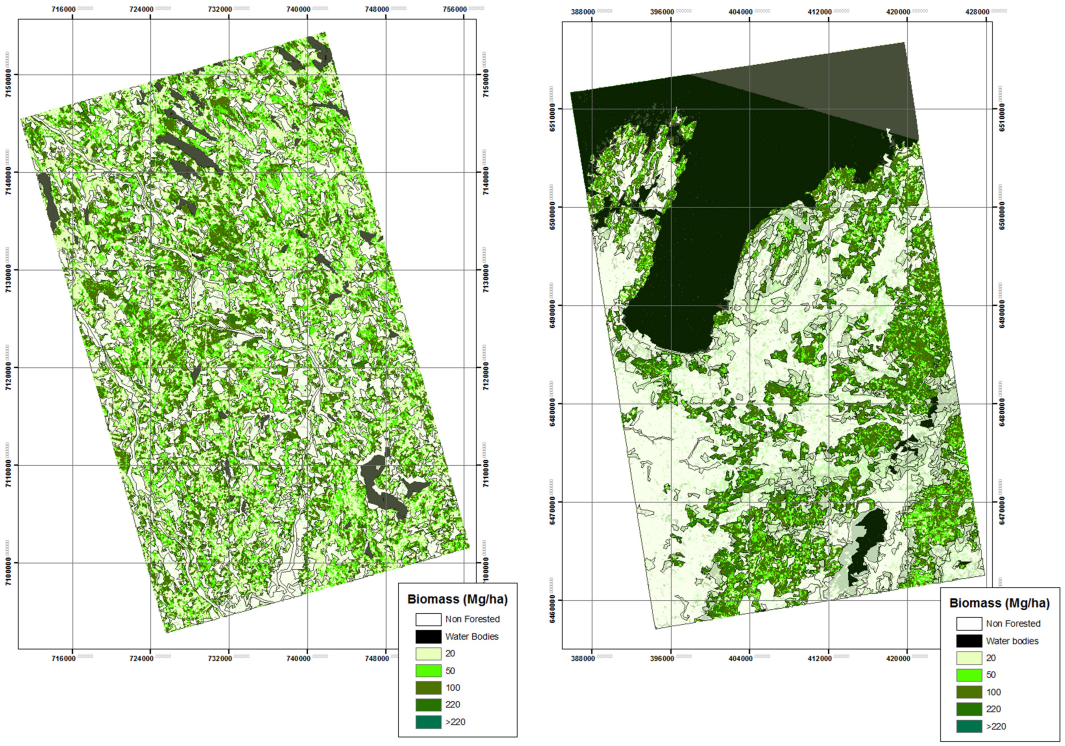

Fig. 22. Biomass classification for Krycklan (2011-02-27), on the left side, and Remningstorp (2012-12-30), on the right side, with overlaid CORINE forest-non forest map . Biomass is grouped in five classes: 0-20, 50-100, 100-220, >220 Mg/ha, from light to dark green. Non-forested areas from CORINE are overlaid in white. Water bodies are represented in black.

and coniferous forest in the rest of the Remningstorp site) are separated by TanDEM-X in five biomass classes.

TABLE 9
CONFUSION MATRIX FOR THE FOREST/ NON FOREST CLASSIFICATION BETWEEN THE KRYCKLAN SINGLE BASELINE WINTER DEM SCENARIO (2011/02/27) AND THE CORINE CLASSIFICATION. OVERALL ACCURACY 53.3%.%.

Krycklan	**CORINE classes**	
TanDEM-Xclassification	Non-forest	Forest
Non-Forest (< 20 Mg/ha)	**0.80**	0.50
Forest (> 20 Mg/ha)	0.20	**0.50**

Confusion matrices have been calculated for both sites. The results for Krycklan are shown in Table 9, and for Remningstorp in Table 10. Results from the matrices are displayed separately here, due to the site-dependency effects that are observed between CORINE and the TanDEM-X data at the large scale. Being the resolution of the maps obtained from TanDEM-X much higher than from CORINE there are many stands (patches of forest) that are recognized by the first and not by the second, and this produces different classification performances depending on the main land cover type of the site. In Krycklan which is a forested area, 80% of the pixels are classified as Non-Forest in both maps, however only a 50% of the pixels are classified as Forest in both of them. This is due to the existence of a high number of small forested areas which have a biomass lower than 20 Mg/ha and are not detected inside of the class that CORINE defines as Forest (another 50% of the pixels). In Remningstorp, being an area dominated by agriculture, the effect is the opposite. An 84% of the pixels are classified as forest in both maps, however a high number of isolated patches classified as forest in the map obtained from TanDEM-X are not detected by the CORINE map inside the classes which correspond to the agricultural areas (61% of the pixels). These patterns can be clearly observed in Figure 22.

TABLE 10
CONFUSION MATRIX FOR THE FOREST/ NON-FOREST CLASSIFICATION BETWEEN THE SINGLE BASELINE REMNINGSTORP WINTER DEM SCENARIO (2011/12/30) AND THE CORINE CLASSIFICATION. OVERALL ACCURACY 65.7%..

Remmingstorp	**CORINE classes**	
TanDEM-X classification	Non-forest	Forest
Non-Forest (< 20 Mg/ha)	**0.39**	0.16
Forest (> 20 Mg/ha)	0.61	**0.84**

VI. DISCUSSION AND CONCLUSION

This paper demonstrates that single baseline X-band interferometric data from the standard DEM mode of Tandem-X are sensitive to forest height and biomass, and they can successfully be used to perform a biomass classification of boreal forests. When only one baseline is available, quite strong assumptions about the volume shape factor and the ground-to-volume ratio are needed. However, it has been shown that a wide range of values for extinction σ and ground-to-volume ratio m can be used without significantly impacting the height estimation accuracy. The winter scenarios appeared to be more suitable for biomass inversion

than the summer scenarios, especially in Krycklan. This site, located further north than Remningstorp, is a typical boreal site with colder winter temperatures and permanent frozen conditions during the winter months.

Moreover, the availability of several interferometric baselines allowed us to investigate different inversion scenarios including baselines. A significant change of the interferometric phase center height (from summer to winter) allows exploiting phase information in a dual baseline inversion scenario and improved the height inversion results.

It was observed that with adequate σ and m assumptions, the results of the single baseline inversion are already very accurate, explained by the assumed homogeneity of the forest structures in the boreal environment. Yet, if forest growth is considered, a general tendency of underestimation in the lower classes is observed. The experimental dual baseline analyses done with data for the summer – summer case and with DEM data for the summer – winter case indicate that a phase center height difference, as it appeared in the summer-winter scenario, is needed in order to improve the classification results. However, two different dual baseline inversion scenarios with Δh (summer – winter) were needed, one for Krycklan and one for Remmingstorp. While in Krycklan Δh seemed to be induced by a changing ground-to-volume ratio in Remningstorp a changing extinction appeared more probable for introducing a Δh between summer and winter. This could be due to two reasons: first, Remningstorp belongs to the ecological class of hemi-boreal forests and has therefore a more diverse structure than pure boreal forests as found in Krycklan. Second, weather conditions during the winter acquisition were different for the two sites (Table 3). In Remningstorp the winter acquisition took place at mild temperatures above 0° C, while Krycklan was acquired at freezing conditions of -10° C and below. Moreover, the right dual baseline inversion approaches have improved the results with respect to the single baseline. In a future boreal biomass classification these effects could be accounted for by differentiating between boreal and hemi-boreal biomes [2] or/and by integrating meteorological data in the inversion process. For the two optimum scenarios selected for the dual inversion in both, Krycklan and Remmingstorp sites, the effects of forest growth could be observed, indicating a higher accuracy in the classification. Due to the lack of data, winter-winter conditions could not be evaluated. However, we would expect a similar performance to the summer-summer data, as changes in σ or m between acquisitions of the same season are unlikely.

The TanDEM-X biomass classification possesses a high spatial resolution, which allows a consistent classification with a single methodology for the entire boreal region at a high resolution. The classification performance has appeared to be similar between the two sites proving the transferability of the allometric equation between boreal sites that represent different weather conditions within the biome. The numbers of classes and the class boundaries have been selected as a result of a sensitivity analysis, studying the error propagation from the height inversion to the biomass inversion. Each class can be associated to a certain forest development stage or management process. Depending on the number of classes, forest development stages or management phases can be associated to them, giving an ecological meaning to each forest biomass class boundaries. From the height inversion analyses (Section IV) a height inversion error between 5% and 10% is expected for the winter and the dual baseline inversion scenarios with Δh (summer – winter) and an inversion error up to 15% for the summer scenarios. According to the sensitivity analyses done in Section II.B four biomass classes could be segregated for pure summer scenarios and five biomass classes for pure winter acquisitions and the dual baseline (summer – winter) scenario. The maximum biomass class is above 220 Mg/ha and until that point no saturation effects could be detected. In both sites, the highest biomass class (>220 Mg/ha for the five classes case and >200 Mg/ha for the four classes case) represent only a very small proportion of the area. Nevertheless, it is a very relevant class as it indicates areas of very high biomass for these forest environments, and can indicate where forest in an old stage are located.

The obtained biomass classification maps can improve thematic mapping in forested areas as provided by CORINE, and is able to discriminate between different biomass levels within a defined CORINE forest class in the boreal forest (e.g. coniferous forest). On the one hand, a higher number of classes provide with more precise biomass information and higher biomass thresholds are especially important for forest management forecasts and carbon estimation. On the other hand, a higher spatial resolution improves the knowledge about biomass distribution and allows forest management in finer scales (below the forest stand scale), as well as a better sensitivity to forest disturbances.

Dual-pol inversions can improve the height estimation accuracy as shown in [36] and therefore may also improve biomass classification accuracy. One extra polarization may allow a height inversion as described in [45] exploiting additionally to the coherence amplitude information, also the phase information. The phase information of a single baseline acquisition makes assumptions about extinction or the ground-to-volume ratio obsolete.

A fully polarimetric (quad-pol) system could further improve the height estimation and, therefore, the classification performance. Longer wavelengths, like L- or P-band [30], in single baseline quad pol spaceborne missions, could help the estimation of new allometries to further compensate biases coming from forest structure diversity [46]. It is therefore possible to conclude that new quad-pol spaceborne single pass missions would have a great potential for improving boreal biomass classifications and are highly necessary to periodically update the classifications for land-cover change detection.

VII. Acknowledgements

The authors would like to thank the TanDEM-X team for the fast access to the data, Pau Prats for his support in data processing and Matteo Pardini for his useful comments and remarks. This work has been partially supported by the HGF - Helmholtz Alliance “Remote Sensing & Earth System Dynamics”.

VIII. REFERENCES.

[1] M. Santoro, C. Beer, O. Cartus, C. Schmullius, A. Shvidenko, I. McCallum, U. Wegmüller and A. Wiesmann, "Retrieval of growing stock volume in boreal forest using hyper-temporal series of Envisat ASAR ScanSAR backscatter measurements", *Remote Sensing of Environment,* vol 114, pp. 490-507, 2011.

[2] Global Forest resource Assessment, Food and Agriculture Organization of the United Nations (FAO): http://www.fao.org/forestry/fra/80298/en/, 10/15/2013.

[3] R. A. Houghton, "Aboveground Forest Biomass and the Global Carbon Balance", *global change Biology*, vol, 11, pp. 945-958, 2005.

[4] FSC: http://iap.esa.int/projects/transparentforests., observed: 22/11/2013

[5] T. Schneider, A. Elatawneh, J. Rahlf, M. Kindu, A. Rappl, A. Thiele, M. Boldt and S. Hinz, "Parameter Determination by RapidEye and TerraSAR-X Data: A Step Toward a Remote Sensing Based Inventory, Monitoring and Fast Reaction System on Forest Enterprise Level", *Earth Observation of Global Changes (EOGC) Lecture Notes in Geoinformation and Cartography*, pp 81-107, 2013.

[6] S. J. Goetz, A. Baccini, N. Laporte, T. Johns, W. S. Walker and coauthors, "Mapping and monitoring carbon stocks with satellite observations: a comparison of methods", *Carbon Balance Manage*. 4. 2009.

[7] R. A. Houghton , "How well do we know the flux of CO2 from land-use change", *International Metereological Institute of Stockholm.* Vol 62B, pp. 337-351, 2010.

[8] CORINE land cover report: http://www.eea.europa.eu/publications/COR0-landcover, observed: 22/11/2013.

[9] P. Mayaux, H. Eva, J Gallego, A. H. Strahler, M. Herold, S. Agrawal, s. Naumov, E. E. De Miranda, C. M. Di Bella, C. Ordoyne, Y. Kopin, P.S. Roy, "Validation of the Global Land Cover 2000 Map, means of L and X band POLInSAR and HUTSCAT scatterometer", *IEEE Transactions on Geoscience and Remote Sensing letters*, vol 44, no 7, pp. 1728 – 1739, 2006.

[10] R. O. Dubayah and J. B. Drake, "Lidar Remote Sensing for Forestry," *Journal of Forestry*, vol. 98, no. 6, pp. 44–46, Jun. 2000.

[11] M. Simard, N. Pinto, J. B. Fisher, and A. Baccini, "Mapping forest canopy height globally with spaceborne LIDAR", *Journal of geophysical research.* Vol 116, G04021, 2011.

[12] A. M. Lefsky, "A global forest canopy height map from the Moderate Resolution Imaging Spectroradiometer and the Geosciences Laser Altimeter", *Geophysical research letters*. Vol 37, L15401, 2010

[13] W. Wagner, A. Luckman, J. Vietmeier, K. Tansey, H, Balzter, C. Schmullius, M.Davidson, D.Gaveau, M. Gluck, T. Le Toan, Shaun Quegan, Anatoly Shvidenkof, A. Wiesmann, and J. J.Yu, "Large-scale mapping of boreal forest in SIBERIA using ERS tandem coherence and JERS backscatter data", *Remote Sensing of Environment*, vol. 85, pp. 125-144, 2003.

[14] C.J. Thiel, C. Thiel and C.C. Schmullius, "Operational Large-Area Forest Monitoring Using ALOS PALSAR Summer Intensities and Winter Coherence", *IEEE Transactions on Geoscience and Remote Sensing*, vol 47, no 12, pp 3993-4000, 2009.

[15] N. Pinto, M. Simard, and R. Dubayah, "Using InSAR Coherence to Map Stand Age in a Boreal Forest," *Remote Sensing*, vol. 5, no. 1, pp. 42–56, Dec. 2012.

[16] BIOMASAR project: http://biomasar.org/, observed: 10/15/2013

[17] G. Krieger, A. Moreira, H. Fiedler, I. Hajnsek, M. Werner, M. Younis, and M. Zink, "TanDEM-X: A Satellite Formation for High-Resolution SAR Interferometry", *IEEE Transactions on Geoscience and Remote Sensing*, vol. 45, no. 11, pp. 3317- 3341, 2007.

[18] R. Treuhaft, F. Goncalves, J. R. dos Santos, M. Palace, M. Keller, S. Madsen, F. Sullivan, and P. Graca, "Exploring Vegetation Profiles from TanDEM-X Phase, Lidar, and Field Measurements in Tropical Forests," in EUSAR 2014; 10th European Conference on Synthetic Aperture Radar; Proceedings of, 2014, pp. 1–3.

[19] J. Praks, F. Kugler, K. P. Papathanssiou, I. Hajnsek and M. Hallikainen, "Tree height estimation for boreal forest by means of L and X band POLInSAR and HUTSCAT scatterometer", *IEEE Transactions on Geoscience and Remote Sensing letters*, 37(3), pp. 466-470, 2007.

[20] F. Kugler and I. Hajnsek, "Forest characterisation by means of TerraSAR-X and TanDEM-X (polarimetric and) interferometric data", *Proceedings of the Geoscience and Remote Sensing Symposium (IGARSS)*, Vancouver July, 2011.

[21] J. I. H. Askne, J. E. S. Fransson, M. Santoro, M. J. Soja, and L. M. H. Ulander, "Model-Based Biomass Estimation of a Hemi-Boreal Forest from Multitemporal TanDEM-X Acquisitions," *Remote Sensing*, vol. 5, no. 11, pp. 5574–5597, Oct. 2013.

[22] S. Solberg, R. Astrup, J. Breidenbach, B. Nilsen, and D. Weydahl, "Monitoring spruce volume and biomass with InSAR data from TanDEM-X," *Remote Sensing of Environment*, vol. 139, pp. 60–67, Dec. 2013.

[23] R. Treuhaft, F. Gonçalves, J. R. dos Santos, M. Keller, M. Palace, S. N. Madsen, F. Sullivan, and P. M. L. A. Graça, "Tropical-Forest Biomass Estimation at X-Band From the Spaceborne TanDEM-X Interferometer," IEEE Geoscience and Remote Sensing Letters, vol. 12, no. 2, pp. 239–243, Feb. 2015.

[24] M. J. Soja, H. Persson, and L. M. H. Ulander, "Estimation of Forest Height and Canopy Density From a Single InSAR Correlation Coefficient," IEEE Geoscience and Remote Sensing Letters, vol. 12, no. 3, pp. 646–650, Mar. 2015.

[25] J. I. H. Askne and M. Santoro, "On the Estimation of Boreal Forest Biomass From TanDEM-X Data Without Training Samples," IEEE Geoscience and Remote Sensing Letters, vol. 12, no. 4, pp. 771–775, Apr. 2015.

[26] J. Rahlf, J. Breidenbach, S. Solberg, E. Næsset, and R. Astrup, "Comparison of four types of 3D data for timber volume estimation," Remote Sensing of Environment, vol. 155, pp. 325–333, Dec. 2014.

[27] S. Solberg, R. Astrup, J. Breidenbach, B. Nilsen, and D. Weydahl, "Monitoring spruce volume and biomass with InSAR data from TanDEM-X," Remote Sensing of Environment, vol. 139, pp. 60–67, Dec. 2013.

[28] J. S. Huxley, *Problems of relative growth*, New York: McVeagh, 1932

[29] P. Burschel and J. Huss, *Grundriss des Waldsbaus*. Pareys Studientexte 49, Berlin, 1997

[30] T. Mette, K. Papathanassiou and I. Hajnsek, "Biomass estimation from polarimetric SAR Interferometry over heterogeneous forest terrain", *Proceedings of the Geoscience and Remote Sensing Symposium (IGARSS)*, Anchorage, USA, September 2004.

[31] A. Van Laar and A. Akça, *Forest Mensuration (Managing Forest ecosystems)*. Doordrecht. Springer. Ch-9, pp-223-227

[32] A. C. Torano, F. Kugler, K. P. Papathanassiou, P. Biber and P. Pretzsch, "Biomass estimation as a function of vertical forest structure and forest height, Potential and limitations for Radar Remote Sensing", *Proceedings of EUSAR*, Aachen, Germany, June 2010.

[33] I. Hajnsek, F. Kugler, S. Lee and K. Papathanassiou, "Tropical Forest Parameter Estimation by means of Pol-InSAR: The INDREX II Campaign", *IEEE Transactions on Geoscience and Remote Sensing*, Cape Town, South Africa, July 2009.

[34] H. Peterson, "Biomassafunktioner för trädfraktioner av tall, gran och björk i Sverige", *SLU*, *Institutionen för skoglig resurshushållning och geomatik*, Arbetsrapport 59, Umeå, 1999, (in Swedish).

[35] R. N. Treuhaft and P. R. Siqueira, "The vertical structure of vegetated land surfaces from interferometric and polarimetric radar", *Radio Science*, Vol. 35, No. 1, pp. 141-177, 2000.

[36] F. Kugler, D. Schulze, I. Hajnsek, H. Pretzsch, and K. P. Papathanassiou, "TanDEM-X Pol-InSAR Performance for Forest Height Estimation," IEEE Transactions on Geoscience and Remote Sensing, vol. 52, no. 10, pp. 6404–6422, Oct. 2014.

[37] R. Bamler and P. Hartl, "Synthetic aperture radar interferometry," Inverse Problems, vol. 14, no. 4, p. R1, Aug. 1998.

[38] R. Touzi and A. Lopes, "Statistics of the Stokes parameters and of the complex coherence parameters in one-look and multilook speckle fields," IEEE Transactions on Geoscience and Remote Sensing, vol. 34, no. 2, pp. 519–531, Mar. 1996.

[39] O. M. Bollandsås, "Estimation of forest stand parameter using airborne laser scanner data; a comparison of Methods", *Proceedings of the ScandLaser Scientific Workshop on Airborne Laser Scanning of Forests*, Sweden, 3–4 September 2003; pp 65-70.

[40] M. Nilsson and J. Holmgren, "Prediction of Forest Variables Using LIDAR Measurements with Different Footprint Sizes and Measurement Densities", *Proceedings of the ScandLaser Scientific Workshop on Airborne Laser Scanning of Forests*, Sweden, 3–4 September 2003; pp. 125-133.

[41] M. Bachman, et al., "Calibration of the TanDEM-X interferometer", *Proceedings of 9th European Conference on Synthetic Aperture Radar (EUSAR)*, Nuremberg, April 2012.

[42] S.R. Cloude and K.P. Papathanassiou, "Three-stage inversion process for polarimetric SAR interferometry", *IEE Proceedings - Radar Sonar and Navigation*, vol. 150, no. 3, pp. 125-134,2003
[43] Weather Spark, historical weather: htttp://www.weatherspark.com, 25/6/2013
[44] H. Balzter, E. Talmon, W. Wagner, D. Gaveau, S. Plummer, J. J. Yu, Shaun Quegan, Malcolm Davidson, Thuy Le Toan, M. Gluck, A. Shvidenko, S. Nilsson, K. Tansey, A. Luckman & and C. Schmullius, "Accuracy assessment of a large-scale forest cover map of central Siberia from synthetic aperture radar", *Canadian Journal of Remote Sensing*, 28(7): 719-737, 2000
[45] K. P. Papathanassiou and S. R. Cloude, "Single-baseline Polarimetric SAR Interferometry", *IEEE Transactions on Geoscience and Remote Sensing*, vol. 39, no. 11, pp. 2352-2363, 2001.
[46] S. K. Lee, F. Kugler, K. P. Papathanassiou and I. Hajnsek, "Quantification of temporal decorrelation effects at L-band for polarimetric SAR interferometry applications". *Selected Topics in Applied Earth Observations and Remote Sensing, 6*(3), pp. 1351-1367, 2013.

Astor Toraño Caicoya was born in Asturias, Spain in 1983. He received his Bhc in Forestry Engineering by the University of Oviedo in 2004, and his MSc also in Forestry Engineering by the Polythecnic University of Valencia (UPV), in Valencia, Spain in 2007. He continued his studies with a MSc in Sustainable Resource Management at the Technische Universtität München (2007-2010). He defended his PhD thesis in April 2016, at the Chair of Forest Growth and Yield from the Technische Universität München, Munich, Germany.

From 2009 to 2015, he worked at the Radar and Microwaves Institute from the German Aerospace Center (DLR – HR), Oberpfaffenhofen, Germany. His research focuses on forest modelling and allometry for the estimation of forest above ground biomass and the development of algorithms for the characterization of 3D forest structures from remote sensing (i.e. SAR tomography and waveform LiDAR) data.

Florian Kugler was born in Bavaria, Germany, in 1974. He received a Diploma degree (Dipl. Ing. silv.) in forestry science from the Technische Universität München, Freising, Germany, in 2004. Since October 2004, he is a research scientist at the German Aerospace Center (DLR). In the frame of his research activities at DLR he received his Ph.D. from the Technische Universität München, Freising, Germany. His research focuses on Remote Sensing on forests, by using Polarimetric SAR Interferometry.

Irena Hajnsek (AM' 01, M'06, SM'09, FM'14) is since November 2009 Professor of Earth Observation at the Swiss Federal Institute of Technology (ETH) Zürich Institute of Environmental Engineering and at the same time head of the Polarimetric SAR Interferometry research group at the German Aerospace Center Microwaves and Radar Institute. Her main research interests are in electromagnetic propagation and scattering theory, radar polarimetry, SAR and interferometric SAR data processing techniques, environmental parameter modelling and estimation. She received her Dipl. degree (Honors) in 1996 from the Free University of Berlin, Germany and the Dr. degree (Honors) in 2001 from the Friedrich Schiller University of Jena, Germany. Since 2010 she is the science coordinator of the German satellite mission TanDEM-X. She was Technical Program Co-chair of the IEEE IGARSS 2012 Symposium in Munich. Since 2013 she is a member of the IEEE GRSS AdCom.

Konstantinos P. Papathanassiou (A'01 – M'06 – SM'09 – F'13) received the Dipl.Ing. (Hons.) and Dr. (Hons.) degrees from the Graz University of Technology, Graz, Austria, in 1994 and 1999, respectively. From 1992 to 1994, he was with the Institute for Digital Image Processing (DIBAG), Joanneum Research, Graz. Between 1995 and 1999, he was with the Microwaves and Radar Institute, German Aerospace Center (DLR-HR), Wessling, Germany. From 1999 to 2000, he was a European Union Postdoctoral Fellow with Applied Electromagnetics, St. Andrews, U.K. Since October 2000, he has been a Senior Scientist with DLR-HR, leading the Information Retrieval Research Group. He is the author or co-author of more than 100 publications in international journals, conferences, and workshops. His main research interests are in polarimetric and interferometric processing and calibration techniques, polarimetric SAR interferometry, and the quantitative parameter estimation from SAR data, as well as in SAR mission design and SAR mission performance analysis.

He was the recipient of the IEEE GRSS IGARSS Symposium Prize Award in 1998, the Best Paper Award of the European SAR Conference in 2002, the DLR Science Award in 2002, and the DLR Senior Scientist Award in 2011.

Dr. Papathanassiou is a member of DLR's TanDEM-X and Tandem-L Science Teams, JAXA's ALOS-2 Cal-Val teams, ESA's BIOMASS mission Advisory Group, SAOCOM-SC Expert Team, JAXA's Carbon and Kyoto Initiative, and NASA's GEDI Mission Science Team.

III

Forest above-ground biomass estimation from vertical reflectivity profiles at L-Band

Astor Toraño Caicoya, Matteo Pardini, Irena Hajnsek and Konstantinos Papathanassiou

***Abstract*— Forest height is an important parameter for the allometric estimation of above-ground forest biomass (AGB). However, variable forest stand densities limit the performance of the allometric estimation of AGB from height measurements alone. Recently, the use of vertical forest structure information as an indicator for the variation of stand density has been proposed and used to improve the allometric estimation of AGB from height measurements. In this work, the use of vertical radar reflectivity profiles at L-band obtained from SAR tomography, as a proxy for vertical forest structure for the allometric estimation of AGB, is investigated. L-band reflectivity profiles, reconstructed from data at different polarisations (HH and HV) and acquired under "moist" and "dry" weather conditions, are investigated. The proposed allometric AGB estimator increases the correlation factor from 0.60 to 0.81 and reduces the RMSE from 50.25 Mg/ha to 36.30 Mg/ha when compared to the AGB estimation from forest height alone. The effect of polarisation and weather conditions on the AGB estimation performance is discussed.**

***Index Terms*— Forest biomass, SAR tomography, L-band, vertical reflectivity profiles, vertical forest structure, forest allometry.**

I. Introduction

Forest above-ground biomass (AGB) represents the amount of carbon stored in forests and is, therefore, a key element in the quantification of the global carbon cycle [1]. At the same time, accurate estimation of AGB requires the knowledge of several forest parameters. At stand level, single parameter allometric relations like the height-to-biomass allometry proposed in [2], [3],[4]

$$\mathrm{AGB} = 0.9\mathrm{H}^{1.58} \tag{1}$$

where H is the forest (stand) top height, can serve for a first order estimation of AGB, but are not sufficient for accurate and robust biomass estimation. The variable stand density for a given stand height [5] introduces a rather large variation in the estimation obtained by [1], especially at smaller stand sizes. Towards an accurate (and general) height-to-biomass allometry the integration of direct or indirect information for forest density is required [6].

Recently, the use of vertical structure information derived from vertical biomass profiles (AGB) has been used in [7] to improve the performance of the height-to-biomass allometry. For this, the vertical distribution of biomass AGB(h), derived from inventory data has been expressed in terms of a Legendre polynomial series

$$\mathrm{AGB(h)} = \sum_{\mathrm{n}} \mathrm{a_n P_n(h)} \tag{2}$$

where $\mathrm{P_n}$ are the Legendre polynomials and a_n the associated Legendre coefficients [7]

$$\mathrm{a_n} = \tfrac{2n+1}{2} \textstyle\int_{-1}^{1} \mathrm{AGB(h) P_n(h) dh}. \tag{3}$$

In order to express the vertical structure independently from absolute biomass the coefficient $\mathrm{a_0}$, which is proportional to the integral of the biomass profile, is not taken into account.

In [7] the first four Legendre coefficients $(\mathrm{a_1}, \cdots, \mathrm{a_4})$ have been used to distinguish between different levels of biomass. The lower frequency contribution given by the first Legendre coefficient $(\mathrm{a_1})$, i.e. the normalized height to the profile's barycenter, is associated to the stem compartment while the higher frequency components given by the next three coefficients $(\mathrm{a_2}, \mathrm{a_3}, \mathrm{a_4})$ are associated to the crown compartment. Accordingly, the structure ratio $\mathrm{S_{rat}}$

$$\mathrm{S_{rat}} = \frac{|\mathrm{a_1}|}{|\mathrm{a_2} + \mathrm{a_3} + \mathrm{a_4}|} \tag{4}$$

may be used as a proxy to stand density to improve the allometric biomass estimation

$$\mathrm{AGB} = 7\mathrm{S_{rat}^{0.8} H^{0.85}}. \tag{5}$$

Thus, for a constant height, if the numerator of the ratio increases (indicating a higher proportion of stem biomass), biomass increases, and if the denominator increases (indicating a higher proportion of crown biomass) biomass decreases. In [7] H and $\mathrm{S_{rat}}$ have been derived from vertical biomass profiles. AGB(h) was obtained from inventory data.

The objective of this work is to evaluate how far (5) can be used to estimate AGB by means of SAR measurements, i.e. using H and $\mathrm{S_{rat}}$ derived from vertical reflectivity profiles at

Manuscript received April xx, 2015; revised month xx, 201x, Current Version published month xx, 201x.

Astor Toraño Caicoya, Matteo Pardini and Konstantinos Papathanassiou are with the Radar Concepts Department, Microwaves and Radar Institute, German Aerospace Center (DLR), (DLR-HR), D-82234 Oberpfaffenhofen, Germany. (e-mail: astor.toranocaicoya@dlr.de, matteo.pardini@dlr.de, kostas.papathanassiou@dlr.de).

Irena Hajnsek is with the Institut für Umweltingenierwissenschaften, ETH Zürich, Schafmattstr. 6, 8093 Zürich. (e-mail: hajnsek@ifu.baug.ethz.ch)

L-band obtained from multi-baseline polarimetric (interferometric) L-band data.

II. Experimental data

A. Test site, ground measurements and SAR data

Traunstein is a managed temperate heterogeneous forest located in the southeast of Germany (47°51'32"N, 12°39'20"E) dominated by Norway spruce, European beech and White fir. Forest stand heights range from 10 up to 40m. The mean biomass level is about 200Mg/ha, and thus significantly higher than other managed forests in the same ecological zone.

The biomass at plot level is estimated using forest inventory data acquired in 2008. The inventory was performed on circular plots of 500m^2 on a grid of 100x100m. For each tree within the plot, the height and measured diameter at breast height (dbh) have been used to estimate vertical biomass distribution using species specific allometry [7]. The vertical biomass distributions of all trees within the plot have been summed up to obtain a vertical biomass profile. These plot-level biomass estimates have then been interpolated to generate a continuous biomass map. The forest ground inventory of 2008 was supported by an airborne LIDAR mapping campaign providing forest height measurements and a digital terrain model (DTM) for the entire site.

Between June 7th and June 20th 2008 DLR's airborne E-SAR system acquired, several L-band multibaseline fully polarimetric SAR data sets over the Traunstein site. Each data set consisted of five flight tracks allowing the formation of interferograms with vertical wavenumbers between 0.05 and 0.4 rad/m and a Rayleigh height resolution limit of about 15 m [8]. For the investigations in this work two of these data sets are considered. The first one was acquired on June 10th after a longer period without rainfall, while the second one was collected on June 12th, the day after a strong rain event [7]. Given the difference in the vegetation and/or soil moisture conditions, in the following the two data sets will be called "dry" acquisition and "moist" acquisition, respectively. Due to the short repeat-pass intervals (< 10 min between tracks and <50 min for the whole data set) and the calm wind conditions during both acquisition days (< 1.2 m/s), wind-induced temporal decorrelation effects can be neglected [9].

B. SAR Tomography: Capon estimator

Vertical reflectivity (i.e. power) profiles can be estimated from the interferometric coherences measured at the different baselines by means of several algorithms, model-based or not [8], [10]. In this work, the Capon spectral estimator, a low-complexity model-free imaging solution that offers height super-resolution and side-lobe rejection, has been used. A known shortcoming of the Capon estimator is its intrinsic radiometric non-linearity, which can lead to biased power estimates due to statistical reasons even with well (phase) calibrated data. However, such power-bias can be mitigated by processing the data with more than 50 independent looks [8]. In this way the relative power difference between height layers is preserved with enough accuracy, although a small absolute bias may still remain.

Concerning the two data sets at hand, the Capon estimator has been applied by processing 80 independent looks, corresponding to a squared multi-look cell with 15m side length. The tomographic analysis in [8] has shown that the difference in moisture conditions before and after a rainfall causes a stand-dependent change of the vertical reflectivity profiles. The most apparent effect is an increase of the canopy extinction in the "moist" acquisition. This was quantified in [8] by means of the relative variation (integrated in height) of the "moist" reflectivity profile with respect to the "dry" profile. This relative variation was estimated to be around 20% on average, at some stands up to 50%. It is also worth noting that a slight worsening of the imaging capabilities of the Capon estimator is observed in the "dry" acquisition with respect to the "moist" acquisition in (some) stands which taller than 30m. Indeed, in those stands the thicker canopy volume together with lower extinction decrease the interferometric coherence, which turns into an increased blurring of the Capon profiles. Conversely, in the "moist" acquisition extinction increases, volume coherences increase, and blurring decreases.

III. Structure characterization for biomass inversion

The algorithm for the estimation of forest biomass from the estimated vertical reflectivity profiles and the corresponding Legendre coefficients can be structured into three steps: (*i*) forest (stand) height estimation, (*ii*) attenuation correction of the reflectivity profiles and (*iii*) the estimation of the structure ratio S_{rat} and application of an empirically derived structure-to-biomass allometric relationship.

A. Height estimation: profile truncation

As already discussed in [7], forest height is a key parameter in the estimation of biomass and by itself can reach correlations up to 60% [2]. While forest height estimation from model-based inversion of MB polarimetric interferometric L-band SAR data has been demonstrated to be accurate and robust [3],[4], in this work forest height is directly estimated from the reflectivity profiles. For this, the estimation of the underlying ground (i.e. zero height) is required. The position of the ground is estimated using the method proposed in [11]. The methodology provides, in all polarizations and scenarios, robust and accurate ground estimates with a root mean square error lower than 2 m, when they are validated against the LIDAR DTM.

Forest height is estimated by using the algorithm proposed in [10] with a slight modification motivated by the assumption that, for taller stands, the vertical resolution of around 15 m may allow to identify more than one physically relevant lobe.

Starting from the estimated ground (i.e. from zero height) and moving along the reflectivity profile upwards, the profile is truncated when the power drops below 30% of the power of the highest physically relevant lobe. Physically relevant are only lobes recognized with power larger than the 20% power of the dominant lobe. These thresholds have been selected after validation on multiple stands in order to obtain optimum

inversion performance for this site. The height at which the profile is truncated corresponds to the forest height estimate. The estimated heights are plotted against the LIDAR reference heights (H100 [12]) in Figure 1. The performance is better for the "moist" conditions (on the left side) and reduces for "dry" conditions (on the right side) characterized by a correlation factor r^2 of 0.95 and 0.92, and the RMSE of 2.04 m and 2.76 m, respectively. An overestimation of tall trees in the "dry" conditions can be noticed in Figure 1. This is related to the blurring of the Capon profiles discussed at the end of Section II.B.

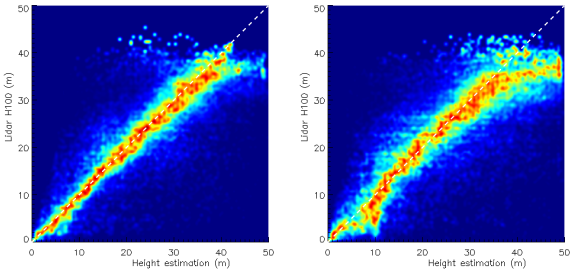

Figure 1: Height estimation vs. Lidar H100. The "moist" acquisition lays on the left (RMSE= 2.04 m and r^2 = 0.95) and the "dry" on the right for HH polarization (RMSE= 2.76 m and r^2 = 0.92).

B. Profile adaptation-exponential correction

The vertical reflectivity profiles cannot directly be interpreted as vertical biomass profiles. Before estimating the structure ratio from the reflectivity profiles, these need to be corrected for attenuation of the representation of lower forest compartments. The correction is performed adaptively for each profile, according to the profile height and the power ratio of the power of the dominant lobe A_{max_pic} to the power of the lowest (closest to the ground) profile lobe A_{first_pic}

$$f_{ex}(h) = e^{-(ah-b)} \quad (6)$$

where $f_{ex}(h)$ is an exponential as a function of height (h), a and b are defined as

$$a = \frac{4.6+b}{H}, \; b = \mathrm{Ln}\left(\frac{A_{max\_pic}}{A_{first\_pic}}\right) \quad (7)$$

and H is the forest height. The ratio $A_{max\_pic}/A_{first\_pic}$ ensures that the corrected power of upper lobes is lower than the lower lobes, as it is expected for vertical biomass distributions. The ratio is affected by ground response which in fact accounts for extinction effects. Furthermore, the value of a vertical biomass profile must be zero at the top height H. For this reason, in the expression of the exponential correction, the value of 4.6 ($-\mathrm{Ln}\,0.01$) is fixed, as an approximation to zero for the value of the function at H, i.e. $f_{exp}(H) = 0.01$. The resulting corrected profile $f_{corr}(h)$ is calculated multiplying the exponential function to original profile f(h): $f_{corr}(h) = f(h) \cdot f_{ex}(h)$.

After correcting the relative powers, the profile lobes become more similar to the vertical biomass profiles. In Figure 2 two profiles (on the left side for a mixed forest and on the right side for a dense coniferous forest), before and after the exponential correction, are shown. The correction effect is obvious: the reflectivity profile approaches the biomass distribution. It is important to remark that the height of the reflectivity lobes corresponds with great accuracy to lobes of the biomass profile. However, the L-band profiles show a reduced sensitivity to some biomass compartments, especially to the biomass contained between the canopy and the ground, which cannot be fully amplified by this exponential correction.

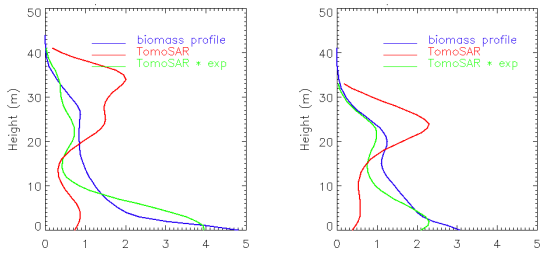

Figure 2: Exponential correction examples in "moist" conditions and HH polarization. Blue is the biomass profile, red the original reflectivity profile and green the profile after exponential correction. All profiles are normalized to the Legendre coefficient a_0.

C. Biomass inversion

After the correction, the profiles are expressed in terms of a Legendre polynomial series and the coefficients of the four first polynomials are used to estimate the structure ratio S_{rat}. With a relationship of the kind of (5), the exponent for S_{rat} changes its sign, accordingly to the given sensitivity to the crown volume response. The inversion parameters need to be also adapted due to the expected smaller range of ratio values, expressed by the higher slope in the S_{rat}-to-Biomass relationship. The allometric relationship is then described by

$$AGB = \alpha S_{rat}^{\beta} H^{\gamma} \quad (8)$$

and the parameters α, β and γ result in: $\alpha = 40, \beta = -0.55$ and $\gamma = 0.85$. Due to the high height estimation accuracy the exponent γ in (8) is equal to exponent c used in (5).

In Figure 3, the biomass maps for Traunstein are shown, obtained from HH in "moist" (top panel) and "dry" (bottom panel) conditions, together with the estimated height and the corresponding S_{rat} maps. The final biomass map has a spatial resolution of 15x15 m (0.2 ha). The height estimation is performed for every resolution cell (15x15 m); however, S_{rat}, being a structural variable is calculated at a ~1 ha grid, to achieve a representative physical horizontal structure [7].

A coherent and reasonable biomass distribution is already apparent, following the forest stands defined by the forest management plan. Several stands which do not reach the maximum height of the site present very high levels of biomass (~400 Mg/ha) due to the high stand density. In these areas, the values of S_{rat} are minimum (in dark blue) and, therefore, have positively corrected for the high stand density.

The biomass range is larger and more apparent in the "moist" acquisition, due to a more sensitive structure characterization,

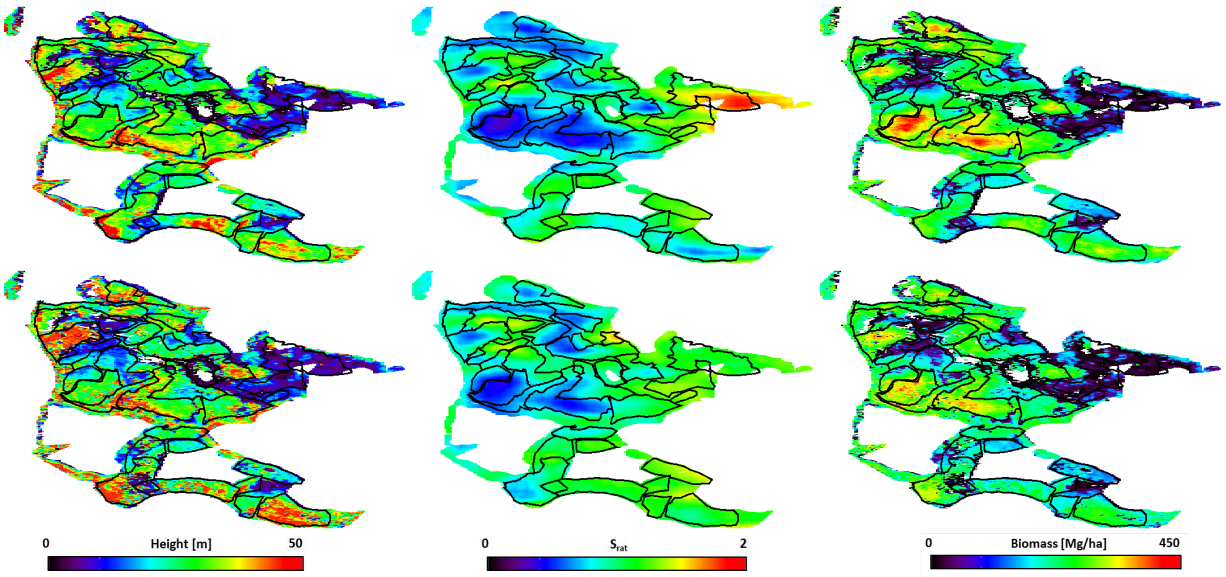

Figure 3: 2D maps of the structure algorithm results. From left to right, estimated height from the profile truncation, structure ratio and biomass inversion results. On the upper panel: "moist" conditions in HH polarization. On the lower panel: "dry" conditions in HH polarization. Overlaid in black: forest management homogenous polygons.

mainly due to a lower effect of the volume decorrelation on Capon imaging (Section II.B). This is visible in a higher variability of the range values in the S_{rat} map, which can be observed by darker colors in the high density area. Even if taller heights tend to be overestimated, the limited capability of the structure ratio to compensate for the stand density can be translated in an underestimation of biomass values.

IV. Validation Results

In Figure 4 (on the left) the estimated height for each stand in "moist" conditions is plotted against the reference biomass results. Each plot is color coded according to the value of S_{rat}. In this plot it is possible to observe the dependencies of the ratio. First, it is inversely correlated to biomass (as expressed in the exponent S_{rat} in (8)) and second, for a constant height the values decrease when biomass increase indicating an inverse correlation to stand density [7]. In Figure 4 (on the right), the inverted biomass using the estimated height in (1) is shown. A typical height-to-biomass correlation value of 0.61 is obtained with a root mean square error (RMSE) of 50.25 Mg/ha.

In Figure 5, the inversions results, for the different weather conditions and polarizations, are shown. The best results correspond to the "moist" acquisition using the HH polarization although the difference to the results obtained using HV polarization, for this acquisition, is very small. In principle, even if the sensitivity of HV to the vertical structure is higher than in HH, a better height estimation performance in HH (due to a lower decorrelation and a better exponential correction due to higher visibility of the ground) leads to overall better inversion results. This effect also influences the inversions in "dry" conditions: due to the lower extinction, the height estimation performance decreases and the reflectivity becomes less sensitive to the forest volumes affecting the performance of the inversion algorithm. Nevertheless, for all scenarios we observe a constant improvement of ~20% when compared to height-only allometry. A slight tendency of underestimation is observed in the stands of highest biomass for the "dry" acquisitions, in both HH and HV polarizations. There is not evident effect of topography on the achieved performance for any of the investigated scenarios and polarizations.

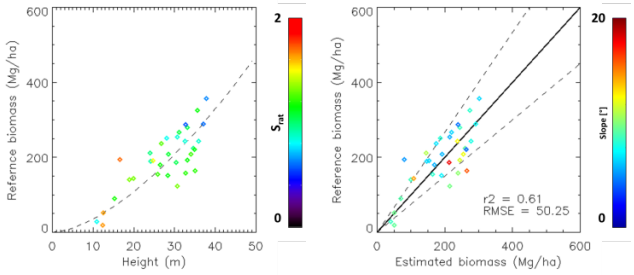

Figure 4: On the left side: Height-to-biomass relation obtained from the validation polygons for HH-moist case. The plots are color coded according to the structure ratio S_{rat}. The dashed curve corresponds to $B = 0.9H^{1.58}$. On the right side: biomass inversion using height-to-biomass allometry on the validation polygons (1). The dashed lines indicate the 20% biomass estimation error. The plots are color coded according to the average terrain slope.

V. Conclusions

In this work, the interpretation of forest structure-to-biomass allometry using vertical reflectivity profiles obtained at L-band from multi-baseline polarimetric (interferometric) data is demonstrated. The proposed AGB estimation algorithm is based on estimates of forest height and structure ratio S_{rat} (interpreted as the ratio, between the stem and the crown compartment) from vertical reflectivity profiles at L-band.

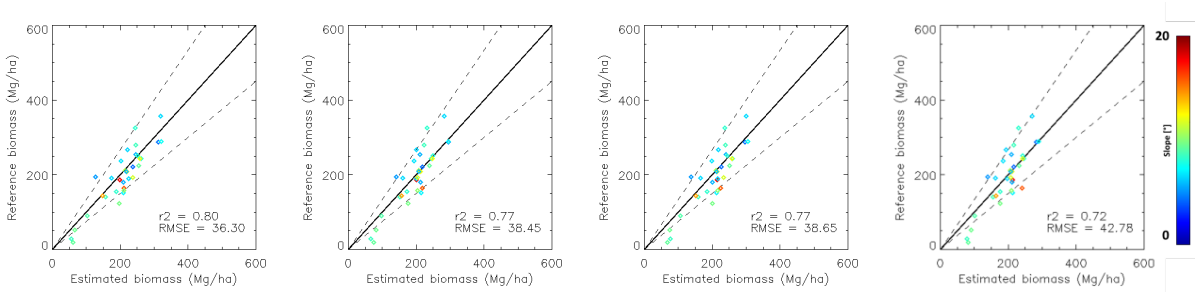

Figure 5: Biomass estimation performance using the structure-to-biomass algorithm. From left to right: HH-moist, HH-dry, HV-moist and HV-dry. The dashed lines indicate the 20% biomass estimation error. The plots are color coded according to the average terrain slope.

First, the reflectivity profiles are estimated from the available SAR data in different polarizations (HH and HV) and different environmental scenarios ("moist" and "dry") using the Capon spectral estimator. Then, forest (stand) height is derived directly from the estimated reflectivity profiles. The retrieval of forest height was for all cases accurate with an error below 10 %. However, the obtained forest heights depend on the shape of the reflectivity profile, which is affected by changing environmental conditions.

The Legendre basis decomposition is used in order to test an allometrically derived algorithm that has been successfully applied to vertical biomass distributions [7]. However, before applying it on reflectivity profiles, these have to be corrected for attenuation. The correction of the height-dependent attenuation, in spite of increasing the sensitivity of S_{rat} to a higher range of structure types, is expected to make the AGB estimation more robust against variations of environmental conditions. After applying the Legendre basis decomposition, the Legendre coefficients are used to derive the structure ratio S_{rat}. The fact that the ratio is based on relative powers reduces the impact of a residual power bias introduced by the Capon estimator. For all scenarios and polarizations the biomass estimation performance is similar (max. deviation ~8%), indicating the compensation of the errors in height estimation error and the estimation of the structure ratio S_{rat}.

The applicability of this methodology to reflectivity profiles derived from different frequencies may show limitations due to the different response of the radar signal to the biomass compartments. The relative proportion between the powers associated to different biomass compartments may modify the structure ratio S_{rat} and therefore the connection to forest density and biomass.

This is a case study developed in a very heterogeneous forest stand, which offers a great potential for the study of structures and is representative of highly diverse temperate forests. However, the average slope on the validation area is generally low (~10°) so a study on higher slopes would be useful to test topographic correction methods. The applicability of the method should be also tested in other forest scenarios in order to generalize the conclusions drawn here.

VI. Acknowledgements

We would like to thank the Chair of Forest Yield of the "Technische Universität München" for providing the inventory and reference data. This work has been partially supported by the HGF-Helmholtz Alliance "Remote Sensing & Earth System Dynamics".

VII. References

[1] R. A. Houghton, "Aboveground Forest Biomass and the Global Carbon Balance," *Glob. Change Biol.*, vol. 11, no. 6, pp. 945–958, Jun. 2005.

[2] T. Mette, K. P. Papathanassiou, I. Hajnsek, and R. Zimmermann, "Forest biomass estimation using polarimetric SAR interferometry," in *Geoscience and Remote Sensing Symposium, 2002. IGARSS '02. 2002 IEEE International*, 2002, vol. 2, pp. 817–819 vol.2.

[3] K. P. Papathanassiou and S. R. Cloude, "Single-baseline polarimetric SAR interferometry," *IEEE Trans. Geosci. Remote Sens.*, vol. 39, no. 11, pp. 2352–2363, Nov. 2001.

[4] R. N. Treuhaft, B. D. Chapman, J. R. dos Santos, F. G. Gonçalves, L. V. Dutra, P. M. L. A. Graça, and J. B. Drake, "Vegetation profiles in tropical forests from multibaseline interferometric synthetic aperture radar, field, and lidar measurements," *J. Geophys. Res. Atmospheres*, vol. 114, no. D23, p. D23110, Dec. 2009.

[5] H. Pretzsch and P. Biber, "A Re-Evaluation of Reineke's Rule and Stand Density Index," *For. Sci.*, vol. 51, no. 4, pp. 304–320, Aug. 2005.

[6] D. H. T. Minh, T. L. Toan, F. Rocca, S. Tebaldini, M. M. d'Alessandro, and L. Villard, "Relating P-Band Synthetic Aperture Radar Tomography to Tropical Forest Biomass," *IEEE Trans. Geosci. Remote Sens.*, vol. 52, no. 2, pp. 967–979, Feb. 2014.

[7] A. C. Toraño, F. Kugler, H. Pretzsch, and K. Papathanassiou, " Forest vertical structure characterization using ground inventory data for the estimation of forest aboveground biomass," Can. J. For. Res., 2015. doi: 10.1139/cjfr-2015-0052

[8] M. Pardini, A. Cantini, F. Lombardini, and K. Papathanassiou, "3-D Structure Of Forests: First Analysis of Tomogram Changes Due to Weather and Seasonal Effects at L-Band," in *EUSAR 2014; 10th European Conference on Synthetic Aperture Radar; Proceedings of*, 2014, pp. 1–4.

[9] S.-K. Lee, F. Kugler, K. P. Papathanassiou, and I. Hajnsek, "Quantification of Temporal Decorrelation Effects at L-Band for Polarimetric SAR Interferometry Applications," *IEEE J. Sel. Top. Appl. Earth Obs. Remote Sens.*, vol. 6, no. 3, pp. 1351–1367, Jun. 2013.

[10] S. Tebaldini and F. Rocca, "Multibaseline Polarimetric SAR Tomography of a Boreal Forest at P- and L-Bands," *IEEE Trans. Geosci. Remote Sens.*, vol. 50, no. 1, pp. 232–246, Jan. 2012.

[11] M. Pardini and K. Papathanassiou, "Sub-canopy topography estimation: Experiments with multibaseline SAR data at L-band," in *Geoscience and Remote Sensing Symposium (IGARSS), 2012 IEEE International*, 2012, pp. 4954–4957.

[12] F. Kugler, D. Schulze, I. Hajnsek, H. Pretzsch, and K. P. Papathanassiou, "TanDEM-X Pol-InSAR Performance for Forest Height Estimation," *IEEE Trans. Geosci. Remote Sens.*, vol. 52, no. 10, pp. 6404–6422, Oct. 2014.